UNIVERSITY OF CALIFORNIA, MERCED

Open system dynamics in quantum optomechanics

A dissertation submitted in partial satisfaction of the
requirements for the degree of
Doctor of Philosophy

in

Physics

by

Dan Hu

Committee in charge:

Professor Jay E. Sharping, Chair
Professor Harish S. Bhat
Professor Kevin A. Mitchell
Professor Lin Tian, Dissertation Advisor

2014

The dissertation of Dan Hu, titled Open system dynamics in quantum optomechanics, is approved, and it is acceptable in quality and form for publication on microfilm and electronically:

Chair _____ Date _____

Professor Jay E. Sharping

_____ Date _____

Professor Harish S. Bhat

_____ Date _____

Professor Kevin A. Mitchell

_____ Date _____

Professor Lin Tian

University of California, Merced

2014

This dissertation is dedicated to my family.

Contents

Abstract

Open system dynamics in quantum optomechanics

by

Dan Hu

Doctor of Philosophy in Physics

University of California, Merced

Professor Lin Tian, Dissertation Advisor

In this dissertation, I theoretically investigate the open system dynamics of cavity optomechanical systems in the quantum limit, where a mechanical resonator couples to a cavity mode via radiation pressure force. Recent developments in nanofabrication and cooling techniques make it possible to optically control and manipulate the motion of micro- and nano-mechanical resonator. Several experiments have demonstrated the possibility of preparing macroscopic mechanical resonators into their quantum ground state, which makes optomechanical systems an ideal candidate for studying the quantum behavior of macroscopic objects. One important direction in quantum optomechanics is the study of the decoherence of optomechanical system due to the interaction with their external environments. This dissertation explores the decoherence effects by considering the influence of the radiation pressure coupling on the interaction between optomechanical system and its environments. Because the effects of the nonlinear interaction vary with the optomechanical coupling strength, three different interaction regimes are fully studied here: the weak coupling, the intermediate coupling and the strong coupling.

In Chapter 1, I introduce the basis of optomechanics and quantum open systems. I first review the current development for the experimentally available optomechanical systems, focusing on the description of the system and its Hamiltonian model, the nonlinear properties of the radiation-pressure interaction and their possible applications. I also provide a brief introduction of the open system theory based on the Born-Markov master equation and Langevin equation method, respectively.

Chapter 2 is concerned with the weak coupling regime where the system can be linearized. We consider the validity of the general linearization procedure of an optomechanical system in the unstable regime, which has been proposed for generating large optomechanical entanglement by a pulsed scheme. Our results show that for a pulse driven optomechanical system there exists a time window where the optomechanical dynamics can be fully characterized by a linearized model. We discuss the

influence of the linearization window on entanglement generation for an optomechanical system in the unstable regime. We also investigate the schemes of improving optomechanical entanglement using time modulation and extend this idea to a three-mode optomechanical system, where two cavity modes interact with one mechanical mode. Our results reveal that with a suitable time modulation of the driving field, the three-mode optomechanical system can have steady-states with significantly improved entanglement between each subsystem, which provides an additional control of entanglement dynamics in optomechanical systems.

In Chapter 3, we treat the nonlinear optomechanical interaction as a small perturbation to the linearized model, which works for the standard optomechanical system with an intermediate radiation pressure coupling. In this regime, the nonlinear part of the optomechanical interaction starts to show its influence while the linearized optomechanical interaction still dominates the dynamics for the system. We propose a perturbative method to study the influence of the nonlinear interaction in the Heisenberg picture. It turns out that the perturbative approach successfully reveals the role of the nonlinear coupling, which is consistent with the results from the general master equation method, while the perturbative method developed in this chapter can be applied to a much broader parameter regime as well as providing clear physical pictures with its analytical form.

Finally, Chapter 4 is about the strong coupling regime, where the strength of the optomechanical coupling is comparable to that of the mechanical frequency. In this ultra-strong coupling regime, both the linearization and perturbation method mentioned previously fail to provide correct dynamics. We establish a dressed-state master equation method to investigate the optomechanical open system dynamics. New coherent dynamics for this strongly coupled system are discovered with this dressed-state master equation. We provide detailed comparison of this dressed-state master equation with that of the standard master equation.

List of Figures

List of Tables

Acknowledgments

I would like to thank my advisor, Professor Lin Tian, for the support and guidance she has provided me throughout my dissertation. Her scientific intuition and insights,which laid the foundation for this work, have always been very helpful. She encouraged me not only to grow as a physicist but also as an independent thinker which will benefit me for the rest of my life. I would also like to thank my committee members Professor Jay Sharping, Professor Kevin Mitchell and Professor Harish Bhat, without whose knowledge and assistance this study would not have been successful.

I want to thank the staff of the School of Natural Sciences, the Center for Research on Teaching Excellence (CRTE) and the Graduate Division at UC Merced, for continuously hiring me as a Teaching Assistant and providing me with necessary financial and technical support. In particular, I want to thank Carrie King, Dr. Carrie Menke and Stefanie Stepp. Because of their help, I really enjoyed my studies and life at UC Merced.

A special thanks to Professor Raymond Chiao and his wife Florence Chiao. Because of their love, we have a real family in Merced. They were so helpful for my study and my family. I also thank my friend Dr. Jian Cai, who has provided helpful advice many times during my graduate school career. I also thank him for many interesting and stimulating discussions throughout the years. My sincere thanks also goes to Dr. Anton V. Sharypov, Dr. Bing He, Dr. Sumei Huang and Dr. Lianghui Du for their helpful discussions in my research projects.

I especially thank my parents JiaShun Hu and Quanmei Wei for all their aid and dedication throughout the years.

Finally and most importantly, I want to thank my beloved wife, Jia Jia, for her true support, continuous encouragement, patience and unwavering love. Without her, I could not have finished all my work, and I am so lucky to have her by my side.

Chapter 1

Introduction

Radiation pressure forces between light and matter come from the exchanges of momentum between the scattered photons and the reflecting object, where the momentum change implies that the light is exerting a force on the object. To estimate the magnitude of this force for a light beam with power P, the momentum change of reflecting light during time Δt is $\Delta p = 2P\Delta t/c$ and, as a result, the radiation force is $F = \Delta p/\Delta t = 2P/c$, which is a very tiny force due to the speed of light. For example, the power of the sun light on earth is about $1.4KW/m^2$ and the corresponding radiation force per square meter is $10^{-5}N$, which is ten orders smaller than the atmospheric pressure force on the same area, i.e. $10^5 N/m^2$. The radiation force was firstly observed in the dust tails of comets by Kepler in the 17^{th} century [1] and has been studied by experiments since the early 20^{th} century. Later, along with the laser technology, radiation pressure forces were successfully applied to experimentally trap and control the atomic system. One remarkable achievement is the laser cooling technique, which allowed and initiated many important applications for atomic experiments, such as the optical atomic clocks, high resolution spectroscopy of stored ions, and the observation of the motional ground state of trapped ions.

Radiation pressure interaction exists not only for microscopic objects but also between the light and macroscopic objects. The fluctuations of radiation pressure on large mechanical objects were investigated by Braginsky and co-workers in the late 1960s[2, 3]. They demonstrated that the quantum fluctuations of radiation fields can limit the precision of position detection in the gravitational wave detectors via the radiation pressure interaction. Recent advances in micro- and nano-fabrication have enabled experimentalists to obtain this interaction between radiation fields and micro- and nano-mechanical objects, which we call the optomechanical interaction and the corresponding systems are called optomechanical systems. Optomechanical systems have been realized experimentally in a variety of systems, including a Fabry-Perot cavity with moving mirror(s) [4, 5], cold atoms in a cavity [6, 7], a nanomechanical resonator coupling with superconducting circuits [8], and photonic

crystal structures[9, 10, 11]. Study of such systems can lead to advances in precision measurements [12, 13] and implementations of quantum information protocols, and the testing of macroscopic quantum effects[14].

In recent experiments, many quantum behaviors of the mechanical modes have been demonstrated [8, 15], which include the cooling to the quantum ground state, the demonstration of strong optomechanical coupling, and conversion of cavity state to the mechanical mode. Therefore the optomechanical system becomes an ideal candidate for studying quantum behavior of macroscopic objects. Putting the mechanical oscillators into the quantum regime could allow us to explore quantum mechanics in entirely new ways, such as observation of the mechanical Schrödinger cat state, creation of entanglement between cavity field and mechanical motion, and control and manipulation of the quantum states for optomechanical system.

In this chapter we introduce the basics of optomechanical systems and lead the reader towards the subject of this dissertation: open system dynamics of optomechanical systems in the quantum limit.

1.1 Cavity Optomechanics

Standard cavity optomechanical system

To investigate the optomechanical interaction between the optical field and mechanical object, an optical cavity is usually employed to resonantly enhance the light-field intensity, which significantly increases the optomechanical effects as the circulating photon repeatedly interacts with the mechanics before it finally leaks out of the cavity. A generic cavity optomechanical system consists of a Fabry-Perot cavity with a movable end-mirror suspended by a mechanical spring and another fixed-mirror as the input-output port for the external laser driving. The motion of the mirror is well approximated by a damped harmonic oscillator interacting with the cavity field. This interaction is caused by the radiation pressure force between the scattered photons and the suspended mirror, where scattering of cavity photons modifies the motion of the mirror. As a result, it changed the length of cavity, which in turn affects the cavity resonance frequency and thus the intensity of the cavity field. The strength of the radiation pressure force is therefore coupled with the mechanical motion. Starting from the equation of motion of the cavity field and the mirror, one could identify the Hamiltonian structure of the system [16], and the resulting Hamiltonian reads,

$$H = \hbar\omega_c \hat{a}_c^\dagger \hat{a}_c + \frac{\hat{p}^2}{2m_{eff}} + \frac{1}{2} m_{eff}\omega_M^2 \hat{x}^2 - \hbar g_0 \hat{x} \hat{a}_c^\dagger \hat{a}_c + \hat{H}_{drive} + \hat{H}_\kappa + \hat{H}_\gamma \tag{1.1}$$

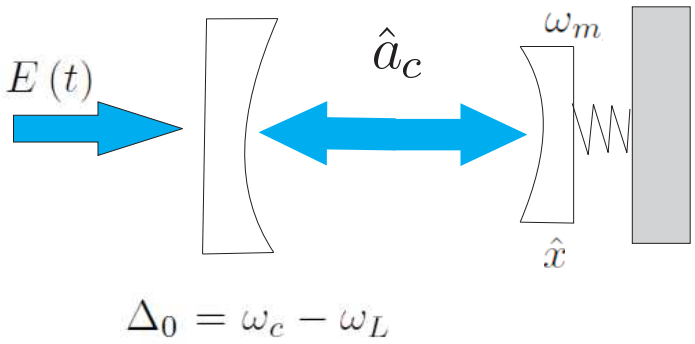

Figure 1.1: Plot of the schematic picture for a standard optomechanical system

with $H_{drive} = i\hbar E\left(e^{-i\omega_L}\hat{a}_c^\dagger - e^{i\omega_L}\hat{a}_c\right)$ and

$$H_\kappa = \int d\omega\hbar\omega\hat{c}^\dagger(\omega)\,\hat{c}(\omega) + i\int d\omega\kappa(\omega)\left(\hat{c}^\dagger(\omega)\,\hat{a}_c - \hat{c}(\omega)\,\hat{a}_c^\dagger\right), \tag{1.2}$$

$$H_\gamma = \frac{1}{2}\sum_j\left[(\hat{p}_j - k_j\hat{x})^2 + \omega_j^2\hat{q}_j^2\right]. \tag{1.3}$$

where $\hat{a}_c$ is the annihilation operator for the cavity field with frequency ω_c. If L is the equilibrium cavity length in the absence of the impinging field, the frequency of the cavity mode will be $\omega_c = n\pi c/L$ and the radiation pressure coupling constant is $g_0 = \omega_c/L$. For the typical materials and geometries one obtains $g_0/\omega_M \sim 10^{-4}$[17]. Operators $\hat{x}$ and $\hat{p}$ are the position and momentum operator of the mechanical oscillator. $\hat{H}_{drive}$ describes the laser driving of the cavity field at frequency ω_L and with E as the driving amplitude. Hamiltonian $\hat{H}_\kappa$ and $\hat{H}_\gamma$ describes the cavity decay and mechanical damping of the oscillator, respectively. The cavity environment is modeled as a bosonic thermal bath with $\hat{c}(\omega)$ as its bosonic operator with frequency ω. The mechanical environment is considered as a finite but very large number of N of harmonic oscillators with j indicating its j-th oscillator mode.

Experimental realizations

The above standard optomechanical model describes a very general optomechanical coupling, and it applies to any situation where the mechanical displacement modifies the resonant frequency of a cavity field. This model has been realized in various experimental systems. The most obvious way to realize optomechanical interactions in a cavity is to suspend one of the cavity mirrors via the micro- or nano-mechanical cantilevers. Due to the flexibility on mirror size and mass, this configuration provides the optomechanical control over a large range of system parameters. Typically, the

mechanical frequencies range from several kHz to tens of MHz, but their bare optomechanical coupling rates are in the order of Hz. Another realization uses optical micro-resonators, where light circulating inside a circular resonator couples the whispering gallery mode to the mechanical vibration mode of the structure. The small size of the micro-resonators allows ultrahigh quality factors with a large optomechanical coupling rate. Optical quality factors of 10^8 are routinely obtained with mechanical frequency at tens of MHz.

Photon crystal and on-chip waveguides provide a different implementation for optomechanical interaction. The periodic structures not only provide localized optical photonic modes but also can localize phononic modes with high mechanical quality, which result in an optomechanical coupling strength that is much larger than regular cavity optomechanical approaches. It provides the possibility to enter the regime of nonlinear photon-phonon interactions. The typical bare optomechanical coupling rates available in experiments are around MHz.

Besides realization of optomechanical system with optical fields, the generic optomechanical model can also be implemented in microwave resonators including LC circuits and the superconducting microwave resonators, where the motion of a mechanical element is capacitively coupled to the microwave field. This enables possibility of creating the hybrid system between an optomechanical system and superconducting qubits. Another approach to realize optomechanical coupling is to replace the solid mechanical element with the ultra-cold atomic gas, where the optical field couples to the collective motion of the atomic ensemble. With a large cavity-atom detuning, the frequency of the cavity field becomes dependent with atoms' positions which provides the optomechanical interactions. Due to the large number of atoms, a strong effective interaction exists between the collective motion and optical field, leading to a strong optomechanical coupling.

To compare the relevant optomechanical parameters for all these experimental implementations, a table summarizing current experimental parameters is provided in the Table 1.1. Although different systems work in different parameter regimes, all these systems share the same dynamical properties of the standard optomechanical model described in Eq.(1.1), details of which we will discuss in the following sections.

1.2 Optomechanical Phenomena

System dynamics and linearized model

Based on the Hamiltonian of the standard optomechanical system in Eq.(1.1), the Heisenberg equations for the mechanical displacement $\hat{x}$, momentum $\hat{p}$ and the cavity operator $\hat{a}_c$ can be written as the following, which are called the quantum Langevin

Experimental System	Reference	$\omega_M/2\pi$[Hz]	$\gamma_M/2\pi$[Hz]	$\kappa/2\pi$[Hz]	κ/ω_M	$g_0/2\pi$[Hz]	g_0/ω_M
Fabry-Perot	Kleckner et al., 2011 [18]	$9.7\cdot10^3$	$1.3\cdot10^{-2}$	$4.7\cdot10^5$	55	$2.2\cdot10^1$	$2.3\cdot10^{-3}$
	Groblacher et al., 2009 [19]	$9.5\cdot10^5$	$1.4\cdot10^2$	$2\cdot10^5$	0.22	3.9	$4.1\cdot10^{-6}$
	Arcizet et al., 2006 [20]	$8.14\cdot10^5$	81	$1\cdot10^6$	1.3	1.2	$1.5\cdot10^{-6}$
	Cuthbertson et al., 1996 [21]	318	$2.5\cdot10^{-6}$	275	0.9	$1.2\cdot10^{-3}$	$3.8\cdot10^{-6}$
Circular resonator	Verhagen et al., 2012 [22]	$7.8\cdot10^7$	$3.4\cdot10^3$	$7.1\cdot10^6$	0.09	$3.4\cdot10^3$	$4.4\cdot10^{-5}$
Photonic crystal	Chan et al., 2011 [23]	$3.9\cdot10^9$	$3.9\cdot10^4$	$5\cdot10^8$	0.13	$9\cdot10^5$	$2.3\cdot10^{-4}$
Microwave Resonator	Teufel et al., 2011 [8]	$1.1\cdot10^7$	32	$2\cdot10^5$	0.02	$2\cdot10^2$	$1.8\cdot10^{-5}$
Atomic gas	Murch et al., 2008 [6]	$4.2\cdot10^4$	$1\cdot10^3$	$6.6\cdot10^5$	15.7	$6\cdot10^5$	14

Table 1.1: Experimental parameters for a representative sampling of published cavity optomechanics experiments (arXiv: 1303.0733v1)

equations (QLEs),

$$\dot{\hat{x}}(t) = \frac{\hat{p}(t)}{m_{eff}}, \tag{1.4a}$$

$$\dot{\hat{p}}(t) = -m_{eff}\omega_M^2\hat{x}(t) - \gamma_M\hat{p}(t) + g_0\hat{a}_c^\dagger(t)\hat{a}_c(t) + \hat{\xi}(t), \tag{1.4b}$$

$$\dot{\hat{a}}_c(t) = -\left(i\Delta_0 + \kappa/2\right)\hat{a}_c(t) + ig_0\hat{a}_c(t)\hat{x}(t) + E + \sqrt{\kappa}\hat{a}_{in}(t), \tag{1.4c}$$

Here $\Delta_0 = \omega_c - \omega_L$ is the cavity detuning under the external driving field. Operator $\hat{\xi}(t)$ is the Brownian stochastic force with zero mean value and obeys the correlation function,

$$\langle\hat{\xi}\left(t\right)\hat{\xi}\left(t'\right)\rangle = \frac{\gamma_M}{\omega_M}\int\frac{d\omega}{2\pi}e^{-i\omega(t-t')}\omega\left[\coth\left(\frac{\hbar\omega}{2k_BT}\right)+1\right] \tag{1.5}$$

and $\hat{a}^{in}(t)$ is the vacuum radiation input noise. For simplicity of discussion, its correlation functions are assumed as

$$\langle\hat{a}_{in}\left(t\right)\hat{a}_{in}^\dagger\left(t'\right)\rangle = \left[N\left(\omega_c\right)+1\right]\delta\left(t-t'\right) \tag{1.6}$$

$$\langle\hat{a}_{in}^\dagger\left(t\right)\hat{a}_{in}\left(t'\right)\rangle = N\left(\omega_c\right)\delta\left(t-t'\right) \tag{1.7}$$

with $N\left(\omega_c\right) = \left[\exp\left(\hbar\omega_c/k_BT\right)-1\right]^{-1}$ as the averaged occupation number for the cavity thermal bath. At optical frequency $\hbar\omega_c/k_BT \gg 1$ so that $N\left(\omega_c\right) \simeq 0$. The above Langevin equations are nonlinear in the sense that the mechanical momentum operator $\hat{p}$ is coupled with cavity field operator in the quadratic form of $\hat{a}_c(t)^\dagger\hat{a}_c(t)$, and it is therefore impossible to obtain a general solution to such a nonlinear quantum Langeivn equations. However, if the fluctuations of the field operator δa_c and the fluctuations of mirror quadratures δx and δp are small compared with the respective mean values, one can linearize the above equations around the mean values. This is equivalent to assume $\hat{x}(t) = \bar{x}(t) + \delta\hat{x}(t)$, $\hat{p}(t) = \bar{p}(t) + \delta\hat{p}(t)$, $\hat{a}_c(t) = \alpha_s(t) + \delta\hat{a}_c(t)$, with the mean values follows the classical dynamics and neglects the high order terms

of the fluctuations operators, the linearized equations are,

$$\frac{d}{dt}\delta\hat{x}(t) = \frac{\delta\hat{p}(t)}{m_{eff}}, \tag{1.8a}$$

$$\frac{d}{dt}\delta\hat{p}(t) = -m_{eff}\omega_M^2\delta\hat{x}(t) - \gamma_M\delta\hat{p}(t) + g_0\left(\alpha_s^*\delta\hat{a}_c(t) + \alpha_s\delta\hat{a}_c^\dagger(t)\right) + \hat{\xi}(t), \tag{1.8b}$$

$$\frac{d}{dt}\delta\hat{a}_c(t) = -\left(i\Delta + \kappa/2\right)\delta\hat{a}_c(t) + ig_0\alpha_s\delta\hat{x}(t) + \sqrt{\kappa}\hat{a}_{in}(t), \tag{1.8c}$$

where $\Delta = \Delta_0 - g_0^2|\alpha_s|^2/m_{eff}\omega_M^2$ and the mean values are chosen as the steady state solutions, $\bar{x} = g_0|\alpha_s|^2/m_{eff}\omega_M^2$, $\bar{p} = 0$ and $\alpha_s = (\kappa - i\Delta)^{-1}E$. With the system under the strong driving, these linearized equations can be used to fully describe optomechanical phenomena, such as optomechanical cooling, optical string effects, quantum entanglement generation, optomechanical induced transparency (OMIT) and squeezing. Note that the above semi-classical linearization procedure can be equivalently derived quantum mechanically with a much more strict form by working with a displacement picture, details of which is provided in Chapter 2.

Classical optomechanical effects

Much of the basic optomechanical physics can be fully understood from the pure classical equations. To do so, one need to replace all quantum operators ($\delta\hat{x}$ and $\delta\hat{a}_c$) of Eq.(2.21) with their average values (δx and $\delta\alpha$) and drop all quantum noise operators. The resulting classical equations of motion read,

$$\frac{d}{dt}\delta\alpha = -\left(i\Delta + \kappa/2\right)\delta\alpha + ig_0\alpha_s\delta x, \tag{1.9}$$

$$m_{eff}\frac{d^2}{dt^2}\delta x = -m_{eff}\omega_M^2\delta x - m_{eff}\gamma_M\dot{\delta}x + g_0\left(\alpha_s^*\delta\alpha + \alpha_s\delta\alpha^*\right) + F_{ext}, \tag{1.10}$$

An external force $F_{ext}(t)$ was added here to investigate the linear response of the standard optomechanical system. This equation is best solved in the frequency domain,

$$-i\omega\delta\alpha(\omega) = -\left(i\Delta + \kappa/2\right)\delta\alpha(\omega) + ig_0\alpha_s\delta x(\omega), \tag{1.11}$$

$$\begin{aligned} -m_{eff}\omega^2\delta x(\omega) &= -m_{eff}\omega_M^2\delta x(\omega) + im_{eff}\gamma_M\delta x(\omega) + F_{ext}(\omega) \\ &+ g_0\left(\alpha_s^*\delta\alpha(\omega) + \alpha_s(\delta\alpha(-\omega))^*\right), \end{aligned} \tag{1.12}$$

Here, $\delta a(\omega) = \int_{-\infty}^{\infty} dt e^{i\omega t}\hat{a}_c(t)$ is the Fourier transformation of $\hat{a}_c$. The corresponding solutions of the above equations read

$$\delta\alpha(\omega) = \frac{g_0\alpha_s}{(\Delta + \omega) - i\kappa/2}\delta x(\omega) \tag{1.13}$$

$$\delta x(\omega) = \chi(\omega)F_{ext}(\omega) \tag{1.14}$$

where $\chi(\omega)$ is the susceptibility of the mechanical oscillator providing the linear responds of the mechanical oscillator to external force $F_{ext}(t)$. Without radiation pressure force ($g_0 = 0$), this susceptibility is given by

$$\chi_0^{-1}(\omega) = m_{eff}(\omega_M^2 - \omega^2) - im_{eff}\gamma_M\omega \tag{1.15}$$

and under radiation pressure force, the susceptibility is modified as following,

$$\chi^{-1}(\omega) = m_{eff}(\omega_M^2 - \omega^2) - im_{eff}\gamma_M\omega - \Sigma(\omega) \tag{1.16}$$

with

$$\Sigma(\omega) = 2m_{eff}\omega_M g^2 \left(\frac{1}{(\Delta - \omega) - i\kappa/2} + \frac{1}{(\omega + \Delta) + i\kappa/2}\right) \tag{1.17}$$

where the relation $g = x_{ZP}g_0|\alpha_s|$ is employed in the above expression and $x_{ZP} = (2m_{eff}\omega_M)^{-1/2}$ is the mechanical zero point fluctuation. $\Sigma(\omega)$ describes the modification of the mechanical properties due to the radiation pressure interaction with the cavity field. Its real part modifies the mechanical frequency causing the optical spring effects for the optomechanical system. The modification of $\Sigma(\omega)$ depends on the detuning of the cavity: with spring-softened mechanical oscillator at red-detuned laser driving ($\Delta > 0$) and spring-hardened for a blue-detuned laser driving ($\Delta < 0$)[24, 25]. The imaginary part of $\Sigma(\omega)$ changes the mechanical damping rate γ_M leading to the mechanical cooling and amplification. However, with a strong external driving field, the standard optomechanical system could enter into an unstable parameter regime where the system shows nonlinear dynamics. We study such a situation in the next chapter, where the stability condition of the standard optomechanical model is discussed in details.

Quantum effects in optomechanical dynamics

Many quantum effects in the standard optomechanical system could also be understood through the above linearized model. To better formalize the theory, we introduce the phonon creation ($\hat{b}_M^\dagger$) and annihilation ($\hat{b}_M$) operators with

$$\hat{x} = x_{ZP}(\hat{b}_M + \hat{b}_M^\dagger), \quad \hat{p} = -im_{eff}\omega_M x_{ZP}(\hat{b}_M - \hat{b}_M^\dagger) \tag{1.18}$$

where $x_{ZP} = \sqrt{\hbar/2m_{eff}\omega_M}$. The linearized equations of Eq.(2.21) now have the following form,

$$\frac{d}{dt}\delta\hat{a}_c(t) = -(i\Delta + \kappa/2)\,\delta\hat{a}_c(t) + ig\left(\delta\hat{b}_M(t) + \delta\hat{b}_M(t)^\dagger\right) + \sqrt{\kappa}\hat{a}_{in}(t), \tag{1.19a}$$

$$\frac{d}{dt}\delta\hat{b}_M(t) = \left(-i\omega_M - \frac{\gamma_M}{2}\right)\delta\hat{b}_M(t) + ig\left(\delta\hat{a}_c(t) + \delta\hat{a}_c^\dagger(t)\right) + \sqrt{\gamma_M}\hat{b}_{in}(t), \tag{1.19b}$$

where $\Delta = \Delta_0 - g_0^2|\alpha_s|^2/m_{eff}\omega_M^2$ and $\Delta_0 = \omega_c - \omega_L$. The effective optomechanical coupling strength is

$$g = x_{ZP} g_0 |\alpha_s| \tag{1.20}$$

The corresponding linearized Hamiltonian has the form of

$$H_s = \hbar\omega_c \delta\hat{a}_c^\dagger \delta\hat{a}_c + \hbar\omega_M \delta\hat{b}_M^\dagger \delta\hat{b}_M + H_{int} \tag{1.21}$$

where $H_{int} = -\hbar g \left(\delta\hat{a}_c^\dagger + \delta\hat{a}_c\right)\left(\delta\hat{b}_M^\dagger + \delta\hat{b}_M\right)$. It is obvious that an effective linear optomechanical interaction is formed between the cavity mode and mechanical mode. Depending on the cavity detuning, three different regimes can be distinguished with respect to this linear interaction. In the red-detuned regime of $\Delta = \omega_M$ and under the rotating-wave approximation (RWA), the interaction H_{int} could be simplified as:

$$H_{int} = -\hbar\left(\delta\hat{a}_c^\dagger \delta\hat{b}_M + \delta\hat{a}_c \delta\hat{b}_M^\dagger\right) \tag{1.22}$$

It describes the exchange of quanta between the cavity mode and the mechanical mode, called the beam-splitter interaction in Quantum Optics. This interaction can be used to implement the mechanical cooling and quantum state transfer between the cavity field and mechanical oscillator [26, 27]. In the blue-detuned regime $\Delta = -\omega_M$, the corresponding interaction under RWA is,

$$H_{int} = -\hbar\left(\delta\hat{a}_c^\dagger \delta\hat{b}_M^\dagger + \delta\hat{a}_c \delta\hat{b}_M\right) \tag{1.23}$$

This effective interaction causes the two modes squeezing and generates the optomechanical entanglement. It is also responsible for the optomechanical parametric amplification [28]. At the resonant detune of $\Delta = 0$, the effective interaction takes the form of

$$H_{int} = -\hbar g \left(\delta\hat{a}_c^\dagger + \delta\hat{a}_c\right)\left(\delta\hat{b}_M^\dagger + \delta\hat{b}_M\right) \tag{1.24}$$

which describes the process of optomechanical displacement measurement and QND detection of the optical amplitude quadrature.

Cavity optomechanical entanglement

One important property in quantum optomechanics is the generation of the entangled cavity-mechanical states, which is basis for many quantum information processes. In order to create reliable entangled states, the red-detuned cavity driving ($\Delta < 0$) is usually applied. In this regime, the system dynamics are well characterized by the linearized optomechanical model and its steady-state entanglement is robust with environment noises. To better understand this topic, We provide a brief introduction to the generation of steady-state optomechanical entanglements in the following two sections.

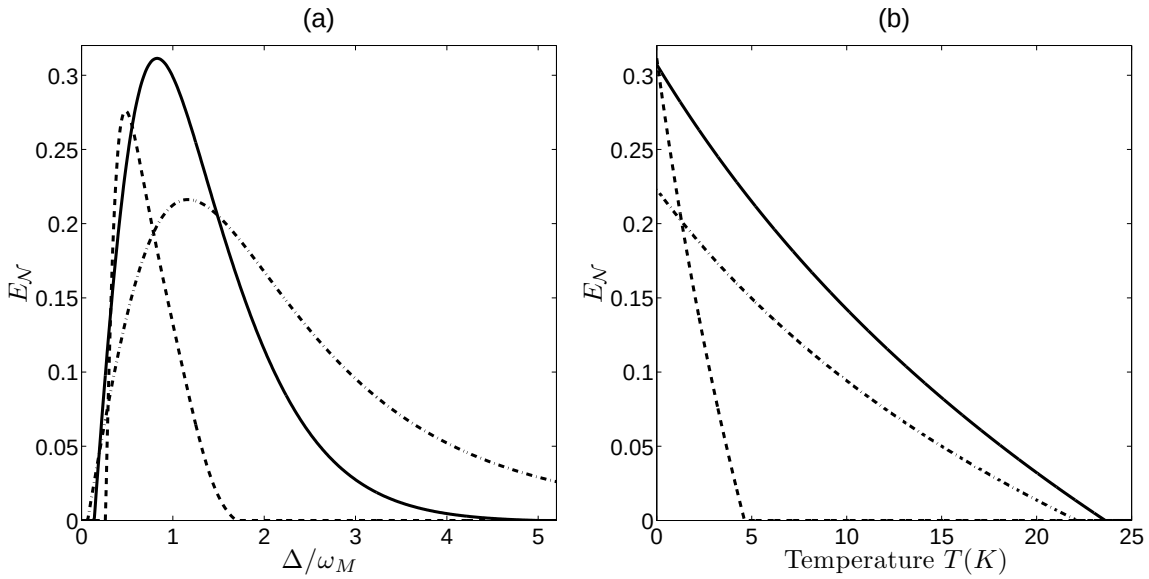

Figure 1.2: (a) Plot of logarithmic negativity $E_{\mathcal{N}}$ as a function of the normalized detuning Δ/ω_M. (b) Plot of logarithmic negativity $E_{\mathcal{N}}$ as a function of mechanical temperature and the detunes are chosen at the maximal entanglement in (a). Parameters are chosen from Ref.[29] as optical cavity length $L = 1mm$, driven by a laser with wavelength 810 nm and power $P = 50\ mW$, mechanical frequency $\omega_M/2\pi = 10\ MHz$ and $\gamma_M/2\pi = 100\ Hz$.

Due to the Gaussian property of the linearized model, the optomechanical dynamics are completely characterized by the covariance matrix,

$$V_{i,j} = \frac{\hat{\xi}_i\hat{\xi}_j + \hat{\xi}_j\hat{\xi}_i}{2} \tag{1.25}$$

with $\hat{\xi} = [\hat{X}_M, \hat{Y}_M, \hat{X}_c, \hat{Y}_c]^T$. Here, $\hat{X}_M = \left(\hat{b}_M + \hat{b}_M^\dagger\right)/\sqrt{2}$ and $\hat{P}_M = -i\left(\hat{b}_M - \hat{b}_M^\dagger\right)/\sqrt{2}$ denote the mechanical amplitude and phase quadratures, while $\hat{X}_c = \left(\hat{a}_c + \hat{a}_c^\dagger\right)/\sqrt{2}$ and $\hat{P}_c = -i\left(\hat{a}_c - \hat{a}_c^\dagger\right)/\sqrt{2}$ denote the cavity amplitude and phase quadratures, respectively. The cavity-mechanical entanglement can be measured by the logarithmic negativity $E_{\mathcal{N}}$ [30],

$$E_{\mathcal{N}} = max[0, -ln2\eta^-] \tag{1.26}$$

Here $\eta^- = 2^{-\frac{1}{2}}[\Sigma(V) - [\Sigma(V)^2 - 4detV]^{\frac{1}{2}}]^{\frac{1}{2}}$ and $\Sigma(V) \equiv detV_M + detV_c - 2detV_{cm}$, with V_c, V_M and V_{cm} as sub-blocks of the covariance matrix,

$$V = \begin{pmatrix} V_M & V_{cm} \\ V_{cm}^T & V_c \end{pmatrix} \tag{1.27}$$

According to the linearized equations in Eq.(1.19), the equation of motion for the covariance matrix is

$$\frac{dV\left(t\right)}{dt}=AV\left(t\right)+V\left(t\right)A^{T}+D \tag{1.28}$$

with $D=Diag(0,\gamma_{M}\left(n_{th}+1/2\right),\kappa/2,\kappa/2)$ and matrix A is the coefficient matrix in Eq.(1.19) with its form given by

$$A=\begin{pmatrix}0 & \omega_{M} & 0 & 0\\ -\omega_{M} & -\gamma_{M}/2 & g & 0\\ 0 & 0 & -\kappa/2 & \Delta\\ g & 0 & -\Delta & -\kappa/2\end{pmatrix} \tag{1.29}$$

The steady-state covariance matrix can be attained from the solution of the following linear equation

$$AV\left(t\right)+V\left(t\right)A^{T}=-D \tag{1.30}$$

which is then applied with Eq.(1.26) to obtain the steady-state optomechanical entanglement. In the red-detuned regime, the entanglement between mechanical and optical mode was first analyzed with the above method in [29, 31]. It was shown that the steady-state entanglement is maximal at the detuning around $\Delta\approx\omega_{M}$, shown in Fig.4.2, where the solid line corresponding to a mass $m=5\ ng$ and finesse $\mathcal{F}=1.07\times10^{4}$. The dashed line refers to $m=50\ ng$ and finesse $\mathcal{F}=3.4\times10^{4}$. The dashed dot line refers to fixed $g/2\pi=16.803\ MHz$ and $\kappa/2\pi=16.822\ MHz$. Fig.4.2(b) shows that the steady state entanglement are also robust with the mechanical temperature. However, such a steady-state entanglement is strongly limited by its stability condition. In oder to obtain highly entangled states, strong cavity drivings are required, but too large driving could make the optomechanical system unstable and break the linearization model. Therefore the obtained entanglement with the steady-state generation scheme is always limited by its driving power. Another approach to overcome this restriction is to work with blue-detuned driving $\Delta<0$ and replace the continuous laser driving with optical pulse, which releases the stability condition, and larger entangled states are created as a result. However, such approach also suffers from the same issue of linearization in the blue-detuned regime and we will come back to this topic in the chapter 2.

Time modulated optomechanics

It was later proposed in [33, 32, 34] that the scheme of steady-state entanglement could be enhanced by a time periodic driving scheme with the following Hamiltonian,

$$H=\hbar\omega_{c}\hat{a}_{c}^{\dagger}\hat{a}_{c}+\frac{\hat{p}^{2}}{2m_{eff}}+\frac{1}{2}m_{eff}\omega_{M}^{2}\hat{x}^{2}-\hbar g_{0}\hat{x}\hat{a}_{c}^{\dagger}\hat{a}_{c}+i\hbar[E(t)e^{-i\omega_{L}t}\hat{a}_{c}^{\dagger}-E^{*}(t)e^{i\omega_{L}t}\hat{a}_{c}] \tag{1.31}$$

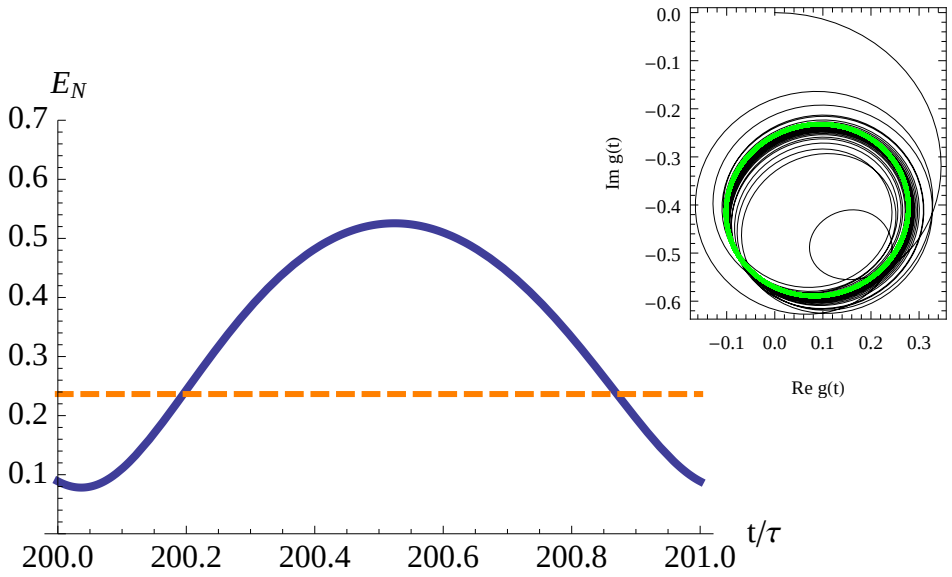

Figure 1.3: Plot of the logarithmic negativity with time dependent driving as a function of time. The solid line refers to a modulated driving ($\Omega = 1.4\omega_M$) while the dotted line corresponds to a non-modulated driving ($\Omega = 0$). The chosen parameters in units of ω_M are: $\kappa = 0.2$, $\gamma_M = 10^{-6}$, $\Delta = 1$, $n_m = 2 \times 10^3$, $n_a = 0$, $g_0 = 4 \times 10^{-6}$, $E_0 = 7 \times 10^4$, $E_\Omega = 2.5 \times 10^4$. The inset shows the trajectory of the effective coupling $\tilde{g}(t) = x_{ZPF} g_0 |\alpha_s(t)|$ in the complex plane due to the time evolution of the optical amplitude $\alpha_s(t)$. The phase space orbit (black line) is numerically simulated from the classical average equations, while the limit cycle (green line) is an analytical approximation (see [32] for more details).

where the driving amplitude $E(t)$ is periodic with $E(t) = E(t + \tau)$. Because of this periodicity, the steady-state solutions become periodic, which causes the linear optomechanical coupling g in Eq.(1.20) to be time dependent,

$$g(t) = x_{ZP} g_0 |\alpha_s(t)| \tag{1.32}$$

In general the driving could be expressed as $E(t) = \sum_{n=0}^{\infty} E_N e^{in\Omega t}$ with $\Omega = 1/\tau$ and the high order modulations of E_N are usually quite small so that one could truncate $E(t)$ as $E = E_0 + E_1 e^{i\Omega t}$. As a result, the above $g(t)$ could be simplified as $g(t) = g_0 + g_\Omega e^{i\Omega t}$, and the corresponding linearized Hamiltonian reads,

$$H_s = \hbar \Delta_c \delta\hat{a}_c^\dagger \delta\hat{a}_c + \hbar\omega_M \delta\hat{b}_M^\dagger \delta\hat{b}_M + H_{int}(t) \tag{1.33}$$

where

$$H_{int}(t) = -\hbar \left(g_0 + g_\Omega e^{i\Omega t}\right) \left(\delta\hat{a}_c^\dagger + \delta\hat{a}_c\right) \left(\delta\hat{b}_M^\dagger + \delta\hat{b}_M\right) \tag{1.34}$$

Previously, with a time independent red-detuned driving, the dominant interaction in H_{int} is dominated by the beam-splitter interaction of Eq.(1.22), which could not be used to create quantum entanglement. However, with a time dependent driving, an effective two-mode squeezing interaction is added in H_{int} as the terms of $g_\Omega e^{i\Omega t}$, which can be used to enhance the optomechanical entanglement. Ref.[32] has shown that, with appropriate choice of rotating frame and some RWA, the Eq.(1.33) could be written as

$$H_s \approx -\hbar g_\Omega e^{i(\Omega-2\omega_M)t}\left(e^{ig_0 t}\hat{c}_+\hat{c}_+ + e^{-ig_0 t}\hat{c}_-\hat{c}_-\right)/2 + h.c. \tag{1.35}$$

with $\hat{c}_\pm = \left(\hat{a}_c \pm \hat{b}_M\right)/\sqrt{2}$. If the modulation frequency were chosen as $\Omega = 2\omega_M - g_0$, the corresponding effective interaction will be

$$H_s \approx -\hbar g_\Omega \left(\hat{c}_\pm\hat{c}_\pm + \hat{c}_\mp^\dagger\hat{c}_\mp^\dagger\right)/2 \tag{1.36}$$

which can be used to cause the squeezing of the hybrid modes $\hat{c}_+$ or $\hat{c}_-$, implying that the time dependent driving really creates an effective interaction to generate entangled optomechanical states. One example from the [32] is provided in Fig.4.3.

Optomechanical induced transparency(OMIT)

Another interesting quantum effect in optomechanical systems is OMIT, analogous to the electromagnetic induced transparency (EIT) in atomic systems. OMIT can be explained as following: If there is only one laser driving (called the probe field) applied resonantly with the cavity, the transmission spectrum of the outgoing probe field will have the standard Lorentz form with a peak at the resonant frequency. Meanwhile, if the cavity field is also driven from its sideband by another laser driving (called the coupling field), the scattered photons of it are at resonant with the cavity but possess an additional $\pi/2$ phase compared with the incoming probe field. Therefore, the probe field is out of the phase with the scattered photons of the coupling field, and they will interfere destructively, leading to a dip in the transmission spectrum of the outgoing probe field at the resonant frequency.

Quantitatively, the Hamiltonian describing the standard optomechanical system with one driving field and one probe field reads

$$H = \hbar\omega_c\hat{a}_c^\dagger\hat{a}_c + \frac{\hat{p}^2}{2m_{eff}} + \frac{1}{2}m_{eff}\omega_M^2\hat{x}^2 - \hbar g_0\hat{x}\hat{a}_c^\dagger\hat{a}_c + \hat{H}_{drive}(t) + \hat{H}_\kappa + \hat{H}_\gamma \tag{1.37}$$

where the driving field

$$\hat{H}_{drive}(t) = i\hbar(E(t)\hat{a}_c^\dagger + E^*(t)\hat{a}_c)$$

has two contributions $E(t) = \varepsilon_c e^{-i\omega_L t} + \varepsilon_p e^{-i\omega_p t}$, with ε_c (ε_p) as the amplitude of the coupling field (the probe field). In a frame rotating at the frequency of the coupling field ω_L, we obtain the equations of motion as:

$$\begin{aligned}
\dot{\hat{x}}(t) &= \hat{p}(t)/m_{eff}, && \text{(1.38a)}\\
\dot{\hat{p}}(t) &= -m_{eff}\omega_M^2\hat{x}(t) - \gamma_M\hat{p}(t) + g_0\hat{a}_c^\dagger(t)\hat{a}_c(t) + \hat{\xi}(t), && \text{(1.38b)}\\
\dot{\hat{a}}_c(t) &= -\left(i\Delta_0 + \kappa/2\right)\hat{a}_c(t) + ig_0\hat{a}_c(t)\hat{x}(t) + \varepsilon_c + \varepsilon_p e^{-i\Omega t} + \sqrt{\kappa}\hat{a}_{in}(t), && \text{(1.38c)}
\end{aligned}$$

To linearize the above equations around the steady-state solutions without the probe field ($\varepsilon_p = 0$), one has to split the quantum operators into its average value and fluctuation operator: $\hat{x} = \bar{x} + \delta\hat{x}$, $\hat{p} = \bar{p} + \delta\hat{p}$ and $\hat{a}_c = \alpha_s + \delta\hat{a}_c$. The mean values of the mechanical amplitude are chosen as $\bar{x} = g_0|\alpha_s|^2/m_{eff}\omega_M^2$ and $\bar{p} = 0$. The average cavity amplitude is $\alpha_s = \varepsilon_c\left(\kappa - i\Delta\right)^{-1}$ and it is chosen as real. The linearized equations read,

$$\begin{aligned}
\frac{d^2}{dt^2}\delta x(t) + \gamma_M\frac{d}{dt}\delta x(t) + \omega_M^2\delta x(t) &= \frac{g_0\alpha_s}{m_{eff}}\left(\delta a_c(t) + \delta a_c^*(t)\right), && \text{(1.39a)}\\
\frac{d}{dt}\delta a_c(t) &= -\left(i\Delta + \kappa/2\right)\delta a_c(t) + ig_0\alpha_s\delta x(t) + \varepsilon_p e^{-i\Omega t}, && \text{(1.39b)}
\end{aligned}$$

Because the probe field is at the frequency of $\Omega = \omega_p - \omega_c$, the general ansatz for the above equations are,

$$\begin{aligned}
\delta a_c(t) &= A_- e^{-i\Omega t} + A_+ e^{i\Omega t} && \text{(1.40a)}\\
\delta x(t) &= X e^{-i\Omega t} + X^* e^{i\Omega t} && \text{(1.40b)}
\end{aligned}$$

When substituting the above relations back into the linearized equations, this yields six different equations ($A_\pm$ are complex amplitude). Because we are only interested in the output field at probe frequency ω_p, only equations of A_- are important:

$$\begin{aligned}
\left(i\left(\Delta - \Omega\right) + \kappa/2\right)A_- - ig_0\alpha_s X &= \varepsilon_p, && \text{(1.41)}\\
\left(-i\left(\Delta + \Omega\right) + \kappa/2\right)A_+^* + ig_0\alpha_s X &= 0, && \text{(1.42)}\\
\left(\omega_M^2 - \Omega^2 - i\gamma_M\Omega\right)X &= \frac{g_0\alpha_s}{m_{eff}}(A_- + A_+^*), && \text{(1.43)}
\end{aligned}$$

The solution for A_- is, therefore,

$$A_- = \frac{1 + if(\Omega)}{i\left(\Delta - \Omega\right) + \kappa/2 - 2\Delta f(\Omega)}\varepsilon_p \qquad \text{(1.44)}$$

with

$$f(\Omega) = \frac{g_0^2\alpha_s^2\chi(\Omega)}{-i\left(\Delta + \Omega\right) + \kappa/2} \qquad \text{(1.45)}$$

and the mechanical susceptibility with

$$\chi(\Omega) = \frac{1}{m_{eff}\left(\omega_M^2 - \Omega^2 - i\Omega\gamma_M\right)} \tag{1.46}$$

Applying the input-output relation, one obtain

$$\hat{a}_{out}(t) = \hat{a}_{in}(t) - \sqrt{\kappa}\hat{a}_c(t) \tag{1.47}$$

the output field amplitude at frequency ω_p is then given by:

$$A_p = \varepsilon_p - \sqrt{\kappa}A_- \tag{1.48}$$

and then the transmission of the probe beam is then given by

$$t_p = \frac{A_p}{\varepsilon_p} = 1 - \frac{\sqrt{\kappa}\left(1 + if(\Omega)\right)}{i\left(\Delta - \Omega\right) + \kappa/2 - 2\Delta f(\Omega)} \tag{1.49}$$

While the amplitude of the probe beam without coupling beam is just the lorentz form and the transmission is,

$$t_p(\alpha_s = 0) = \frac{A_p(\alpha_s = 0)}{\varepsilon_p} = 1 - \frac{\sqrt{\kappa}}{i\left(\omega_c - \omega_p\right) + \kappa/2} \tag{1.50}$$

The OMIT was first predicted theoretically [35] for the standard optomechanical system with the linearized model and then observed experimentally by [36, 37]. More recently, there were three groups theoretically proposing observation of the OMIT created by the nonlinear optomechanical interactions [38, 39, 40], where the OMIT is caused by the destructive inference between the second sideband driving laser and the probe beam. This new type of OMIT could only be understood by the nonlinear optomechanical coupling. The perturbation method developed in chapter 3 provides another alternative theoretical frame to understand this nonlinear OMIT phenomena.

1.3 Nonlinear Quantum Optomechanical System

Quantum optomechanical effects beyond the linearized model have been studied recently, demonstrating that the standard optomechanical system possesses enormously rich nonlinear phenomena, such as multistabilities with both static and dynamical[41, 42], photon blockade [43, 44], and non-Gaussian states [45]. To observe these nonlinear effects, the mechanical mode needs to be strongly coupled with cavity field. Consequently, multiple optical sidebands, as well as multi-photon transitions, are involved for the standard optomechanical system in this strong coupling regime, showing interesting photon-photon, phonon-phonon or photon-phonon correlations.

However, due to its nonlinearity and complexity, the theoretical tools to deal with such a system are limited, especially when the optomechanical open system dynamics with the external environments are included. Perturbations based on assumptions of weak nonlinear coupling or weak driving are usually employed to deal with the optomechanical open system dynamics. In this dissertation, we investigate the various roles of the nonlinear optomechanical interaction on the open system dynamics of the standard optomechanical system for different parameter regimes and focus on developing new theoretical tools for investigating the dynamical behaviors of the standard optomechanical system.

In Chapter 2, we deal with the validity of the linearized optomechanical model in the unstable blue-detuned regime. We propose a linearization time window for this regime and prove that in this time window, the linearized model could be utilized to fully describe the optomechanical dynamics even if the system is unstable. Such a linearization time window is useful for entanglement generation in the blue-detuned regime, where the system tends to be unstable while the dominated linearized optomechanical interaction is preferred for creation of large bipartite entanglement between the cavity field and the mechanical oscillator. Consequently, the linearization time window imposes new limits on available optomechanical entanglement obtained in this regime.

Going beyond the linearization time window, the optomechanical system behaves nonlinearly, and the linearized model fails to describe the optomechanical dynamics. In Chapter 3, a new perturbation method in the Heisenberg picture was developed to deal with a weak nonlinear interaction, where we treated the nonlinear interaction as perturbations to the linearized optomechanical model. The new method shows that, under the first order perturbation, both the optical amplitude and the mechanical quadratures are influenced by this weak nonlinear interaction. While the cavity photon numbers are modified only by another higher order perturbation, which makes the analytical analyze really involved. In order to overcome these weaknesses, a master equation approach in the next chapter was developed to deal with nonlinear interactions, which is much easier to apply numerically.

Chapter 4 is about the strongly coupled optomechanical systems, where the nonlinear effects are dominate and could not be treated as perturbations. In order to characterize the dynamics in this regime, a new master equation based on the dressed-state basis was developed. In chapter 4 we shows that the transient dynamics of the optomechanical system are significantly influenced by the strong coupling and, as a result, the the cavity decay is coupled with the mechanical damping. The traditional treatment of the standard master equation with independent decoherence model may not provide a correct insight for the optomechanical dynamics in this regime. We provide detailed comparison of this dressed-state master equation with that of the standard master equation.

Chapter 2

Linearized Optomechanical Interaction

For the typical materials and dimensions, the optomechanical coupling g_0 in most experimental optomechanical systems usually has a very small value ($g_0/\omega_M \sim 10^{-4}$), which makes the optomechanical effect difficult to observe. One way to enhance the optomechanical interaction is to apply a strong driving field to the optical cavity which leads to an effective linear optomechanical interaction. Such a field-enhanced linear optomechanical interaction has been proved to be responsible for the cooling of the mechanical motion [46, 47, 48], as well as, the creation of various quantum correlations between the cavity light field and mechanical oscillator [29, 31]. As a result, most studies in the weak coupling regime considered a pure linearized interaction while neglecting the nonlinear part of the optomechanical interaction. However, this linearization procedure is not always guaranteed in the weak coupling regime: when the weak coupled optomechanical system becomes unstable, the influence of the nonlinear interaction on optomechanical dynamics can grow exponentially and finally destroy the linearized model.

In this chapter, we propose a practical approach to investigate the validity of the linearization procedure for the standard optomechanical system working in the unstable parameter regime. As we will show, a pulsed laser driving ensures a linearization time window, in which the optomechanical dynamics can be fully characterized by the linearized model. We provide the analytical form of the linearization time window for blue-detuned optomechanical systems and concentrate on its applications for entanglement generation in the unstable parameter regime. Our results show that the optimization of optomechanical entanglement for the pulsed scheme relies sensitively on the validity of the linearized optomechanical model that the pulse duration should be strictly limited by the linearization time window. Otherwise, the breakdown of the linearized optomechanical model often leads to unrealistic optimized

cavity-mechanical entanglement, which finally invalidates the pulsed driving scheme for the optomechanical system in the unstable parameter regime.

Another interesting subject of the linearized optomechanical system is to improve the steady-state optomechanical entanglement utilizing a time periodic driving. This topic has been studied recently for the standard optomechanical system of one cavity mode interacting with one mechanical mode [33, 32, 34], showing that with a suitable time modulation on the amplitude of the cavity driving field or on the mechanical frequency, it is possible to significantly improve the bipartite entanglement between the cavity field and the mechanical oscillator. In the second part of this chapter, we extend this idea one step further and apply it to investigate the influence of the time periodic driving scheme for a three-mode optomechanical system, where two cavity modes interact with one mechanical mode. Our results show that, with a slightly modified scheme, the time modulation technique can be implemented to enhance the obtained entanglement for the three-mode optomechanical system. By controlling the modulation strength, it is possible to increase or decrease the entanglement between two cavity-cavity modes, or between each cavity mode and the mechanical mode, providing an additional control on the entanglement dynamics for the three-mode optomechanical system. We also study the influence of the time periodic driving on the global tripartite entanglement existing in this model.

2.1 Blue-detuned Optomechanics

Introduction

Optomechanical interaction via radiation pressure force is an effective way to generate the coupling between the macroscopic mechanical oscillator and cavity optical fields. With its ability to measure the mechanical position with high accuracy, the optomechanical system can be applied in various fields of physics, such as ultrahigh precision measurements [12] and gravitational wave detection [13]. Furthermore, the optomechanical coupling could be used for cooling mechanical oscillators down to the quantum ground state, allowing us to explore quantum mechanics in entirely new ways [49, 14]. The quantum behavior of the mechanical oscillator has been experimentally observed [15, 8], indicating the realization of the quantum mechanical motion. One important characteristic of the quantum behaviors of the mechanical oscillator are the entangled optomechanical states, which provide useful resources for many quantum information processes, such as continuous-variable quantum teleportation [50], quantum state transfer [51] and entanglement swapping [52]. It could even be possible to build quantum-communication networks using optomechanical systems[52, 53].

While optomechanical entanglement shows promising applications in quantum information science, generating a high enough, reliable entanglement for an optomechanical system remains challenging. Steady-state optomechanical entanglement, which is robust against thermal noise and cavity decay, has been broadly investigated [29, 31]. However, the stability requirement of steady-state entanglement strongly restricts the strength of the effective radiation-pressure coupling, which, in turn, limits its ability to generate high-entangled optomechanical states [46]. Another approach to generate optomechanical entangled states is based on applying a pulsed driving to the cavity field [54]. This scheme does not rely on the existence of a stable steady state and could be used to generate high optomechanical entangled states in an unstable regime. The problem with the preceding approach is that its linearization procedure still depends on an assumption that all quantum operators must have small fluctuations which is not always guaranteed in the unstable optomechanical system. In order to obtain a workable pulsed driving scheme for the unstable optomechanical system, the fluctuation effects in the unstable parameter regime must be studied and taken into consideration for the generation of optomechanical entanglement.

In this section, we aim to study the entanglement generation in an unstable regime, including the effect of fluctuations and the optimization of the parameters for high entanglement outcome. We will show a pulsed driven scheme ensures a time window, in which entanglement is optimized and can be fully characterized with the linearized optomechanical model.

Optomechanical system

We consider a driven Fabry-Perot cavity with one moving end mirror. The cavity mode is coupled to the mechanical motion of the mirror via radiation pressure interaction. The Hamiltonian of the system reads [16]

$$H_s = \hbar\omega_c \hat{a}_c^\dagger \hat{a}_c + \frac{\hat{p}^2}{2m_{eff}} + \frac{1}{2} m_{eff}\omega_M^2 \hat{x}^2 - \hbar G_0 \hat{x} \hat{a}_c^\dagger \hat{a}_c + i\hbar E \left(\hat{a}_c^\dagger e^{-i\omega_L t} - \hat{a}_c e^{i\omega_L t}\right)$$

Here $\hat{a}_c$ is the annihilation operator for the cavity mode, $\hat{x}$ and $\hat{p}$ are mirror quadrature operators. If L is the equilibrium cavity length in the absence of the driving field, the frequency of the cavity mode is $\omega_c = n\pi c/L$, and the radiation pressure coupling constant is $G_0 = \omega_c/L$. The external driving laser has a frequency of ω_L and amplitude of E.

By including the cavity decay and mechanical damping, in the rotating frame at driving frequency ω_L, the equations of motion for the optomechanical system are fully

characterized by the following nonlinear Quantum Langevin Equations (QLEs),

$$\frac{d}{dt}\hat{b}_M(t) = -i\omega_M\hat{b}_M(t) - \frac{\gamma_M}{2}(\hat{b}_M(t) - \hat{b}_M^\dagger(t)) - ig_0\hat{a}_c^\dagger(t)\hat{a}_c(t) - \sqrt{\gamma_M}\hat{b}_{in}(t), \tag{2.1a}$$

$$\frac{d}{dt}\hat{a}_c(t) = -(i\Delta_0 + \kappa)\,\hat{a}_c(t) - ig_0(\hat{b}_M(t) + \hat{b}_M^\dagger(t))\hat{a}_c(t) + E(t) - \sqrt{2\kappa}\hat{a}_{in}(t), \tag{2.1b}$$

Here γ_M is the mechanical damping rate and $\hat{b}_{in}$ is the Brownian stochastic input noise caused by the mechanical thermal bath, which has the correlation functions (in the limit of $\omega_M/\gamma_M \gg 1$)

$$\langle\hat{b}_{in}^\dagger(t)\hat{b}_{in}(t')\rangle = \bar{n}\delta(t-t') \tag{2.2}$$

$$\langle\hat{b}_{in}(t)\hat{b}_{in}^\dagger(t')\rangle = (\bar{n}+1)\delta(t-t') \tag{2.3}$$

with $\bar{n} = [\exp(\hbar\omega_M/k_BT) - 1]^{-1}$. The cavity decay rate is denoted as κ, and $\hat{a}_{in}$ is the input field operator due to the outside vacuum bath with the correlation functions,

$$\langle\hat{a}_{in}(t)\,\hat{a}_{in}^\dagger(t')\rangle = [N(\omega_c)+1]\,\delta(t-t') \tag{2.4}$$

$$\langle\hat{a}_{in}^\dagger(t)\,\hat{a}_{in}(t')\rangle = N(\omega_c)\,\delta(t-t') \tag{2.5}$$

Here $N(\omega_c) = [\exp(\hbar\omega_c/k_BT) - 1]^{-1}$ is the average occupation number for the cavity thermal bath, at optical frequency $\hbar\omega_c/k_BT \gg 1$, $N(\omega_c) \simeq 0$. Cavity detuning is denoted as $\Delta_0 = \omega_c - \omega_L$. Coefficient $g_0 = x_{ZP}G_0$ is the vacuum optomechanical coupling strength and it quantifies the interaction between a single photon and the mechanical mode, often called single photon coupling constant.

Semi-classical dynamics of the nonlinear optomechanical system

To introduce the essential dynamical features of the standard optomechanical system of Eq.(2.1) in the unstable parameter regime, we first consider its purely classical dynamics. To do so, one needs to replace the operator $\hat{a}_c(t)$ and $\hat{b}_M(t)$ by their complex field amplitudes, $\alpha(t)$ and $\beta(t)$ respectively. The classical equations of motion then read,

$$\begin{aligned}\dot{\beta}(t) &= -i\omega_M\beta(t) - \frac{\gamma_M}{2}(\beta(t) - \beta^*(t)) - ig_0|\alpha(t)|^2,\\ \dot{\alpha}(t) &= -(i\Delta_0 + \kappa)\,\alpha(t) - ig_0(\beta(t) + \beta^*(t))\alpha(t) + E(t),\end{aligned} \tag{2.6}$$

where quantum fluctuation operators have been set to zero and all the products of operators have been replaced by the products of the corresponding amplitudes that will be valid for sufficiently strong cavity driving. The above equation could be treated as the expectation values of the quantum operator equations of Eq.(2.1). According to

the standard linearization analysis, the fixed points of the above nonlinear equations are obtained by setting all of the derivatives as zero, which yields the fixed points as $(\alpha_{ss}, \beta_{ss}) = \left(E(t)\left(-i\Delta+\kappa\right)^{-1}, -g_0|\alpha|^2/\omega_M\right)$. The stability of Eq.(2.6) is determined by the eigenvalues of the Jacobian Matrix at these fixed points. If all the eigenvalues are negative, then the system is stable, as in the situation discussed in the previous optomechanical steady-state entanglement schemes [29, 31]. However, here we are interested in the unstable regime where at least one of eigenvalues is positive and we denote the maximal positive one as λ_+. It is known that the dynamics of the nonlinear equations Eq.(2.6) can be well approximated by a set of linear equations within the time duration of $t < \lambda_+^{-1}$, which is true even for the unstable system.

Based on the above discussion, we hypothesize that for an unstable optomechanical system there is a time window that the fluctuations of all the quantum operators are guaranteed to be small and the system dynamics can be fully described by a linearized model. We assume that the time window is determined by the maximal positive eigenvalue λ_+ of the Jacobian Matrix of Eq.(2.1) as $t < \lambda_+^{-1}$. Since small fluctuations are guaranteed in this time window, so as the linear optomechanical model, which could be still utilized to study the behavior of the quantum optomechanical system in the unstable regime, details of which are shown in the following sections.

Linearization in the unstable parameter regime

To linearize QLE of Eq.(2.1) around the general fixed points (including both stable and unstable fixed points), we need to work in a displacement picture with the cavity and mechanical displacement amplitude chosen as $\alpha = E(t)/\left(-i\Delta+\kappa\right)$ and $\beta = -g_0/\omega_M|\alpha|^2$, respectively. The total Hamiltonian of the optomechanical system in this displaced picture takes the following form,

$$\bar{H}\left(t\right) = \mathcal{U}H\mathcal{U}^{-1} = \bar{H}_s + \bar{H}_\kappa + \bar{H}_\gamma$$

where the unitary transformation operator $\mathcal{U} = D_c\left(\alpha\right)D_M\left(\beta\right)$ and the displacement operator for the i-th mode is defined $D_i\left(\xi\right) = \exp\left(-\xi\hat{a}_i^\dagger + \xi^*\hat{a}_i\right)$ and $\hat{a}_i$ stands for the field operator of the cavity mode and the mechanical mode. Here $\bar{H}_\kappa$ ($\bar{H}_\gamma$) describes the interactions between the surrounding thermal bath and the cavity mode (the mechanical mode), while $\bar{H}_s$ describes the coupled cavity-mechanical Hamiltonian in the displacement picture,

$$\begin{aligned}\bar{H}_s = \;& \hbar\Delta\hat{a}_c^\dagger\hat{a}_c + \hbar\omega_M\hat{b}_M^\dagger\hat{b}_M + \hbar g_0\left(\alpha\hat{a}_c^\dagger + \alpha^*\hat{a}_c\right)\left(\hat{b}_M^\dagger + \hat{b}_M\right) \\ & + \left[\hbar\left(\Delta\alpha + iE\right)\hat{a}_c^\dagger + \hbar\left(\omega_M\beta + g_0\left|\alpha\right|^2\right)\hat{b}_M^\dagger + h.c.\right] \end{aligned} \tag{2.7}$$

with $\Delta = \Delta_0 + g_0(\beta^* + \beta)$. Notice that an nonlinear term of $\hat{H}_{int} = \hbar g_0 \hat{a}_c^\dagger \hat{a}_c \left(\hat{b}_M^\dagger + \hat{b}_M\right)$ has been neglected through the assumption that, within the linearization time window, the fluctuation operators $\hat{a}_c$ and $\hat{b}_M$ are small compared with the displacement amplitude α and β, respectively. By defining the vector of $\hat{u}(t) = (\hat{b}_M(t), \hat{b}_M^\dagger(t), \hat{a}_c(t), \hat{a}_c^\dagger(t))^T$ and $\hat{n}(t) = (-\sqrt{\gamma_M}\hat{b}_{in}(t), -\sqrt{\gamma_M}\hat{b}_{in}^\dagger(t), -\sqrt{2\kappa}\hat{a}_{in}(t), -\sqrt{2\kappa}\hat{a}_{in}^\dagger(t))^T$, the corresponding equations of motion for the linearized dynamics read,

$$\frac{d}{dt}\hat{u}(t) = M\hat{u}(t) + \hat{n}(t) \tag{2.8}$$

where its coefficient matrix M is given as

$$M = \begin{pmatrix} -i\omega_M - \gamma_M/2 & \gamma_M/2 & -ig & -ig \\ \gamma_M/2 & i\omega_M - \gamma_M/2 & ig & ig \\ ig & ig & -i\Delta - \kappa & 0 \\ -ig & -ig & 0 & i\Delta - \kappa \end{pmatrix} \tag{2.9}$$

Here the effective optomechanical coupling strength is $g = g_0\alpha$, indicating that the optomechanical interaction has been enhanced by a factor of the cavity light steady-state amplitude α through the strong external driving. To further simplify the discussion, we focus on the case of blue-detuned driving, where $\Delta = \omega_c - \omega_L = -\omega_M$. As discussed in Chapter 1, the effective Hamiltonian in the blue-detuned optomechanical system is dominated by the down-conversion type interaction, which is preferred for entanglement generation but can easily cause the system to become unstable. However, with the new linearization procedure developed here, we are going to show that, within the linearization time window, the dynamics of the optomechanical system could still be linearized even for the system in the unstable parameter regime. Based on the rotating wave approximation (RWA) [29], the coefficient matrix M of the linearized equation Eq.(2.8) in the blue-detuned regime can be simplified into,

$$M = \begin{pmatrix} -\frac{\gamma_M}{2} & 0 & 0 & -ig \\ 0 & -\frac{\gamma_M}{2} & ig & 0 \\ 0 & -ig & -\kappa & 0 \\ ig & 0 & 0 & -\kappa \end{pmatrix} \tag{2.10}$$

The eigenvalues of M are $\lambda_{1,2} = (-2\kappa - \gamma_M - \Omega)/4$ and $\lambda_{3,4} = (-2\kappa - \gamma_M + \Omega)/4$ with $\Omega = \sqrt{(4g)^2 + (2\kappa - \gamma_M)^2}$. The solutions of the linearized equations of Eq.(2.8)

can be obtained as,

$$\begin{aligned}\hat{a}_c(t) &= g_1(t)\cdot\hat{a}_c(0) - f(t)\cdot\hat{b}_M^\dagger(0) - \sqrt{2\kappa}\int_0^t ds g_1(t-s)\hat{a}_{in}(s) \\ &+ \sqrt{\gamma_M}\int_0^t ds f(t-s)\,\hat{b}_{in}^\dagger(s), \qquad (2.11a)\\ \hat{b}_M(t) &= g_2(t)\cdot\hat{b}_M(0) - f(t)\cdot\hat{a}_c^\dagger(0) - \sqrt{\gamma_M}\int_0^t ds g_2(t-s)\,\hat{b}_{in}(s) \\ &+ \sqrt{2\kappa}\int_0^t ds f(t-s)\hat{a}_{in}^\dagger(s), \qquad (2.11b)\end{aligned}$$

where $f(t) = 2ig\Omega^{-1}\left(e^{\lambda_3 t} - e^{\lambda_1 t}\right)$, $g_1(t) = A\cdot e^{\lambda_1 t} + B\cdot e^{\lambda_3 t}$ and $g_2(t) = A\cdot e^{\lambda_3 t} + B\cdot e^{\lambda_1 t}$ with the amplitudes $A = (\Omega + 2\kappa - \gamma_M)/2\Omega$ and $B = (\Omega - 2\kappa + \gamma_M)/2\Omega$. Note that the commutation relations $[\hat{a}_c(t), \hat{a}_c^\dagger(t)] = 1$ and $[\hat{b}_M(t), \hat{b}_M^\dagger(t)] = 1$ are fulfilled by the above solutions at any time.

Linearization time window

For the blue-detuned optomechanical system, $\lambda_{1,2}$ are always negative and the stability of the system relies only on the negativity of $\lambda_{3,4}$. When $g^2/\kappa > \gamma_M/2$, the system is always unstable. As mentioned previously that the upper limit of the linearization time window is $t = \lambda_3^{-1}$, we will show that the maximal entanglement is achieved at the time scale of $|\lambda_1|^{-1} \sim \kappa^{-1}$ which provides the lower bound for the linearization time window. As a consequence, the linearization time window with optimized optomechanical entanglement takes the following form,

$$\kappa^{-1} < t < \left(\frac{-2\kappa - \gamma_M + \Omega}{4}\right)^{-1} \qquad (2.12)$$

In Fig. 2.1 and Fig. 2.2, the solutions of Eq.(2.11) for the linearized optomechanical model are compared with the master equation approach of the standard optomechanical model without linearization. It is known that the master equation approach can correctly describe the optomechanical dynamics as long as the system dynamics are limited within a finite Fock subspace. Here, we have set the initial state as a vacuum state for the cavity mode and the mechanical mode, corresponding to initialize the system around the fixed points of $\alpha = E(t)/(-i\Delta + \kappa)$ and $\beta = -g_0/\omega_M|\alpha|^2$. With a weak driving field, such that the relation of $g < \kappa$ is kept, the system dynamics in the displacement picture can be well restricted within finite Fock spaces. As a consequence, the master equation approach is sufficient to characterize the optomechanical dynamics in this parameter regime.

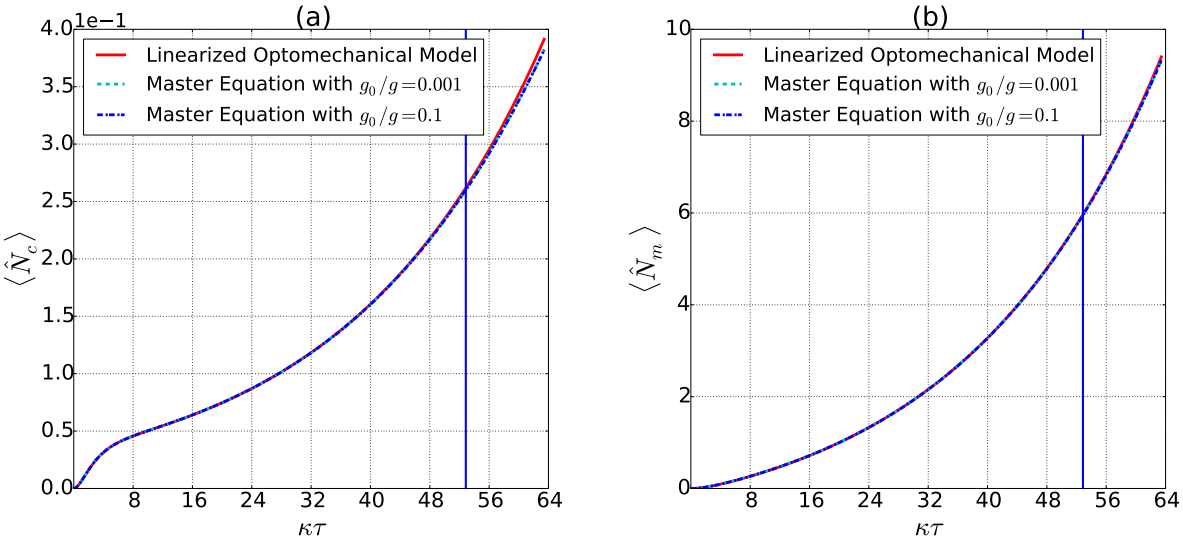

Figure 2.1: Plot of (a) the photon number and (b) phonon number as a function of pulse duration. The blue solid vertical line shows the upper bound of the time window, i.e. $\tau = \lambda_3^{-1}$. Parameters are chosen as $\omega_M/2\pi = 3.2$ MHz and mechanical quality factor $Q = \omega_M/\gamma_M = 10^5$, with an average thermal bath phonon number as $n_{th} = 0$, $\kappa = 0.5\omega_M$ and $g = 0.05\omega_M$.

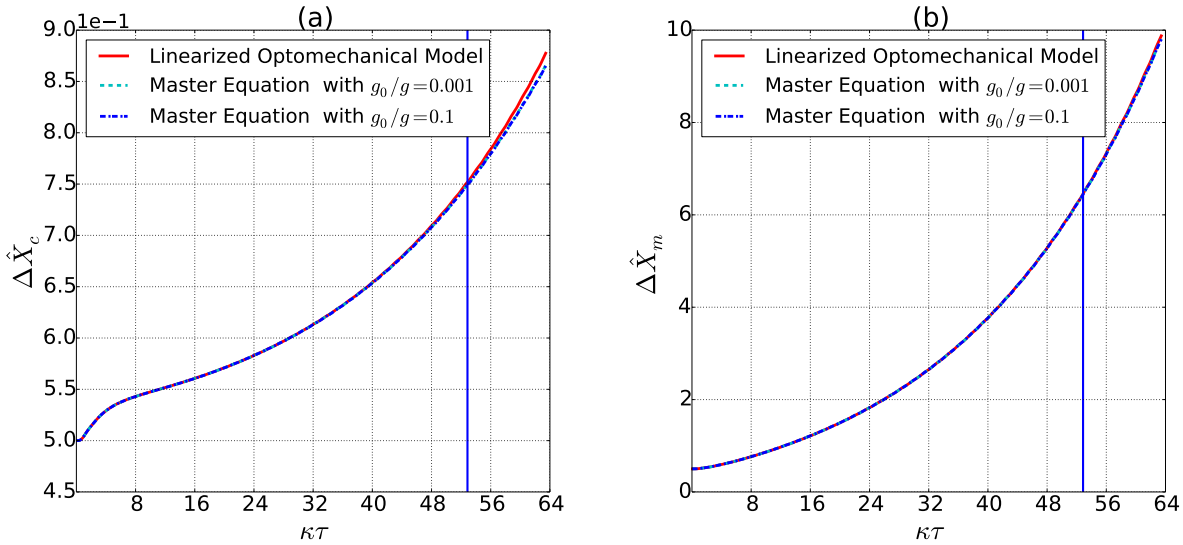

Figure 2.2: Plot of variance of (a) cavity amplitude quadrature X_c and (b) mechanical amplitude quadrature X_m. The blue solid vertical line shows the upper bound of the time window, i.e. $\tau = \lambda_3^{-1}$. Parameters are the same as Fig. 2.1.

Fig. 2.1 shows the evolution of the cavity photon number and the mechanical phonon number in the displacement picture, where the upper bound of the linearization time window is shown as a blue vertical line. It is evident from Fig. 2.1 that, within the linearization time window, both the cavity photon dynamics and the mechanical phonon dynamics are well characterized by the linearized optomechanical model, while large deviations from the master equation approach appear outside the linearization time window. Fig. 2.2 also confirms that the fluctuations of the quantum field operators are small compared with their average values inside the time window, indicating the assumption that all operators have small fluctuations is guaranteed within the linearization time window. Therefore, as long as the dynamics are limited within the linearization time window, the linearized optomechanical model provides exactly the same dynamics as the master equation approach of the standard optomechanical model without any linearization approximation. While outside the time window, the nonlinear interaction terms start to dominate the dynamics where the linearized optomechanical model starts to deviate the solutions from the master equation approach. Notably, for both figures, we have chosen the optomechanical system in the unstable parameter regime. In Fig. 2.2, the fluctuations of the cavity field amplitude and mechanical amplitude are studied within the linearization time window. It is evident that, inside the linearization time window, the fluctuations of these amplitudes are limited, which is consistent with our expectation of the small fluctuations for the linearized optomechanical model.

Intra-cavity optomechanical entanglement

To obtain an analytical description and physical understanding of blue-detuned cavity entanglement dynamics in the unstable parameter regime, we start considering the influence of the linearization time window on the optomechanical entanglement generation process for the pulsed driving scheme. In this section, we are going to introduce two different approach of measuring the optomechanical entanglement: the EPR-Variance method and the logrithmic negativity of covariance matrix. We will show how the linearization time window influences the maximal available optomechanical entanglement measured by these two different methods.

EPR-Variance Approach

For any quantum separable state $\varrho(t)$, the EPR-variance Δ_{EPR} is known to be always bigger than two [55],

$$\Delta_{EPR} = \langle(\Delta\hat{u})^2\rangle_\varrho + \langle(\Delta\hat{v})^2\rangle_\varrho > 2$$

where the two body quantum operators $\hat{u}$ and $\hat{v}$ are defined as $\hat{u} = \hat{P}_c + \hat{x}$ and $\hat{v} = \hat{X}_c + \hat{p}$. Here, the cavity amplitude quadrature (phase quadrature) is denoted as $\hat{X}_c$ ($\hat{P}_c$) and the operator $\hat{x}$ ($\hat{p}$) is the mechanical displacement operator (moment

operator). The EPR-variance Δ_{EPR} provides a direct way to characterize the quantity of entanglement between the cavity mode and mechanical mode, by which the smaller value of the variance indicates the larger the entanglement of the optomechanical quantum state. Under the assumption of RWA, one can prove that $\langle(\Delta\hat{u})^2\rangle_\varrho = \langle(\Delta\hat{v})^2\rangle_\varrho$ and

$$\begin{aligned}\langle(\Delta\hat{u})^2\rangle_\varrho =& G_1\cdot e^{2\lambda_1 t}+G_2\cdot e^{(\lambda_1+\lambda_3)t}+G_3\cdot e^{2\lambda_3 t}\\ &+\Gamma_1\frac{e^{2\lambda_1 t}-1}{2\lambda_1}+\Gamma_2\frac{e^{(\lambda_1+\lambda_3)t}-1}{(\lambda_1+\lambda_3)}+\Gamma_3\frac{e^{2\lambda_3 t}-1}{2\lambda_3}\end{aligned} \tag{2.13}$$

where

$$\begin{aligned}G_1 &= \frac{1}{2}\left(A+\frac{2g}{\Omega}\right)^2+\left(n_0+\frac{1}{2}\right)\left(B+\frac{2g}{\Omega}\right)^2,\quad G_2=n_0\frac{4g\left(2\kappa-\gamma_M\right)}{\Omega^2},\\ G_3 &= \frac{1}{2}\left(B-\frac{2g}{\Omega}\right)^2+\left(n_0+\frac{1}{2}\right)\left(A-\frac{2g}{\Omega}\right)^2\\ \Gamma_1 &= \kappa\left(A+\frac{2g}{\Omega}\right)^2+\gamma_M\left(n_{th}+\frac{1}{2}\right)\left(B+\frac{2g}{\Omega}\right)^2,\\ \Gamma_2 &= \frac{4g\left(2\kappa-\gamma_M\right)}{\Omega^2}\left(\gamma_M\left(n_{th}+\frac{1}{2}\right)-\kappa\right),\\ \Gamma_3 &= \kappa\left(B-\frac{2g}{\Omega}\right)^2+\gamma_M\left(n_{th}+\frac{1}{2}\right)\left(A-\frac{2g}{\Omega}\right)^2,\end{aligned}$$

with $A=\left(\Omega+2\kappa-\gamma_M\right)/2\Omega$, $B=\left(\Omega-2\kappa+\gamma_M\right)/2\Omega$ and $\Omega=\sqrt{(4g)^2+\left(2\kappa-\gamma_M\right)^2}$. Initially, at $t=0$, $\langle(\Delta\hat{u})^2\rangle_\varrho = n_0+1$, leading to $\Delta_{EPR}=2n_0+2>2$, showing that the system is in a separable state, and it is consistent with the separability of our initial state.

The analytical form of the EPR-variance obtained here could be applied to various parameters regimes and to achieve the same results as previous studies [29, 31, 46, 54]. One example is for the case of no environmental noises, where $\kappa=\gamma_M=0$, the calculation for the EPR-variance of Eq.(2.13) yields $\Delta_{EPR}=2\left(n_0+1\right)e^{-2gt}$, showing that radiation pressure interaction helps the system to build up optomechanical entangled states [54]. Another well known case is the stable blue-detuned optomechanical system, in which the corresponding steady state EPR-variance Δ_{EPR} could be calculated from Eq.(2.13),

$$\left(\Delta_{EPR}\right)_{ss}=2\langle(\Delta\hat{u})^2\rangle_{\varrho_{ss}}=\left(-\frac{1}{\lambda_1}\right)\cdot\Gamma_1+\left(-\frac{1}{\lambda_3}\right)\cdot\Gamma_2+\left(-\frac{2}{\lambda_1+\lambda_3}\right)\cdot\Gamma_3, \tag{2.14}$$

indicating that the steady-state entanglement is sensitive to the temperature [29, 31]. In this expression, it is possible to choose the system parameters so that Γ_3 is negative, indicating the appearance of entanglement. The maximal entanglement is obtained at $n_{th} = 0$ with the maximal optomechanical coupling chosen as $g = \sqrt{2\kappa\gamma_M}$ due to the restriction of the stability condition. The corresponding entanglement is

$$min\left(\Delta_{EPR}\right)_{ss} = \frac{1}{4}\left(1 - \sqrt{\frac{2\gamma_M}{\kappa}} - \frac{3}{2}\left(\frac{\gamma_M}{\kappa}\right) - 11 \times \left(\frac{\gamma_M}{2\kappa}\right)^{3/2}\right) + \left(2n_{th}+1\right)\left(\frac{\gamma_M}{2\kappa}\right)^{3/2}, \tag{2.15}$$

showing that $\Delta_{EPR} > \frac{1}{4}$, and it disappears with high n_{th}, consistent with [46].

More importantly, our results could be applied to the case of unstable optomechanical system, i.e. $\lambda_3 > 0$. For the blue-detuned cavity optomechanical system in unstable parameter regime, our formula shows that the time scale for the system to build up entanglement is κ^{-1}. In Eq.(2.13), EPR-variance $\langle(\Delta\hat{u})^2\rangle_\varrho$ decreases exponentially with $e^{2\lambda_1 t}$ and $e^{(\lambda_1+\lambda_3)t}$ where both of these two terms are in the time scale of κ^{-1} and all other terms are monotonically increasing functions with t. Physically, Γ_1, Γ_2 and Γ_3 are caused via the cavity decay and mechanical damping, destroying the obtained optomechanical entanglement. G_3 describes the feedback of the environment on the radiation pressure coupling. However, it is known that the EPR-variance approach only detects limited kinds of entangled optomechanical states, and many optomechanical entangled states are out of its ability. In fact, most optomechanical entangled states could be measured by the logarithmic negativity of the system's covariance matrix, details of which we will focus on in the following section.

Covariance matrix approach

Another alternative way to characterize the entanglement dynamics for the optomechanical system is the logarithmic negativity of the covariance matrix, which will be described in this section. Since we have shown that the linearized optomechanical model is guaranteed within the linearization time window, the dynamics of the unstable optomechanical system can be fully characterized by the covariance matrix of $V_{ij} = \langle u_i(t)u_j(t) + u_j(t)u_i(t)\rangle/2$ inside the linearization time window, where $u^T(t) = \left[X_c(t), Y_c(t), x(t), p(t)\right]$. According to the dynamics of $u(t)$ in Eq.(2.8), the equation of motion for the covariance matrix $V(t)$ is

$$\frac{dV(t)}{dt} = AV(t) + V(t)A^T + D, \tag{2.16}$$

This is a direct result from the linearized QLEs without any additional approximations, and once it has been solved, all the dynamics of the optomechanical system

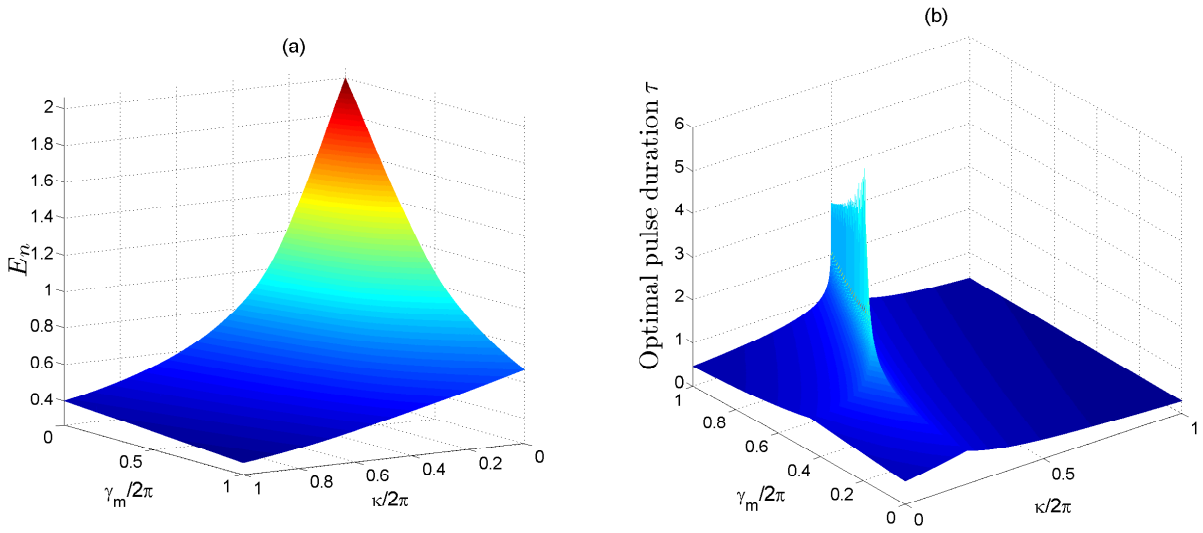

Figure 2.3: Plot of Zero-temperature maximal entanglement and the corresponding optimal pulse duration. (a) The dependence of logarithmic negativity on mechanical damping rate γ_M (MHz) and cavity decay rate κ (MHz).(b) The corresponding optimal pulse duration τ (us) inside the linearization time window. The mechanical coupling rate is fixed as $g = 0.3MHz$ and mechanical frequency is chosen as $\omega_M = 500MHz \gg \kappa, g$

could be inferred from it. However, the general analytical expression is too convolved to be reported here. Under RWA the expression could be further simplified, which are present in the Appendix A.1. Here we focus on the numerical solutions of Eq.(2.16).

At zero thermal temperature, the dependence of the maximal optomechanical entanglement on the cavity decay rate κ and the mechanical damping γ_M are reported in Fig. 2.3. The maximal values are obtained by searching within the linearization time window. Our results show entanglement is maximized in the regime where both γ_M and κ are small, consistent with the expectation that entanglement is optimized with small cavity decay and less mechanical damping. Fig. 2.3 also shows that the pulse duration of the optimal entanglement is larger at smaller cavity decay rate κ, which is consistent with our previous discussion that $\kappa^{(-1)}$ is the time scale for optimal optomechanical entanglement.

For non-zero temperatures, we study the dependence of optimal entanglement on the mechanical temperature n_{th} for the blue-detuned cavity optomechanical system in the unstable parameter regime. The results are shown in Fig. 3.2. Because of the existence of the linear time window in this weak driving unstable regime, the entanglement is very strong against the thermal noise and the non-zero negativity is

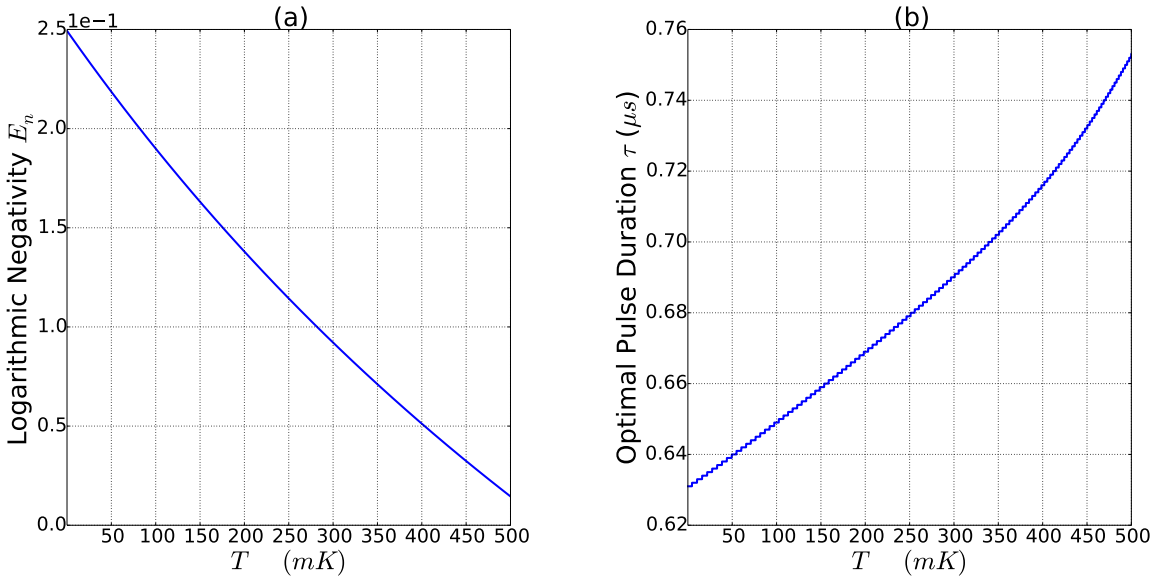

Figure 2.4: (a) Temperature dependence of the maximal values of logarithmic negativity $E_n(t)$ inside the linearization time windows with fixed $\omega_M/2\pi = 3.8MHz$, $\gamma_M = \omega_M/Q(Q = 10^5)$, $g/2\pi = 0.3MHz$ and $\kappa/2\pi = 0.3MHz$ (b) The corresponding optimal pulse duration τ. Note that the linearization windows here is $t < 0.858$ (μs) and in our case the entanglement E_n always get maximal before the system lose linearization.

obtained at $T = 500$ mK. For the steady-state entanglement scheme, the restrictions from the stability condition make the existence of high temperature optomechanical entanglement impossible. But in our pulsed driving scheme, because the linearization is guaranteed in the linearization time window, the stability condition is released, and the optomechanical entangled states are, therefore, possible for very high mechanical temperatures.

In Fig. 3.3, we show the optimized optomechanical entanglement on the strength of optomechanical coupling g and the cavity decay rate κ within the restrictions from the linearization time window, and the corresponding time duration is shown in Fig. 3.4. The mechanical damping and its thermal temperature are fixed at $\gamma_M/\omega_M = 10^5$ and $n_{th} = 1100$, respectively. It shows that for the unstable parameter regime at non-zero temperatures, the linearization time window tends to create large entanglement at smaller cavity decay rate κ with larger optomechanical coupling strength g which is consistent with the expectation. However, the pulse duration shows some special behavior that for the special choice of g and κ, the duration for optimal entanglement is significantly large. The reason is that in these regimes, although the system is unstable, its linearization time window could last for a very time duration, while in

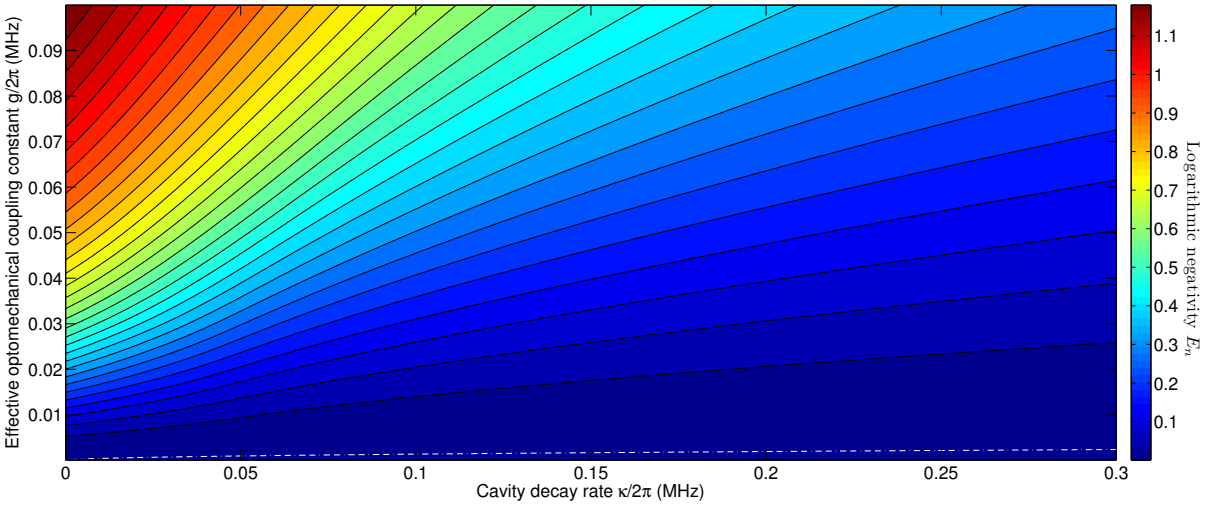

Figure 2.5: Maximum values of optomechanical entanglement E_n as a function of interaction constant $g/2\pi$ and cavity dacay rate $\kappa/2\pi$. The mechanical oscillator has fixed frequency of $\omega_M/2\pi = 3.8$ MHz and its damping rate is set as $\gamma_M/2\pi = 3.8\times10^{-5}$ MHz. The phonon number of the thermal bath is given as $n_{th} = 1100$. The white dotted line is the boundary between stable parameters regime and unstable regime, i.e. above this line, the optomechanical system is unstable due to the large interaction strength g, i.e. $g > \sqrt{\kappa \times \gamma_M/2}$.

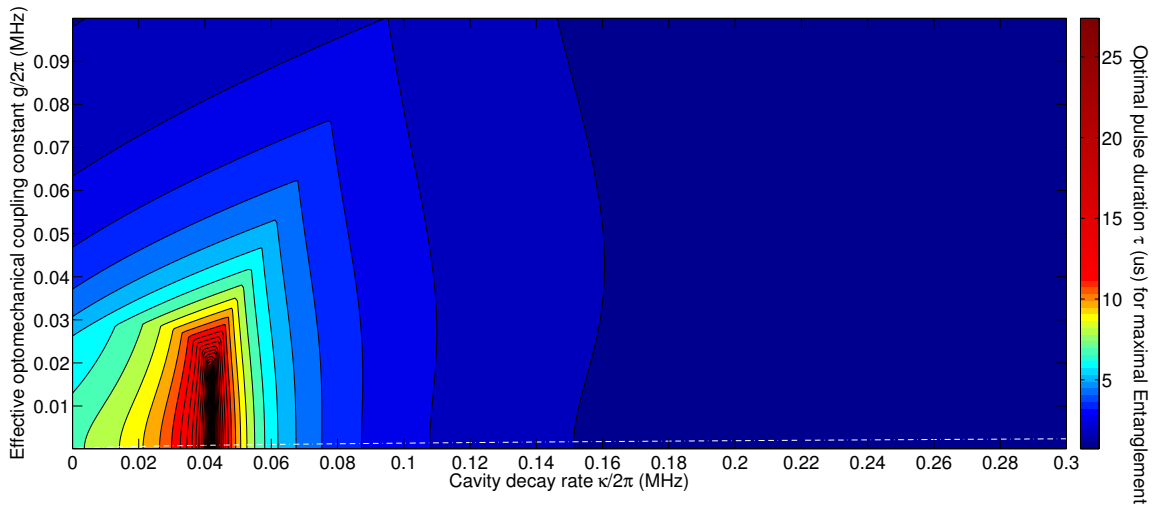

Figure 2.6: The corresponding optimal pulse duration τ for the maximal entanglement. Parameters are the same as Fig. 3.3. The optimal duration τ is found by searching maximal entanglement inside the time window where the linearization is always guaranteed.

these regimes, the time scale of optimal entanglement is solely controlled by κ^{-1}, which is also a large number.

In practice, people are more interested with the entanglement between the output field and the mechanical oscillator since we can only measure the outgoing optical field in experiment. It is, therefore, important to have theoretical tools to characterize such an entanglement, and this is done in the Appendix A.2, where we propose a realistic scheme to connect the intra-cavity entanglement with the entanglement among the output field and mechanical oscillator.

Conclusions

In this study, we successfully established a quantitative description of the linear time window for the unstable optomechanical system under blue-detuned cavity driving. It turns out that the standard optomechanical dynamics within linear time window could be well characterized by the linear optomechanical model, while outside the time window, a nonlinear description is necessary. We also provided a detail study on how such a time window influences the entanglement generation for the unstable blue-detuned optomechanical system. Two different approaches have been employed to characterize the optomechanical entanglement, one with the simple analytical expression and clear physics pictures. Another could be implemented with broader parameter regimes. All these studies show that the linear time window has a strong influence on the optimal schemes generating entanglement in the unstable regime. In order to investigate the experimental measurement on the cavity entanglement, an input-output formalism has been developed to describe the entanglement between the output field and the mechanical oscillator.

However, the current study is based on RWA, where it requires $\omega_M \gg \kappa$, and outside such a parameter regime, the general form for the linear time window is really involved and has not been fully studied, where it could show new characteristics for the linear time window. Another possible direction for this study is to investigate the linear time window beyond the standard optomechanical model, which could involve several cavity modes interacting with several mechanical modes. Whether the stability condition will relax or restrict the linear time window is still an open question and needs further study.

2.2 Optomechanical System With Periodic Driving

Introduction

One interesting question about the optomechanical system is how to improve the obtained optomechanical entanglement for the steady-state entanglement generation scheme proposed by [29, 31]. The previous section has provided one way to enhance the optomechanical entanglement via a pulsed driven optomechanical system working in an unstable parameter regime. However, the complexity of the pulse control along with the instability issues make it difficult to implement such a scheme experimentally. Recently, it has been proposed that with a suitable time modulation of the driving field, the standard optomechanical system could have steady states with significantly improved entanglement between the cavity light field and the mechanical mode[33, 32, 34]. As outlined in Chapter 1, the periodic time modulation of the driving field leads to an effective two-mode squeezing interaction for the standard optomechanical system, which helps to produce highly entangled optomechanical steady states.

In this section, we extend this idea one step further and apply it to the optomechanical system beyond the standard optomechanical model, where our system includes two cavity modes interacting with one single mechanical mode—a three-mode optomechanical system. Such a system has been proposed for the frequency transmission between optical and microwave fields [26, 27], which has many important applications in various research [31, 56, 57, 58]. This section focuses on the improvement of entanglement for the three-mode optomechanical system by means of suitable time modulation of the driving field. Our results show that the periodic driving field in the three-mode optomechanical system can not only be utilized to enhance the cavity-mechanical entanglement as well as the entanglement between the two cavity modes. It could also be used to reduce the entanglement by controlling the modulation amplitude, which provide an effective way to improve the quantum communication scheme. The new scheme present here has the ability to establish or break the entanglement channels freely. Moreover, at the end of this section, we also study the influence of the time modulation on the dynamics of the tripartite entanglement for the three-mode optomechanical system. We show that the genuine tripartite entanglement is sensitive to the external driving and, with appropriate time modulation, the tripartite entanglement of the three-mode optomechanical system can be enhanced.

Three-mode Optomechanical system

We consider a optomechanical system composed of two cavity modes coupling with a single mechanical mode via the radiation pressure interaction. One cavity is driven

by a red-detuned laser field with frequency ω_r to generate anti-Stokes process, and another cavity is driven by a blue-detuned laser field at frequency ω_b to generate Stokes process. The Hamiltonian of this system reads,

$$\begin{aligned} H_s &= \hbar\omega_1\hat{a}_1^\dagger\hat{a}_1 + \hbar\omega_2\hat{a}_2^\dagger\hat{a}_2 + \frac{1}{2}\hbar\omega_M\left(\hat{p}^2+\hat{q}^2\right) - \sum_{i=1,2}\hbar g_i\hat{a}_i^\dagger\hat{a}_i\hat{q} \\ &+ i\hbar E_1\left(1+\eta cos\left(\Omega t\right)\right)\left(e^{-i\omega_r t}\hat{a}_1^\dagger - e^{i\omega_r t}\hat{a}_1\right) + i\hbar E_2\left(e^{-i\omega_b t}\hat{a}_2^\dagger - e^{i\omega_b t}\hat{a}_2\right) \end{aligned} \tag{2.17}$$

where $\omega_{1,2}$ are the frequencies of the two cavities and $\hat{a}_i$ is the corresponding annihilation operator. Here the amplitude of the red detuned driving field is time modulated with a strength ηE_1 and frequency Ω. Operators $\hat{p}$ and $\hat{q}$ are the dimensionless operator for the mechanical oscillator with communicator $[\hat{q},\hat{p}] = i$. The corresponding equations of motion read,

$$\dot{\hat{q}} = \omega_M\hat{p}, \tag{2.18a}$$
$$\dot{\hat{p}} = -\omega_M\hat{q} - \gamma_M\hat{p} + g_1\hat{a}_1^\dagger\hat{a}_1 + g_2\hat{a}_2^\dagger\hat{a}_2 + \xi(t), \tag{2.18b}$$
$$\dot{\hat{a}}_1 = -[\kappa_1 + i\Delta_r]\hat{a}_1 + ig_1\hat{a}_1\hat{q} + E_1 + \eta E_1 cos\left(\Omega t\right) + \sqrt{2\kappa_1}\hat{a}_1^{in}, \tag{2.18c}$$
$$\dot{\hat{a}}_2 = -[\kappa_2 + i\Delta_b]\hat{a}_2 + ig_2\hat{a}_2\hat{q} + E_2 + \sqrt{2\kappa_2}\hat{a}_2^{in}, \tag{2.18d}$$

with the cavity detunings given as $\Delta_r = \omega_1 - \omega_r > 0$ and $\Delta_b = \omega_2 - \omega_b < 0$. To investigate the essential features of the periodic time modulation on such a three-mode optomechanical system, we first consider its purely classical dynamics. To do so, we replace each operator with its average value. The classical equations of motion then read,

$$\langle\dot{\hat{q}}\rangle = \omega_M\langle\hat{p}\rangle, \tag{2.19a}$$
$$\langle\dot{\hat{p}}\rangle = -\omega_M\langle\hat{q}\rangle - \gamma_M\langle\hat{p}\rangle + g_1|\langle\hat{a}_1\rangle|^2 + g_2|\langle\hat{a}_2\rangle|^2, \tag{2.19b}$$
$$\langle\dot{\hat{a}}_1\rangle = -[\kappa_1 + i\Delta_r]\langle\hat{a}_1\rangle + ig_1\langle\hat{a}_1\rangle\langle\hat{q}\rangle + E_1 + \eta E_1 cos\left(\Omega t\right), \tag{2.19c}$$
$$\langle\dot{\hat{a}}_2\rangle = -[\kappa_2 + i\Delta_b]\langle\hat{a}_2\rangle + ig_2\langle\hat{a}_2\rangle\langle\hat{q}\rangle + E_2, \tag{2.19d}$$

The above equations could be solved numerically, as it is done in the following sections. Another way is to solve the above nonlinear equations via the perturbation method based on the smallness of the weak optomechanical coupling g_i. Since all the nonlinearities of the above equations are associated with g_i and if we further assume $g_1 \sim g_2 \sim g_0$ is small enough, a power series ansatz could be employed,

$$\langle\hat{O}\rangle = \sum_{n=0}^{\infty} O_n g_0^n$$

where $\hat{O}$ stands for any quantum operator in the above nonlinear equations. Once we substitute this expression back into Eq.(2.19) and collect terms of different orders of g_0, one will arrive at a set of linear equations. To solve this set of equations, we focus on the asymptotic solutions, where all the transient dynamics have died out and the steady-state amplitudes oscillate as the sidebands of the modulation frequency Ω. This leads to the following improved ansatz for Eq.(2.19),

$$\langle \hat{O} \rangle = \sum_{n=0}^{\infty} \sum_{\ell=-\infty}^{\infty} O_{n.\ell} g_0^n e^{i\ell\Omega t} \tag{2.20}$$

As a result, the classical steady-state solutions are all periodic due to the time periodic driving, which provides the basis for the following linearization process of the quantum Langevin equations Eq.(2.18), and we will discuss it in more detail in the next section.

Linearization of the three-mode optomechanical system

With the classical solutions obtained in the previous section, one could continue to linearize the quantum Langevin equations of Eq.(2.18) around the asymptotic quasiperiodic orbits, which are then used to study the second moments of system operators—the quantum correlations of the three-mode system.

By expanding the quantum operator $\hat{\Omega}(t)$ as average value and its fluctuation operator, i.e. $\hat{\Omega}(t) = \langle \hat{\Omega(t)} \rangle + \delta\hat{\Omega}(t)$, and by using the assumption of small fluctuations of the stable three-mode optomechanical system, Eq.(2.18) could be linearized around the classical solutions into the following first order inhomogeneous differential equations,

$$\frac{du}{dt} = A(t)u(t) + n(t) \tag{2.21}$$

with the vector defined as $u(t) = [\delta\hat{q}, \delta\hat{p}, \delta\hat{X}_1, \delta\hat{Y}_1, \delta\hat{X}_2, \delta\hat{Y}_2,]^T$ and the noise vector is $n(t) = (0, \xi(t), \sqrt{2\kappa_1}\hat{X}_1^{in}, \sqrt{2\kappa_1}\hat{Y}_1^{in}, \sqrt{2\kappa_2}\hat{X}_2^{in}, \sqrt{2\kappa_2}\hat{Y}_2^{in})^T$. The coefficient matrix is given by,

$$A(t) = \begin{pmatrix} 0 & \omega_M & 0 & 0 & 0 & 0 \\ -\omega_M & -\gamma_M & G_{1,x}(t) & G_{1,y}(t) & G_{2,x}(t) & G_{2,y}(t) \\ -G_{1,y}(t) & 0 & -\kappa_1 & \Delta_1(t) & 0 & 0 \\ G_{1,x}(t) & 0 & -\Delta_1(t) & -\kappa_1 & 0 & 0 \\ -G_{2,y}(t) & 0 & 0 & 0 & -\kappa_2 & \Delta_2(t) \\ G_{2,x}(t) & 0 & 0 & 0 & -\Delta_2(t) & -\kappa_2 \end{pmatrix} \tag{2.22}$$

where the coefficient matrix A(t) contains the time modulated cavity detuning and optomechanical coupling as $\Delta_1(t) = \Delta_r - g_1\langle\hat{q}(t)\rangle$ and $\Delta_2(t) = \Delta_b - g_2\langle\hat{q}(t)\rangle$,

$$G_i(t) = \sqrt{2}g_i\langle\hat{a}_i(t)\rangle \equiv G_{i,x}(t) + iG_{i,y}(t) \tag{2.23}$$

Due to the linearity of Eq.(2.21) and the Gaussian nature of the noise operators, the dynamics of this three-mode optomechanical system are always kept in Gaussian and are completely characterized by its symmetrized 6×6 covariance matrix, with its elements given by,

$$V_{ij}(t) = \frac{1}{2}\langle \hat{u}_i(t)\hat{u}_j(t) + \hat{u}_j(t)\hat{u}_i(t)\rangle \tag{2.24}$$

The corresponding equation of motion for the covariance matrix could be obtained as,

$$\frac{dV(t)}{dt} = A(t)V(t) + V(t)A^T(t) + D \tag{2.25}$$

where D=diag$(0,\ \gamma_M(2n_{th}+1),\ \kappa_1,\ \kappa_1,\ \kappa_2,\ \kappa_2)$. Combing the solutions of Eq.(2.19) and Eq.(2.25), one can solve for the dynamics for the three-mode optomechanical system under the periodic driving.

Dynamics of the three-mode optomechanical system

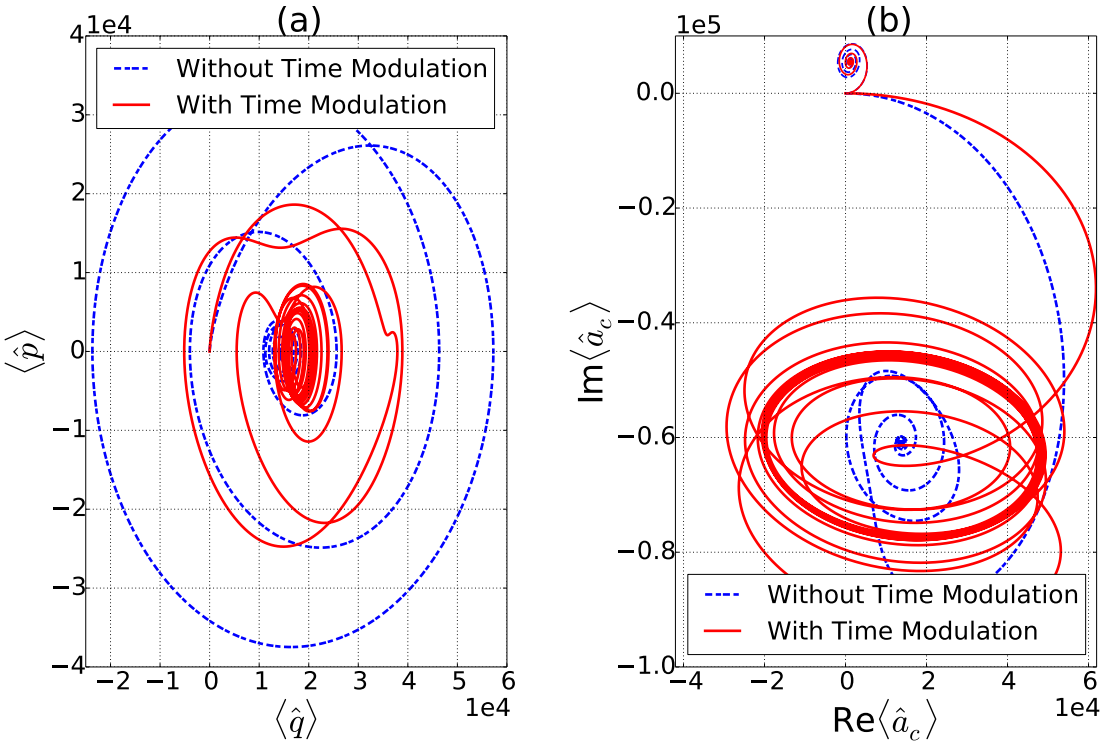

Figure 2.7: The dynamics of the classical solution for the three-mode optomechanical system with and without time modulation on the red-detuned driving. (a) Phase Plot of mechanical oscillator. (b) Phase Plot of the cavity modes, the upper ones are blue detuned cavity mode and the lower ones are the red-detuned cavity modes. The parameters are: $\omega_M/2\pi = 1\ MHz$, $\gamma_M/2\pi = 1\ Hz$ with thermal temperature at $n_{th} = 0$. One cavity is red-detuned at $\Delta_r = \omega_M$ with amplitude $E_1 = 3.80 \times 10^{11}$ Hz and another cavity is blue-detuned at $\Delta_b = -\omega_M$ with amplitude $E_2 = 0.1E_1$. Both cavities have the same decay rate of $\kappa_1 = \kappa_2 = 1.35\ MHz$. The modulation frequency is $\Omega = 2\omega_M$ with amplitude $E_\Omega = 0.45E_1$. The optomechanical couplings are $g_1/2\pi = g_2/2\pi = 3.8\ Hz$.

The phase space trajectories of the first moments of the mechanical oscillator and cavity fields are shown in Fig. 2.7 (solid curves) and compared with the case of no time modulation(dashed line curves). Fig. 2.7 shows that the dynamics of the mechanical oscillator (red curve in Fig. 2.7(a)) and of the red-detuned cavity (red curve in Fig. 2.7(b)) are strongly imparted by the time modulation, specifically limit circles rather than fixed points appear for the time modulated dynamics. The blue detuned cavity mode (blue dashed curve in Fig. 2.7(b)) is almost unaffected by the time

modulation. This is because only the red-detuned driving field is time modulated, which influences the blue-detuned cavity field via the weak optomechanical coupling, making its influence on the blue-detuned cavity mode one order smaller than its influence on the red-detuned cavity mode.

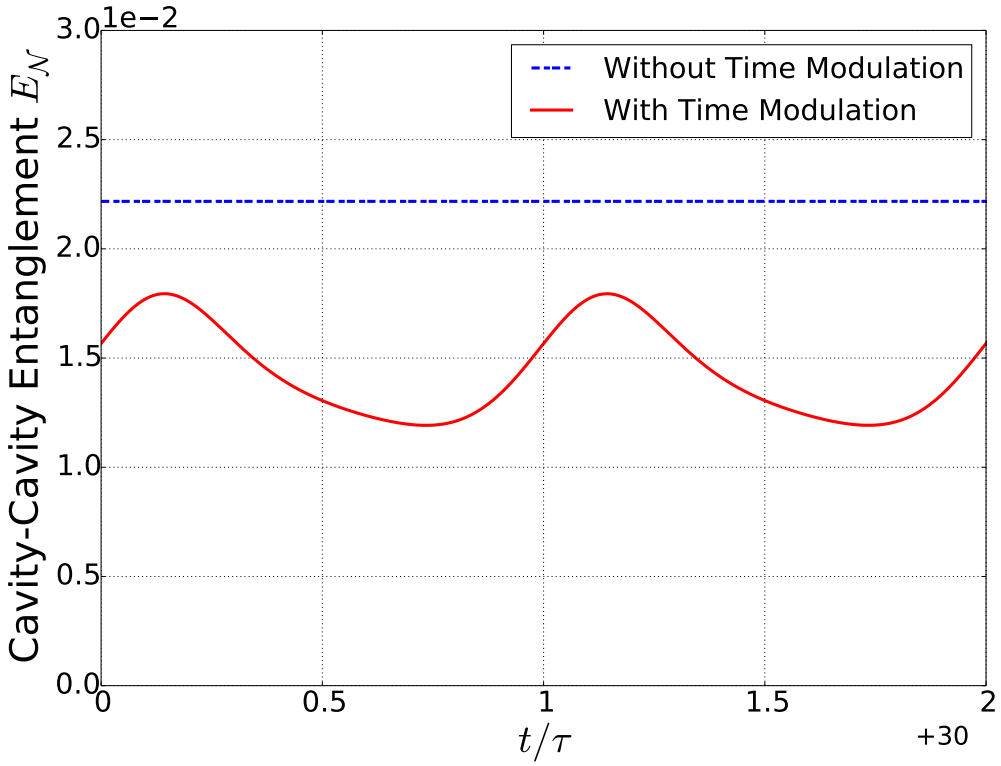

Figure 2.8: The entanglement dynamics under the time modulation. Solid cures are the dynamics with time modulated red-detuned driving and dashed lines are without time modulation. Parameters are the same as Fig. 2.7

As discussed previously, the quantum fluctuations around the classical orbits are well characterized by Eq.(2.21), from which the dynamics of the optomechanical quantum correlations can be obtained. One important quantum correlation is the bipartite entanglement between the cavity fields and mechanical mode. We use the logarithmic negativity of the covariance matrix as a measure of the optomechanical entanglement [29], of which the definition is provided in the Chapter 1 with Eq.(1.26). Fig. 2.8 and Fig. 2.9 show the entanglement dynamics under the time modulation of the red detuned cavity driving (red curves), which are compared with the case of no time modulation (blue dashed curves). It is evident that both the entanglement between the red-detuned cavity mode and mechanical mode (Fig.2.9(a)), and the entanglement between the blue-detuned cavity mode and mechanical mode (Fig.2.9(b)) are improved

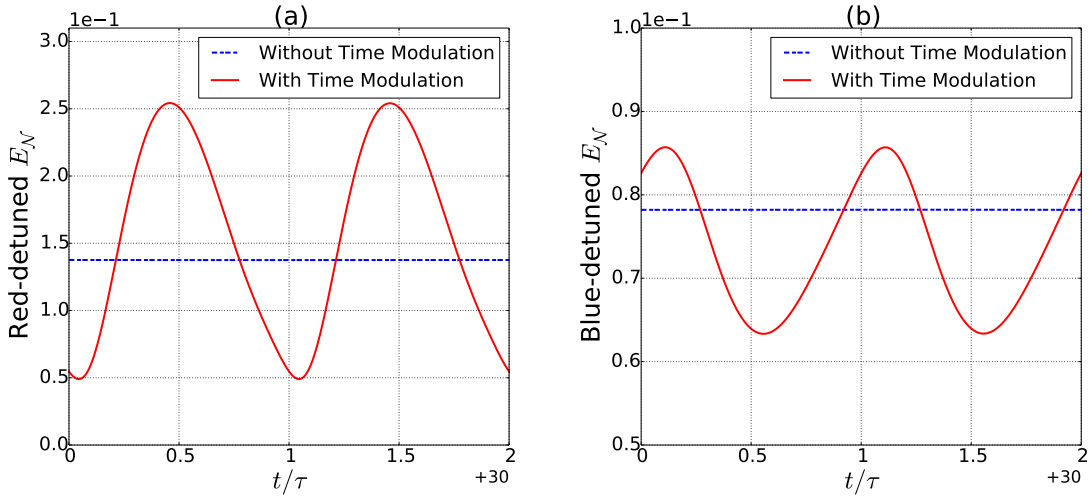

Figure 2.9: The entanglement dynamics under the time modulation. (a) the entanglement between the red-detuned cavity and mechanical mode. (b) the entanglement between the blue-detuned cavity and mechanical mode. Solid cures are the dynamics with time modulated red-detuned driving and dashed lines are without time modulation. Parameters are the same as FIG.2.7

by the time modulation, while the cavity-cavity entanglement (Fig.2.8) is depressed by the time modulation. This is due to the fact that the time modulation was added on the red-detuned driving laser, which generates an effective down-conversion interaction between the red-detuned cavity field and mechanical mode, leading to a large improvement for the red-detuned optomechanical entanglement.

It is also possible to enhance the cavity-cavity entanglement through the time modulation. One example for the case of the time modulated red-detuned cavity driving is given in Fig. 2.10(a), where we have fixed the effective cavity detuning as $\Delta_1 = \omega_M$ and $\Delta_2 = -\omega_M$. It shows that the cavity-cavity entanglement is significantly improved from 1.15 to 1.48 as result. However, the assumption with a time independent cavity detuning under the time modulation could cause some experimental difficulties. With another set of parameters, we release this restriction, but only a slightly enhanced cavity-cavity entanglement is observed. The time modulating of the blue-detuned cavity driving could also be employed to enhance the steady cavity-cavity entanglement and Fig. 2.10(b) shows one example with the time modulation applied to the blue detuned cavity. It clearly shows that the cavity-cavity entanglement is enhanced from $E_{\mathcal{N}} = 0$ with no time modulation to $E_{\mathcal{N}} \approx 0.35$ with time modulation. However, we also observed that the bipartite entanglement between the blue-detuned cavity and mechanical mode is reduced. This is due to the fact that the time modulation induced an effective beam splitter interaction between them.

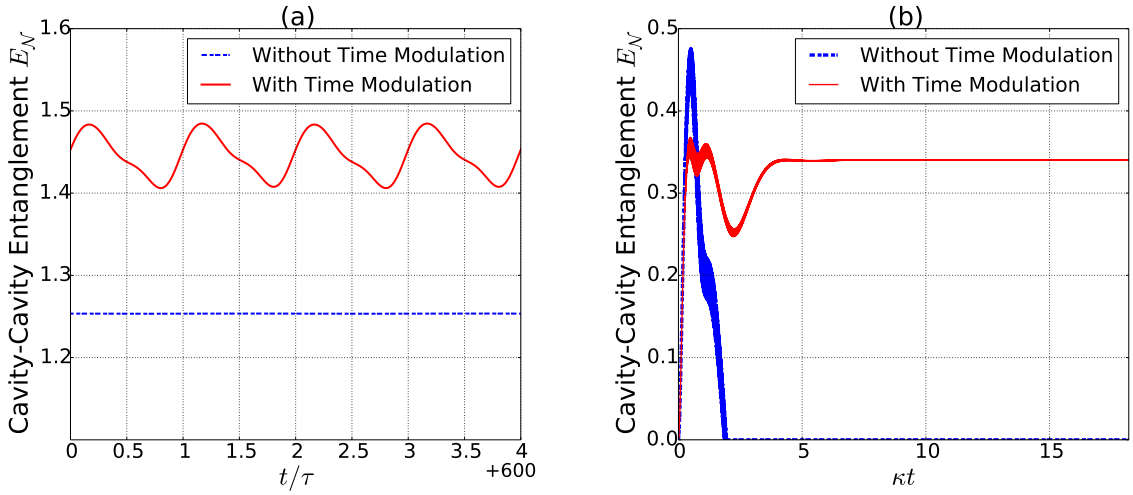

Figure 2.10: (a) Steady-state cavity-cavity entanglement with the cavity detunings fixed at $\Delta_1(t) = \omega_M$ and $\Delta_2(t) = -\omega_M$. The mechanical frequency is chosen as $\omega_M/2\pi = 10\ MHz$ and damping as $\gamma_M/2\pi = 0.4\ MHz$ with thermal temperature at $n_{th} = 0$. The optomechanical couplings are $g_1/2\pi = g_2/2\pi = 1.63\ Hz$, the cavity decay rate is $\kappa_1/2\pi = \kappa_1/2\pi = 25\ kHz$, with $E_1 = 7.35 \times 10^{13}$, $E_2 = 5.44 \times 10^{13}$ and the modulation amplitude is $E_\Omega = 4.41 \times 10^{13}$. (b) Steady-state entanglement under the time modulation on the driving field of the blue detuned-cavity. Parameters are the same with (a) except the driving amplitudes $E_1 = 6.67\times10^{12}\ Hz$, $E_2 = 7.79\times10^{12}$ Hz. The modulation amplitude is $E_\Omega = 0.8\ E_1$.

The effective linear Hamiltonian

To explain the above observed influence of the time modulation on entanglement generation, one reasonable argument is to obtain an effective Hamiltonian from the linearized Langevin equation Eq.(2.21) and apply a similar argument as it has been in [32]. To do so, one must work with several rotating frames and use the RWA to obtain an effective Hamiltonian responsible for creating entanglement among different subsystems. The original effective Hamiltonian for the time modulation with the red-detuned driving reads,

$$\begin{aligned} H_s &= \hbar\omega_M \hat{b}_M^\dagger \hat{b}_M + \hbar\Delta_1 \hat{a}_1^\dagger \hat{a}_1 + \hbar\Delta_2 \hat{a}_2^\dagger \hat{a}_2 - \frac{1}{2}\left(G_1(t)^* \hat{a}_1 + G_1(t)\hat{a}_1^\dagger\right)\left(\hat{b}_M + \hat{b}_M^\dagger\right) \\ &- \frac{1}{2}\left(G_2(t)^* \hat{a}_2 + G_2(t)\hat{a}_2^\dagger\right)\left(\hat{b}_M + \hat{b}_M^\dagger\right) \end{aligned} \tag{2.26}$$

Here we consider the situation of the strength of the red-detuned driving field is much stronger than the blue detuned driving field, i.e. $E_1 > E_2$. One could treat $G_2(t)$ as time-dependent while treating $G_1(t)$ as a constant, i.e. $G_1(t) = G_1 + G_\Omega e^{-i\Omega t}$ and

$G_2(t) = G_2$. The system Hamiltonian could be expressed as $H_s = H_0 + H_1 + H_2$ and

$$H_0 = \hbar\omega_M \hat{b}_M^\dagger \hat{b}_M + \hbar\Delta_1 \hat{a}_1^\dagger \hat{a}_1 + \hbar\Delta_2 \hat{a}_2^\dagger \hat{a}_2, \tag{2.27}$$

$$H_1 = -\frac{1}{2}G_1\left(\hat{a}_1 + \hat{a}_1^\dagger\right)\left(\hat{b}_M + \hat{b}_M^\dagger\right) - \frac{1}{2}G_2\left(\hat{a}_2 + \hat{a}_2^\dagger\right)\left(\hat{b}_M + \hat{b}_M^\dagger\right), \tag{2.28}$$

$$H_2 = -\frac{1}{2}G_\Omega\left(e^{i\Omega t}\hat{a}_1 + e^{-i\Omega t}\hat{a}_1^\dagger\right)\left(\hat{b}_M + \hat{b}_M^\dagger\right), \tag{2.29}$$

By setting $\Delta_1 = \omega_M$ and $\Delta_2 = -\omega_M$, in the rotating frame of H_0 and applying the RWA, one could further simplify H_1 and H_2 as

$$H_1' \simeq -\frac{1}{2}G_1\left(\hat{a}_1\hat{b}_M^\dagger + \hat{a}_1^\dagger\hat{b}_M\right) - \frac{1}{2}G_2\left(\hat{a}_2\hat{b}_M + \hat{a}_2^\dagger\hat{b}_M^\dagger\right), \tag{2.30}$$

$$H_2' \simeq -\frac{1}{2}G_\Omega\left(e^{i(\Omega-2\omega_M)t}\hat{a}_1\hat{b}_M + e^{-i(\Omega-2\omega_M)t}\hat{a}_1^\dagger\hat{b}_M^\dagger\right), \tag{2.31}$$

where the fast oscillating terms have been dropped by the RWA. By introducing the Bogoliubov modes: $\hat{\beta}_A = \cosh r\hat{a}_1 + \sinh r\hat{a}_2^\dagger$, $\hat{\beta}_B = \sinh r\hat{a}_1^\dagger + \cosh r\hat{a}_2$ and $\hat{C}_\pm = \hat{\beta}_A \pm \hat{b}_M/\sqrt{2}$ with $\tanh r = G_2/G_1$, the Hamiltonian H_1' becomes diagonal, i.e.

$$H_1' \simeq -\frac{1}{2}\tilde{G}\left(\hat{\beta}_A^\dagger\hat{b}_M + \hat{\beta}_A\hat{b}_M^\dagger\right) = -\frac{1}{2}\tilde{G}\left(\hat{C}_+^\dagger\hat{C}_+ - \hat{C}_-^\dagger\hat{C}_-\right) \tag{2.32}$$

Here, $\tilde{G} = \sqrt{G_1^2 - G_2^2}$. We now preform the second rotating frame of H_1', in which the Hamiltonian H_2' has the following form,

$$H_2' \simeq -\frac{1}{2}G_\Omega\left(e^{i(\Omega-2\omega_M)t}\left(\frac{\cosh r}{2}\hat{H}_{CC}(t) - \frac{\sinh r}{\sqrt{2}}\hat{H}_{BC}(t)\right) + h.c.\right) \tag{2.33}$$

with $\hat{H}_{CC}(t) = e^{i\tilde{G}t}\hat{C}_+\hat{C}_+ - e^{-i\tilde{G}t}\hat{C}_-\hat{C}_-$ and $\hat{H}_{BC}(t) = e^{-i\frac{\tilde{G}}{2}t}\hat{\beta}_B^\dagger\hat{C}_+ + e^{i\frac{\tilde{G}}{2}t}\hat{\beta}_B^\dagger\hat{C}_-$. Here are four different resonant frequencies: $\Omega = 2\omega_M \pm \tilde{G}$ and $\Omega = 2\omega_M \pm \frac{\tilde{G}}{2}$. The corresponding four different resonant Hamiltonian are given by

$$H_{2,1}' = -\frac{\cosh r}{4}G_\Omega\left(\hat{C}_+\hat{C}_+ + \hat{C}_+^\dagger\hat{C}_+^\dagger\right), \quad H_{2,2}' = \frac{\cosh r}{4}G_\Omega\left(\hat{C}_-\hat{C}_- + \hat{C}_-^\dagger\hat{C}_-^\dagger\right) \tag{2.34}$$

$$H_{2,3}' = \frac{\sinh r}{2\sqrt{2}}G_\Omega\left(\hat{\beta}_B^\dagger\hat{C}_+ + \hat{C}_+^\dagger\hat{\beta}_B\right), \quad H_{2,4}' = \frac{\sinh r}{2\sqrt{2}}G_\Omega\left(\hat{\beta}_B^\dagger\hat{C}_- + \hat{C}_-^\dagger\hat{\beta}_B\right) \tag{2.35}$$

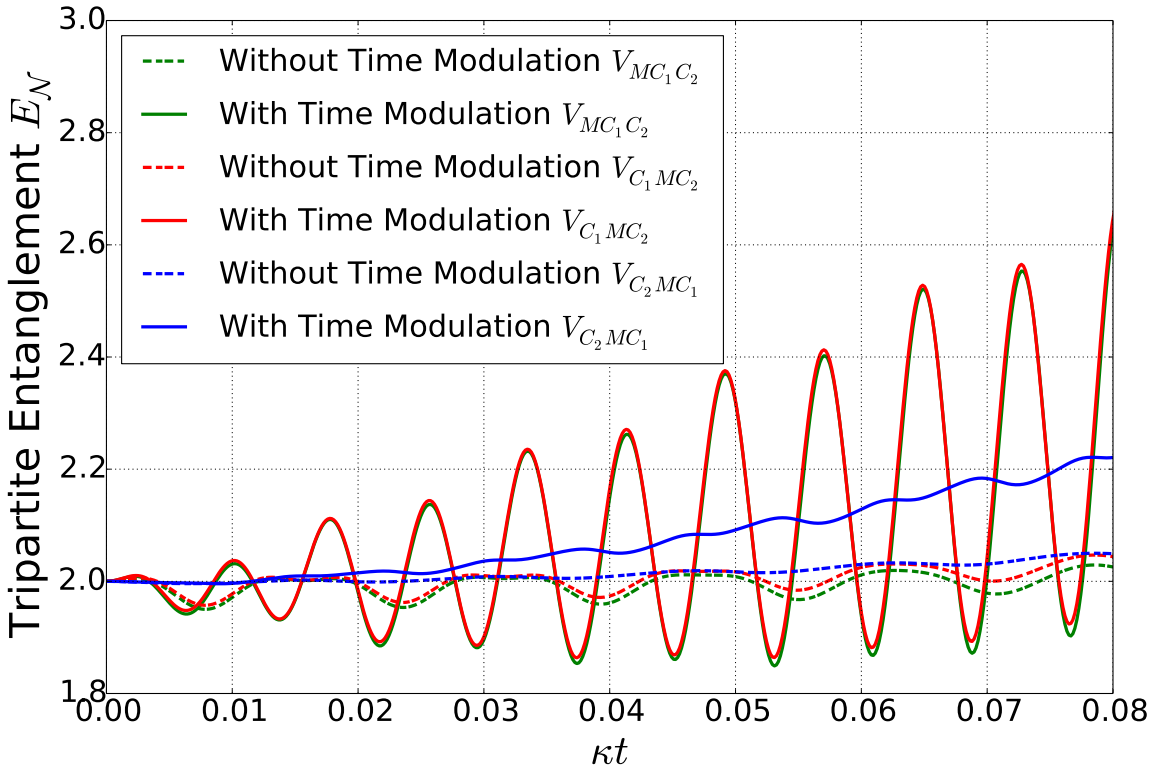

Figure 2.11: The dynamics of tripartite entanglement with time modulation. Dashed cures are the results without time modulation. The mechanical frequency is $\omega_M/2\pi = 10\ MHz$ with its damping as $\gamma_M/2\pi = 400\ Hz$ and the temperature $n_{th} = 0$. The optomechanical couplings are $g_1/2\pi = g_2/2\pi = 1.63\ Hz$. The cavity decay rate is $\kappa_1/2\pi = \kappa_1/2\pi = 25\ kHz$, with $E_1 = 9.024 \times 10^{12} e^{i\pi/2}\ Hz$ and $E_2 = 1.36 \times 10^{12} e^{-i\pi/2}\ Hz$. The time modulation amplitude $E_\Omega = 0.6E_1$.

From the above Hamiltonian, it is shown that if the time modulation frequency was properly tuned, one could arrive at tripartite entanglement using the three-mode squeezing Hamiltonian of Eq.(2.34), or by exchanging state of two cavity modes to achieve the global tripartite entanglement through Eq.(2.35). One example is shown in Fig. 2.11 where the tripartite entanglement is measured by van Loock and Furusawa criterion[59] that the genuine tripartite entanglement exists only if at least one

of the following relation was kept,

$$V_{MC_1C_2} = \Delta\left(\delta\hat{q} - \frac{\delta\hat{X}_1 + \delta\hat{X}_2}{\sqrt{2}}\right)^2 + \Delta\left(\delta\hat{p} + \frac{\delta\hat{Y}_1 + \delta\hat{Y}_2}{\sqrt{2}}\right)^2 < 2, \tag{2.36}$$

$$V_{C_1MC_2} = \Delta\left(\delta\hat{X}_1 - \frac{\delta\hat{q} + \delta\hat{X}_2}{\sqrt{2}}\right)^2 + \Delta\left(\delta\hat{Y}_1 + \frac{\delta\hat{p} + \delta\hat{Y}_2}{\sqrt{2}}\right)^2 < 2, \tag{2.37}$$

$$V_{C_2MC_1} = \Delta\left(\delta\hat{X}_2 - \frac{\delta\hat{X}_1 + \delta\hat{q}}{\sqrt{2}}\right)^2 + \Delta\left(\delta\hat{Y}_2 + \frac{\delta\hat{Y}_1 + \delta\hat{p}}{\sqrt{2}}\right)^2 < 2, \tag{2.38}$$

where $\Delta(\hat{A})^2 = \langle\hat{A}^2\rangle - \langle\hat{A}\rangle^2$. As it is evident from Fig. 2.11, the tripartite entanglement for the three-mode optomechanical system is transient and under the time modulation the system tends to stay with the tripartite entanglement for a longer time.

Conclusions

In this study, we successfully demonstrated that the time modulated driving could be employed to enhance the quantum correlations for the three-mode optomechanical system, as this chapter shows that the cavity-cavity entanglement or cavity-mechanical mode entanglement is enhanced by the periodic driving. Our study provides one additional way to optically control the quantum property of the optomechanical system, which has the potential applications in the field of quantum communication, where the mechanical oscillator works as a transistor for different cavity modes which carry the quantum information to implement the communication. The time modulation scheme discussed in this research provides one approach to control the communication via enhancing or reducing the quantum correlations between different cavity modes.

However, the current research did not consider the relation among the time modulation and the many body entanglement behaviors of the three-mode optomechanical system, although, one example for quantum tripartite entanglement is demonstrated at the end of this chapter. Such a many body behavior may have potential applications for quantum communication. The effective Hamiltonian approach developed here could be the basis for the future research in this direction.

Chapter 3

Nonlinear Optomechanical Effects with Perturbation

As discussed in the previous chapters, the linearized optomechanical model, based on the approximation that all quantum fluctuations are small, has been successfully applied to fully describe many interesting optomechanical phenomena, including optomechanical cooling [60, 20, 61], OMIT[35, 36, 37], steady-state optomechanical entanglement generation [29, 31] and optical string effects [62, 63]. However, even the linearized optomechanical model itself could be used to predict the breakdown of its basic assumption of the small fluctuations. As discussed in Chapter 2, with a large enough driving field and proper cavity detuning, the optomechanical system could become unstable. As a result, the mechanical amplitude grows exponentially with time, and any initial fluctuations would become extra large, which breaks down the basic approximation of the linearized model, and causes it to fail to correctly characterize the dynamics for the optomechanical system in the unstable regime.

Even for the stable optomechanical system, provided that the radiation pressure coupling is strong enough, many details of the optomechanical dynamics due to the nonlinear optomechanical interactions are not resolved by the linearized optomechanical model, which provides another reason for us to study the nonlinear effects in the optomechanical system. However, there are few theoretical tools to deal with the influence of nonlinear interaction in the optomechanical dynamics, especially with the open system dynamics of both the cavity decay and the mechanical damping involved. This chapter is, therefore, devoted to investigate the influence of the nonlinear optomechanical interaction in the system dynamics under an intermediate radiation pressure coupling strength, where the nonlinear terms could be treated as perturbations to the linearized optomechanical model.

We address the problem by dealing with the perturbations of the quantum operator equations in the Heisenberg picture, which are known as the quantum Langevin equations. Because of the weak optomechanical coupling, the nonlinear terms in

the quantum Langevin equations could be treated as perturbations of the linear optomechanical interaction. Therefore one can expand all the operators in terms of the different orders of this weak coupling. The zero order operator equations correspond to the case of the linearized optomechanical model, with its solutions easily obtainable as it has been done in the previous chapters; while in the higher order operator equations, the original nonlinear terms appear as time dependent driving terms, made up with the solutions from the lower order equations. In this way, the nonlinear optomechanical quantum Langevin equations are converted into a set of inhomogeneous linear operator equations, and one could, therefore, solve them order by order, details of which are shown in this chapter.

3.1 Introduction

The radiation pressure interaction in the standard optomechanical system is essentially a nonlinear interaction in the sense that its Heisenberg equations for the field operators are nonlinear. However, with the strong classical driving, the standard optomechanical system is well approximated with the linearized model, where the radiation pressure interaction in the system Hamiltonian becomes quadratic of the field operators, corresponding to an effective beam-splitter like interaction, or two-mode squeezing interaction, experimentally tuned at will via the control of the driving laser frequency. This linearized approach has been used to study various interesting features of the standard optomechanical system, such as the ground-state cooling of mechanical oscillators [46], quantum standard limit for the displacement detection [64] and optomechanical squeezing of cavity field [65, 66]. However, the linearized optomechanical model breaks down when the system is unstable or with a strong optomechanical coupling g_0, where the pure linear model fails to describe the nonlinear effects of the standard optomechanical system. Most studies today could only treat this nonlinearity in the classical regime with large cavity driving, while the influence of the nonlinearity in the dynamical behavior for the quantum optomechanical system is still unclear to us.

In this study, we address this problem for the optomechanical system with an intermediate radiation pressure coupling strength, where the influence of the nonlinearity could be treated as perturbations to the linear model. We deal with the open system dynamics in the Heisenberg picture via the nonlinear Langevin equations for field operators. It turns out that by treating the optomechanical coupling as a small parameter, one could convert the nonlinear quantum Langevin equations into a set of linear equations with nonlinear terms replaced by time dependent driving, which can then be solved with the standard perturbation approach.

3.2 Optomechanical System

The system we considered is a standard optomechanical system with a continuous driving laser at frequency ω_L and amplitude E, for which the system Hamiltonian reads

$$H_s = \hbar\Delta_0\hat{a}_c^\dagger\hat{a}_c + \hbar\omega_M b^\dagger b + \hbar g_0\left(\hat{b}_M^\dagger + \hat{b}_M\right)\hat{a}_c^\dagger\hat{a}_c + i\hbar E\left(\hat{a}_c^\dagger - \hat{a}_c\right) \tag{3.1}$$

with $\hat{a}_c$ and $\hat{b}_M$ as the annihilation operator of the cavity mode and mechanical mode, respectively. Here $\Delta_0 = \omega_c - \omega_L$ is the cavity detuning showing the difference between the driving laser frequency ω_L and the cavity resonance ω_c. To express our perturbation effectively, we need to work in a displacement picture described by the unitary transformation of $\mathcal{U} = D_c\left(\alpha_{ss}\right) D_M\left(\beta_{ss}\right)$, with complex amplitudes $\alpha_{ss} = \left(-i\Delta + \kappa\right)^{-1} E$, $\beta_{ss} = -g_0|\alpha_{ss}|^2/\sqrt{2}\omega_M$. Here the cavity displacement operator $D_c(\alpha)$ is defined as $D_c(\alpha) = e^{\alpha^*\hat{a}_c - \alpha\hat{a}_c^\dagger}$ and similarly for the mechanical displacement operator $D_M(\beta)$. In this displacement picture, the system's Hamiltonian reads

$$\bar{H}_s = \mathcal{U}H_s\mathcal{U}^{-1} = \hbar\Delta\hat{a}_c^\dagger\hat{a}_c + \hbar\omega_M\hat{b}_M^\dagger\hat{b}_M + \hbar g\left(\hat{a}_c^\dagger + \hat{a}_c\right)\left(\hat{b}_M^\dagger + \hat{b}_M\right) + \hbar g_0\hat{a}_c^\dagger\hat{a}_c\left(\hat{b}_M^\dagger + \hat{b}_M\right) \tag{3.2}$$

with $g = g_0\alpha_{ss}$ and $\Delta = \Delta_0 + g_0\left(\beta_{ss}^* + \beta_{ss}\right)$. Under the strong driving, the above treatment is equivalent to the standard linearization process, where the small nonlinear terms (the last term of Eq.(3.2)) are instead neglected. However, in the intermediate coupling regime, the contribution from the g_0 is non-zero, and its influence is observable from its dynamics. The full dynamical equations, including the cavity decay and the mechanical damping, are

$$\frac{d\hat{u}(\tau)}{d\tau} = M\cdot\hat{u}(\tau) + \hat{n}(\tau) + \epsilon\cdot G(\hat{u}(\tau)) \tag{3.3}$$

with the system operator vector defined as $\hat{u}(\tau) = \left(\hat{b}_M(\tau),\ \hat{b}_M^\dagger(\tau),\ \hat{a}_c(\tau),\ \hat{a}_c^\dagger(\tau)\right)^T$ and noise vector as $\hat{n}(\tau) = g^{-1}\left(-\sqrt{\gamma_M}\hat{b}_{in}(\tau),\ -\sqrt{\gamma_M}\hat{b}_{in}^\dagger(\tau),\ -\sqrt{2\kappa}\ a_{in}(\tau),\ -\sqrt{2\kappa}\ a_{in}^\dagger(\tau)\right)^T$. Here we have rescaled the time t as $\tau = gt$ so that the dimensionless small number $\epsilon = g_0/g$ is shown in the above equation. The coefficient matrix M is

$$M = \begin{pmatrix} -i\tilde{\omega}_M - \frac{\tilde{\gamma}_M}{2} & \frac{\tilde{\gamma}_M}{2} & -i & -i \\ \frac{\tilde{\gamma}_M}{2} & i\tilde{\omega}_M - \frac{\tilde{\gamma}_M}{2} & i & i \\ -i & -i & -i\tilde{\Delta} - \tilde{\kappa} & 0 \\ i & i & 0 & i\tilde{\Delta} - \tilde{\kappa} \end{pmatrix} \tag{3.4}$$

and the nonlinear terms are denoted as

$$G(\hat{u}\left(\tau\right)) = \left(-i\hat{N}_c(\tau), i\hat{N}_c(\tau), -i\hat{a}_c(\tau)\hat{X}_M(\tau), i\hat{a}_c^\dagger(\tau)\hat{X}_M(\tau)\right)^T$$

with $\hat{N}_c(t) = \hat{a}_c^\dagger(\tau)\hat{a}_c(\tau)$ and $\hat{X}_M(t) = \hat{b}_M^\dagger(t) + \hat{b}_M(t)$. All the parameters with tilde indicate they have been divided by g, for example, $\tilde{\omega}_M = \omega_M/g$. Here $\hat{a}_{in}$ is the vacuum radiation input noise whose nonzero correlation function at optical frequency $\hbar\omega_c/k_BT \gg 1$ is

$$\langle \hat{a}_{in}(t)\, \hat{a}_{in}^\dagger(t')\rangle = \delta(t-t') \tag{3.5}$$

and $\hat{b}_{in}$ describes the Brownian motion for the mechanical oscillator. The correlation functions are chosen as,

$$\langle \hat{b}_{in}^\dagger(t)\hat{b}_{in}(t')\rangle = \bar{n}\delta(t-t') \tag{3.6a}$$

$$\langle \hat{b}_{in}(t)\hat{b}_{in}^\dagger(t')\rangle = (\bar{n}+1)\delta(t-t') \tag{3.6b}$$

with $\bar{n} = \left(e^{\hbar\omega_M/K_BT} - 1\right)^{-1}$, and we assumed that the mechanical quality factor $Q_M = \omega_M/\gamma_M \gg 1$.

3.3 Perturbation in the Heisenberg Picture

With a strong cavity driving amplitude E and the dimensionless number $\epsilon = g_0/g \sim E^{-1} \ll 1$, we could treat ϵ as a small number and solve Eq.(3.3) in a perturbational way,

$$\hat{u}(\tau,\epsilon) = \hat{u}^{(0)}(\tau) + \epsilon\hat{u}^{(1)}(\tau) + \epsilon^2\hat{u}^{(2)}(\tau) + \dots \tag{3.7}$$

By inserting it back into Eq.(3.3) and collect different orders of ϵ, one arrives at a set of linear equations. The equation for the zero order of ϵ is given by

$$\frac{d\hat{u}^{(0)}(\tau)}{d\tau} = M\cdot\hat{u}^{(0)}(\tau) + \hat{n}(\tau), \tag{3.8}$$

and the initial condition is $\hat{u}^{(0)}(0) = (\hat{b}_M, \hat{b}_M^\dagger, \hat{a}_c, \hat{a}_c^\dagger)^T$, the same equation obtained in the linearized optomechanical model. The first order of ϵ shows that

$$\frac{d\hat{u}^{(1)}(\tau)}{d\tau} = M\cdot\hat{u}^{(1)}(\tau) + \mathrm{g}(\hat{u}^{(0)}(\tau)) \tag{3.9}$$

with $\hat{u}^{(1)}(0) = 0$ as the initial condition and the inhomogeneous term $\mathrm{g}(\hat{u}^{(0)}(\tau)) = (-i\hat{N}_c^{(0)}(\tau), i\hat{N}_c^{(0)}(\tau), -i\Xi_\tau^{(0)}, i\Xi_\tau^{(0),\dagger})^T$, where $\Xi_\tau^{(0)} = \hat{a}_c^{(0)}(\tau)\hat{X}_M^{(0)}(\tau)$. With the solutions of Eq.(3.8), term of $\mathrm{g}(\hat{u}^{(0)})$ is a known time dependent function so that the above equation is still a linear equation. Similarly, the second order of ϵ shows that

$$\frac{d\hat{u}^{(2)}(\tau)}{d\tau} = M\cdot\hat{u}^{(2)}(\tau) + \mathrm{g}(\hat{u}^{(0)}(\tau), \hat{u}^{(1)}(\tau)) \tag{3.10}$$

with $\hat{u}^{(2)}(0) = 0$ as the initial condition and the inhomogeneous term $\mathrm{g}(\hat{u}^{(0)}(\tau), \hat{u}^{(1)}(\tau)) = (-i\hat{N}_c^{(0,1)}(\tau), i\hat{N}_c^{(0,1)}(\tau), -i\Xi_{(\tau)}^{(0,1)}, i\Xi_{(\tau)}^{(0,1),\dagger})^T$ with $\hat{N}_c^{(0,1)}(\tau) = \hat{a}_c^{(0),\dagger}(\tau)\hat{a}_c^{(1)}(\tau) + \hat{a}_c^{(1),\dagger}(\tau)\hat{a}_c^{(0)}(\tau)$ and $\Xi_{(\tau)}^{(0,1)} = \hat{a}_c^{(0)}(\tau)\hat{X}_M^{(1)}(\tau) + \hat{a}_c^{(1)}(\tau)\hat{X}_M^{(0)}(\tau)$. In practice, we stop at the second order and focus on the solutions for the above linear operator equations.

Perturbative solutions

The Langevin equations for the zero order $\hat{u}^{(0)}(\tau)$ can be solved by diagonalizing the coefficient matrix M,

$$U \cdot M \cdot U^{-1} = diag[\lambda_1, \lambda_2, \lambda_3, \lambda_4] \equiv D \tag{3.11}$$

and defining the canonical vector as

$$\hat{\xi}^{(0)}(\tau) = U \cdot \hat{u}^{(0)}(\tau) \tag{3.12}$$

Here the equation of motion for $\hat{\xi}^{(0)}(\tau)$ reads

$$\frac{d\hat{\xi}^{(0)}(\tau)}{d\tau} = D \cdot \hat{\xi}^{(0)}(\tau) + U \cdot \hat{n}(\tau) \tag{3.13}$$

Because the matrix D has the diagonal form, $\hat{\xi}^{(0)}(\tau)$ can be easily integrated out as,

$$\hat{\xi}^{(0)}(\tau) = e^{Dt}\hat{\xi}^{(0)}(0) + e^{Dt}\int_0^\tau dt' e^{-Dt'} U \cdot \hat{n}(t') \tag{3.14}$$

with $e^{\pm Dt} \equiv diag[e^{\pm\lambda_1 t}, e^{\pm\lambda_2 t}, e^{\pm\lambda_3 t}, e^{\pm\lambda_4 t}]$. By taking the inverse matrix of U, one arrives at the solution for $\hat{u}^{(0)}$,

$$\hat{u}^{(0)}(\tau) = U^{-1} \cdot \hat{\xi}^{(0)}(\tau) = U^{-1}e^{Dt}U \cdot \hat{u}^{(0)}(0) + U^{-1}e^{Dt}\int_0^\tau dt' e^{-Dt'} U \cdot \hat{n}(t') \tag{3.15}$$

we can solve the first order and second order equations with a similar approach as the zero order, and the only difference is that $\hat{n}(t)$ should be replaced by the corresponding g functions, the solutions are

$$\hat{u}^{(1)}(\tau) = U^{-1}e^{Dt}\int_0^\tau dt' e^{-Dt'} U \cdot \mathrm{g}(\hat{u}^{(0)}(t')), \tag{3.16}$$

$$\hat{u}^{(2)}(\tau) = U^{-1}e^{Dt}\int_0^\tau dt' e^{-Dt'} U \cdot \mathrm{g}(\hat{u}^{(0)}(t'), \hat{u}^{(1)}(t')), \tag{3.17}$$

Here $\mathrm{g}(\hat{u}^{(0)}(t'))$ and $\mathrm{g}(\hat{u}^{(0)}(t'), \hat{u}^{(1)}(t'))$ are defined in the preceding section. Combining all these orders yields the second order solution for the system operators,

$$\hat{u}(\tau) \approx \hat{u}^{(0)}(\tau) + \epsilon\hat{u}^{(1)}(\tau) + \epsilon^2\hat{u}^{(2)}(\tau) \tag{3.18}$$

with $\epsilon = g_0/g \ll 1$.

3.4 Applications of the Perturbation Solutions

Field amplitude

In this part, we focus on the application of the above formalism in finding the field amplitude operators, such as $\langle \hat{a}_c \rangle$ and $\langle \hat{b}_M \rangle$, under the first order perturbation. Starting from Eq.(3.18), one can show that the average values of the operator vector is

$$\langle \hat{u}(\tau) \rangle \approx \langle \hat{u}^{(0)}(\tau) \rangle + \epsilon \langle \hat{u}^{(1)}(\tau) \rangle \tag{3.19}$$

By choosing the system's initial state characterized by the correlation matrix,

$$V = \langle \hat{u}(\tau = 0) \hat{u}^T(\tau = 0) \rangle \tag{3.20}$$

and the noise correlation functions of the standard optomechanical system in Eq.(3.5) and Eq.(3.6), one could prove that the second moment of the system under the first order perturbation reads (Appendix B.1)

$$\begin{aligned} \langle \hat{u}_i^{(0)}(t) \hat{u}_j^{(0)}(t) \rangle &= \sum_{l,l',n,n'} e^{(\lambda_l + \lambda_{l'})t} U_{il}^{-1} U_{jl'}^{-1} U_{ln} U_{l'n'} V_{nn'} \\ &\quad + \sum_{l,l'} \frac{e^{(\lambda_l + \lambda_{l'})t} - 1}{g \cdot (\lambda_l + \lambda_{l'})} U_{il}^{-1} U_{jl'}^{-1} W_{l,l'} \end{aligned} \tag{3.21}$$

and $W_{l,l'} = \bar{n}\tilde{\gamma}_M U_{l2} U_{l'1} + (\bar{n}+1)\tilde{\gamma}_M U_{l1} U_{l'2} + 2\tilde{\kappa} U_{l3} U_{l'4}$. This yields the i-th element of $\langle \hat{u}^{(1)}(\tau) \rangle$,

$$\langle \hat{u}^{(1)}(\tau) \rangle_i = i \sum_k U_{ik}^{-1} \Big((U_{k2} - U_{k1}) \cdot G_1(k,\tau) - U_{k3} F_1(k,\tau) + U_{k4} F_2(k,\tau) \Big) \tag{3.22}$$

Here G_1 describes the nonlinear contributions of the radiation force on the mechanical oscillator, while F_i characterizes the nonlinear feedbacks of the mechanical oscillator on the cavity field. Their expressions could be found in the Eq.(B.17) of Appendix B.1. As a result, the amplitude of the field operator is expressed as,

$$\begin{aligned} \langle \hat{u}(\tau) \rangle_i &\approx \sum_{k,l} U_{i,k}^{-1} e^{\lambda_k \tau} U_{k,l} \cdot \langle \hat{u}^{(0)}(0) \rangle_l \\ &+ i\epsilon \cdot \sum_k U_{ik}^{-1} \Big((U_{k2} - U_{k1}) \cdot G_1(k,\tau) - U_{k3} F_1(k,\tau) + U_{k4} F_2(k,\tau) \Big) \end{aligned} \tag{3.23}$$

Combined with U calculated from the coefficient matrix M of Eq.(3.3), we could apply the above results to study the influence of the nonlinear optomechanical interaction

on the linearized optomechanical model, which can be done both numerically and analytically. In general, the form of U is usually involved, however, in the appendix B.3, we discuss special situations where the analytical form of U is available and, therefore, all our results could be analytically expressed. Here, we will focus on the numerical application of Eq.(3.23).

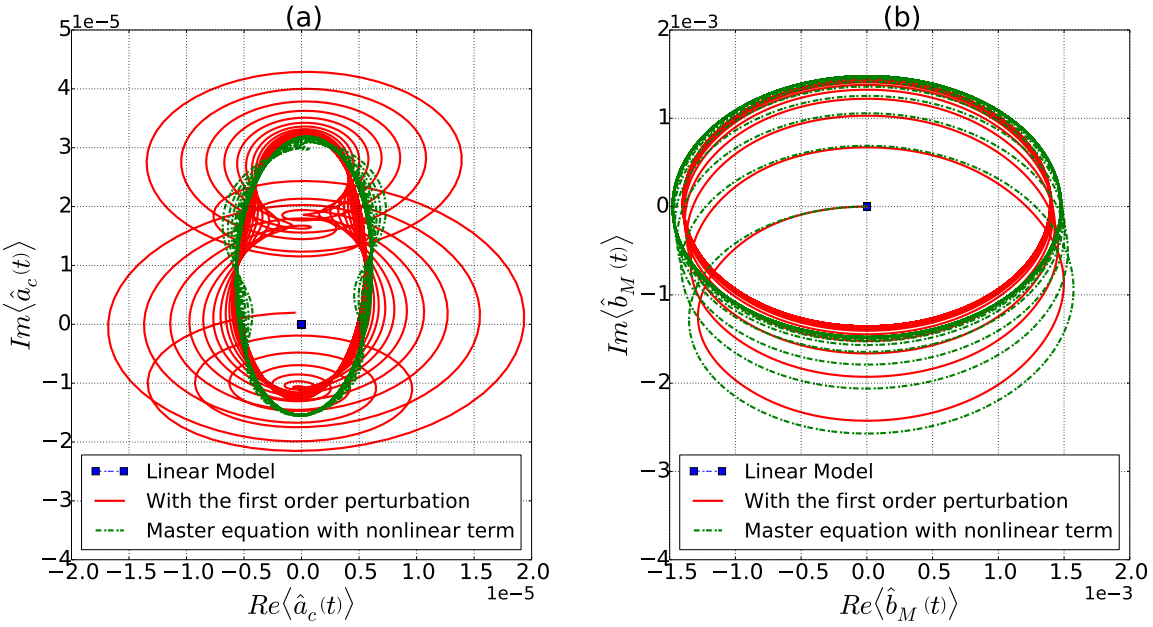

Figure 3.1: The dynamics of (a) cavity field amplitude and (b) mechanical amplitude under the perturbation method. System parameters are : the mechanical frequency $\omega_M/2\pi = 1$ MHz; $\gamma_M = \omega_M/10^5$; and the mechanical thermal bath temperature is $n_{th} = 1$. The cavity field is red-detuned at $\Delta = 4\omega_M$, with cavity decay rate $\kappa = 0.05\omega_M$, $g = 0.05\omega_M$ and $g_0 = 0.3\kappa$.

The first example we studied here is about the optomechanical dynamics starting from a thermal initial state. The parameters are shown in Fig. 3.1 and the initial thermal occupation number is $\bar{n} = 1$ for both the cavity field and the mechanical mode. Green curves are the solution of the master equation method of the standard optomechanical model with the nonlinear interaction terms included. Red curves are the results of the first order perturbation, and blue squares are the result of the linearized optomechanical model. With this choice of initial state, the initial amplitude of the fluctuation operators are zero, which is, in fact, the steady-state for the linearized optomechanical model (blue square in the figure) and, therefore, the linearized equations have no dynamics in this case. However, when the contribution from the nonlinear optomechanical interaction are considered, the system dynamics reappear (green and red curves). This has been captured by both the master equation

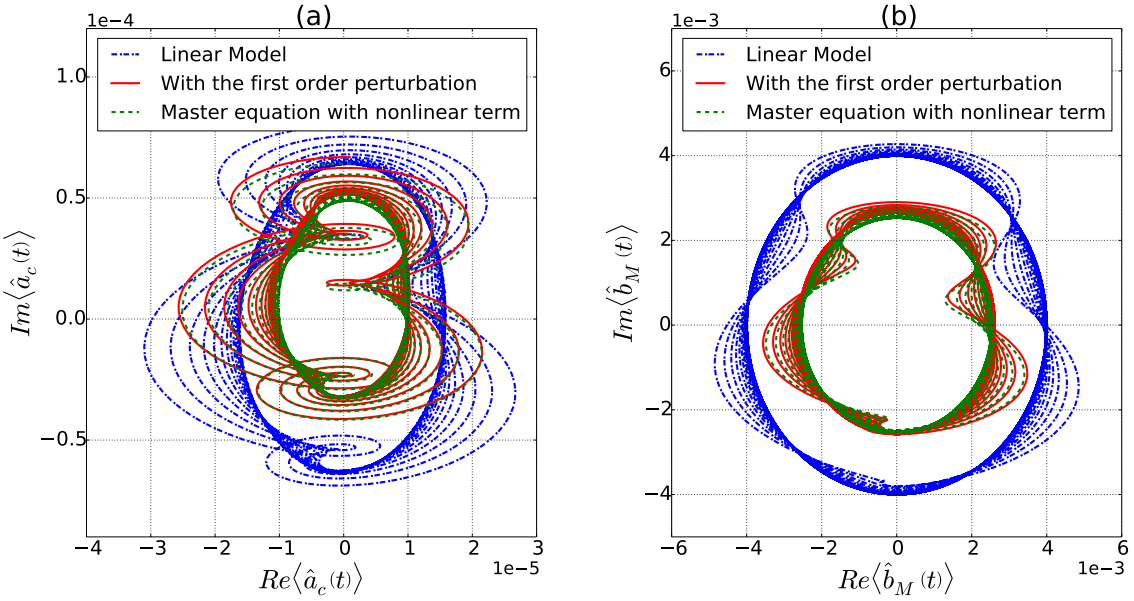

Figure 3.2: The dynamics of (a) cavity field amplitude and (b) mechanical amplitude under the perturbation method. System parameters are : The mechanical frequency $\omega_M/2\pi = 1$ MHz, $\gamma_M = \omega_M/10^5$ and the mechanical thermal bath temperature is $n_{th} = 1$. The cavity field is red detuned at $\Delta = 4\omega_M$, with cavity decay rate $\kappa = 0.05\omega_M$, $g = 0.03\omega_M$ and $g_0 = 0.03\kappa$.

approach and the first order perturbation approach. Fig. 3.1 also confirms that the first order perturbation gives similar dynamics to the master equation method.

The scenario with the nonzero linearized dynamics is also studied here with the following initial state,

$$\rho_{initial} = |\alpha\rangle_c\langle\alpha| \otimes \rho_{thermal} \tag{3.24}$$

Fig. 3.2 compares the results of the first order perturbation, as well as, the master equation approach to the linearized optomechanical model. Here the cavity field amplitude $\alpha = 1$, and the average mechanical phonon occupation number $\bar{n} = 1$. It shows that the linearized dynamics are not only different from the perturbation results but it arrives at a different steady-state, indicating that the nonlinear interaction must be taken into consideration for this scenario. It is important to note that the cavity detuning is the leading factor for such different dynamics. Because at the cavity detuning of $\Delta = 4\omega_M$, the nonlinear optomechanical is at resonance, while the linear optomechanical interaction is depressed by being out of resonance. When the cavity detuning becomes resonant with linearized optomechanical interaction, such as $\Delta = \omega_M$, the linearized optomechanical model and the perturbation yields similar dynamics. This is reported in Fig. 3.3 with all three color curves become indistinguishable. Furthermore, we found that the influence of the nonlinear terms increases

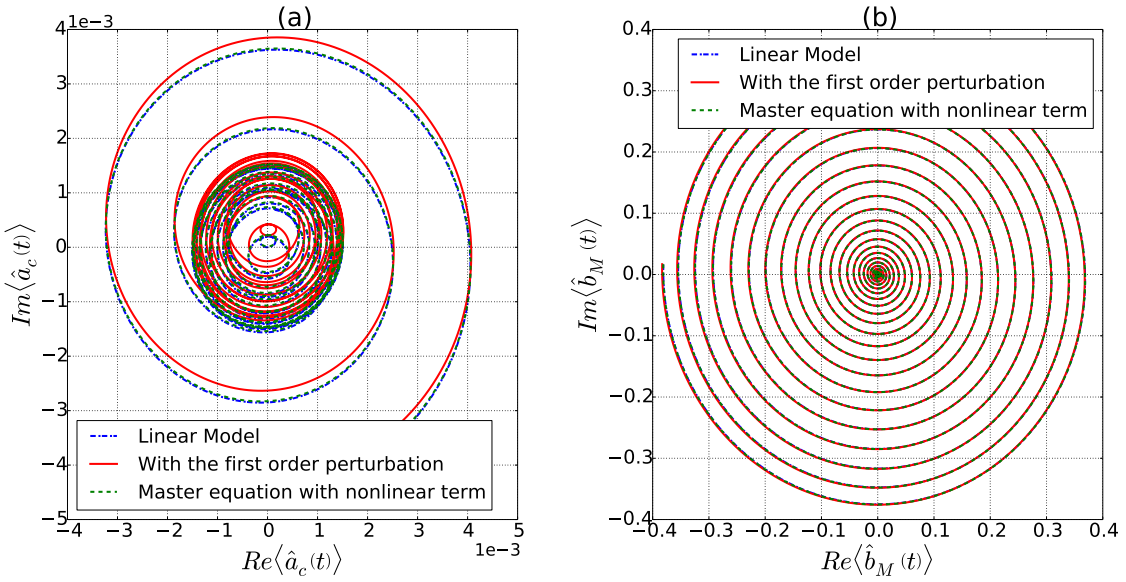

Figure 3.3: The dynamics of (a) cavity field amplitude and (b) mechanical amplitude under the perturbation method. System parameters are the same as Fig. 3.2 but with a different detuning at $\Delta = \omega_M$.

with the optomechanical coupling g_0. One such example is shown in Fig. 3.4, where the optomechanical coupling strength is increased to $g_0 = 0.1\kappa$ and the resulting difference between the linearized optomechanical model and the perturbation method is increased while the perturbation approach is still consistent with the master equation approach.

Quantum optomechanical correlations

In this section, we focus on the influence of nonlinear optomechanical interaction on the dynamics of the second moment of the standard optomechanical system, from which the quantum optomechanical correlation can be extracted. Under the first perturbation theory, the solution of the system operators are given by

$$\hat{u}(\tau) \approx \hat{u}^{(0)}(\tau) + \epsilon \cdot \hat{u}^{(1)}(\tau) \tag{3.25}$$

where the zero order solution $\hat{u}^{(0)}(\tau)$ is in Eq.(3.15) and the first order solution $\hat{u}^{(1)}(\tau)$ in Eq.(3.16). The second moment of the system could, therefore, be expressed as

$$\langle\hat{u}_i(\tau)\hat{u}_j(\tau)\rangle = \langle\hat{u}_i^{(0)}(\tau)\hat{u}_j^{(0)}(\tau)\rangle + \epsilon \cdot \langle\Big(\hat{u}_i^{(1)}(\tau)\hat{u}_j^{(0)}(\tau) + \hat{u}_i^{(0)}(\tau)\hat{u}_j^{(1)}(\tau)\Big)\rangle \tag{3.26}$$

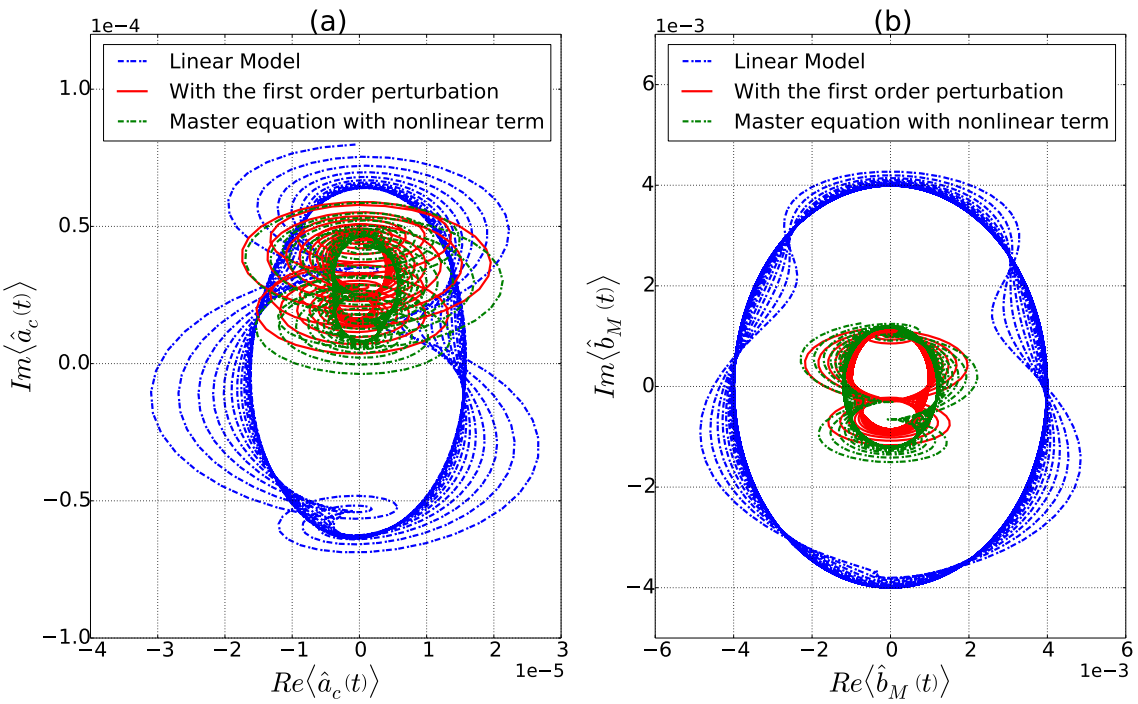

Figure 3.4: The dynamics of (a) cavity field amplitude and (b) mechanical amplitude under the perturbation method. System parameters are the same as FIG.3.2 but with a different optomechanical coupling at $g_0 = 0.1\kappa$.

If all the third moment for the initial state are known, one could simplify the above results as

$$\langle\hat{u}_i^{(1)}(\tau)\hat{u}_j^{(0)}(\tau)\rangle = i\sum_k U_{ik}^{-1}\Big(\Delta U_k\Lambda_1(k,\tau) - U_{k3}\Lambda_2(k,\tau) + U_{k4}\Lambda_3(k,\tau)\Big), \tag{3.27}$$

$$\langle\hat{u}_i^{(0)}(\tau)\hat{u}_j^{(1)}(\tau)\rangle = i\sum_k U_{jk}^{-1}\Big(\Delta U_k\Lambda_1'(k,\tau) - U_{k3}\Lambda_2'(k,\tau) + U_{k4}\Lambda_3'(k,\tau)\Big), \tag{3.28}$$

Here $\Delta U_k = U_{k2} - U_{k1}$ and the analytical form of U, Λ_i and Λ_i' are provided in Appendix B.2 with detailed derivations. Fig. 3.5 shows the resulting dynamics of the cavity photon number and mechanical phonon number, indicating that the first order perturbation has no influence on the cavity photons while slightly modifies the mechanical phonon dynamics. Such a result is expected since the nonlinear optomechanical interaction commute with the cavity photon number operator, indicating that the cavity photon number should be unperturbed by the nonlinear optomechanical interaction.

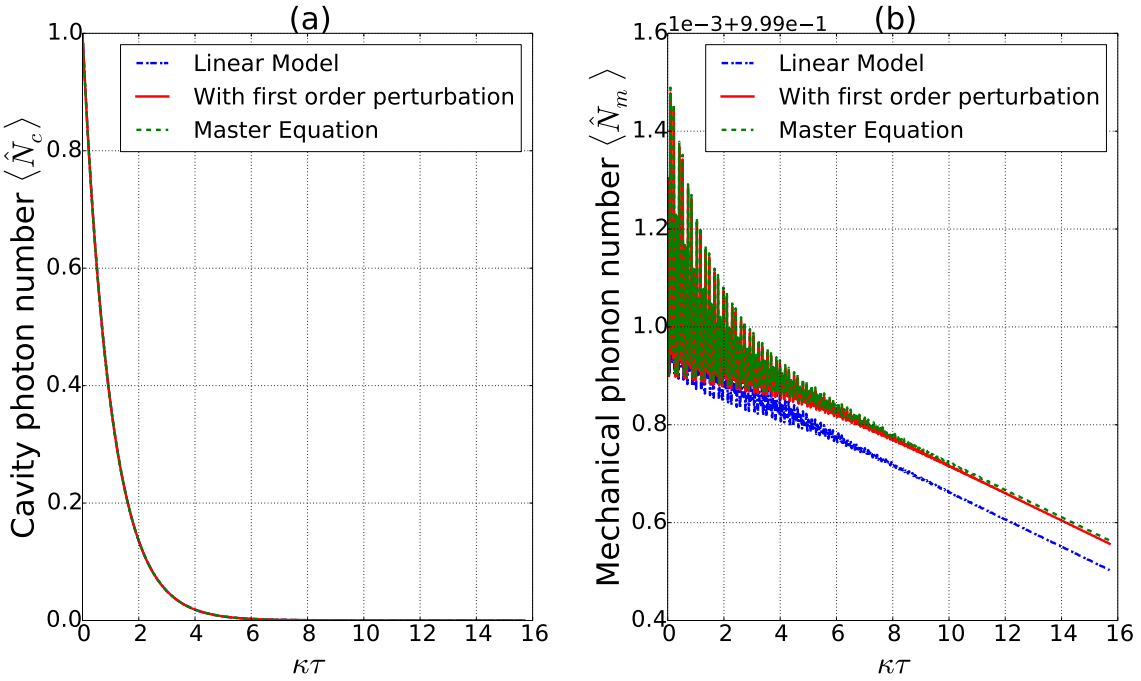

Figure 3.5: The dynamics of (a) cavity photon numbers and (b) the mechanical phonon numbers under the perturbation method. System parameters are the same as FIG.3.2.

We also investigate the influence of the nonlinear interaction on the entanglement generation for the standard optomechanical system. In order to quantify the optomechanical entanglement with nonlinear interaction, which is non-Gaussian in this case, we employ the method developed in [67] where the moments of field operators are employed to characterize the entanglement for a continuous variable system, equivalent to the positive partial transpose criteria (PPT). With the second moments calculated from the first perturbation theory above, we could build the entanglement criteria equivalent to Simon's criteria of [68] with

$$E_n = -det \begin{vmatrix} 1 & \langle \hat{a}_c \rangle & \langle \hat{a}_c^\dagger \rangle & \langle \hat{b}_M^\dagger \rangle & \langle \hat{b}_M \rangle \\ \langle \hat{a}_c^\dagger \rangle & \langle \hat{a}_c^\dagger \hat{a}_c \rangle & \langle \hat{a}_c^{\dagger 2} \rangle & \langle \hat{a}_c^\dagger \hat{b}_M^\dagger \rangle & \langle \hat{a}_c^\dagger \hat{b}_M \rangle \\ \langle \hat{a}_c \rangle & \langle \hat{a}_c^2 \rangle & \langle \hat{a}_c \hat{a}_c^\dagger \rangle & \langle \hat{a}_c \hat{b}_M^\dagger \rangle & \langle \hat{a}_c \hat{b}_M \rangle \\ \langle \hat{b}_M \rangle & \langle \hat{a}_c \hat{b}_M \rangle & \langle \hat{a}_c^\dagger \hat{b}_M \rangle & \langle \hat{b}_M^\dagger \hat{b}_M^\dagger \rangle & \langle \hat{a}_c^2 \rangle \\ \langle \hat{b}_M^\dagger \rangle & \langle \hat{a}_c \hat{b}_M^\dagger \rangle & \langle \hat{a}_c^\dagger \hat{b}_M^\dagger \rangle & \langle \hat{b}_M^{\dagger 2} \rangle & \langle \hat{b}_M \hat{b}_M \rangle \end{vmatrix} \tag{3.29}$$

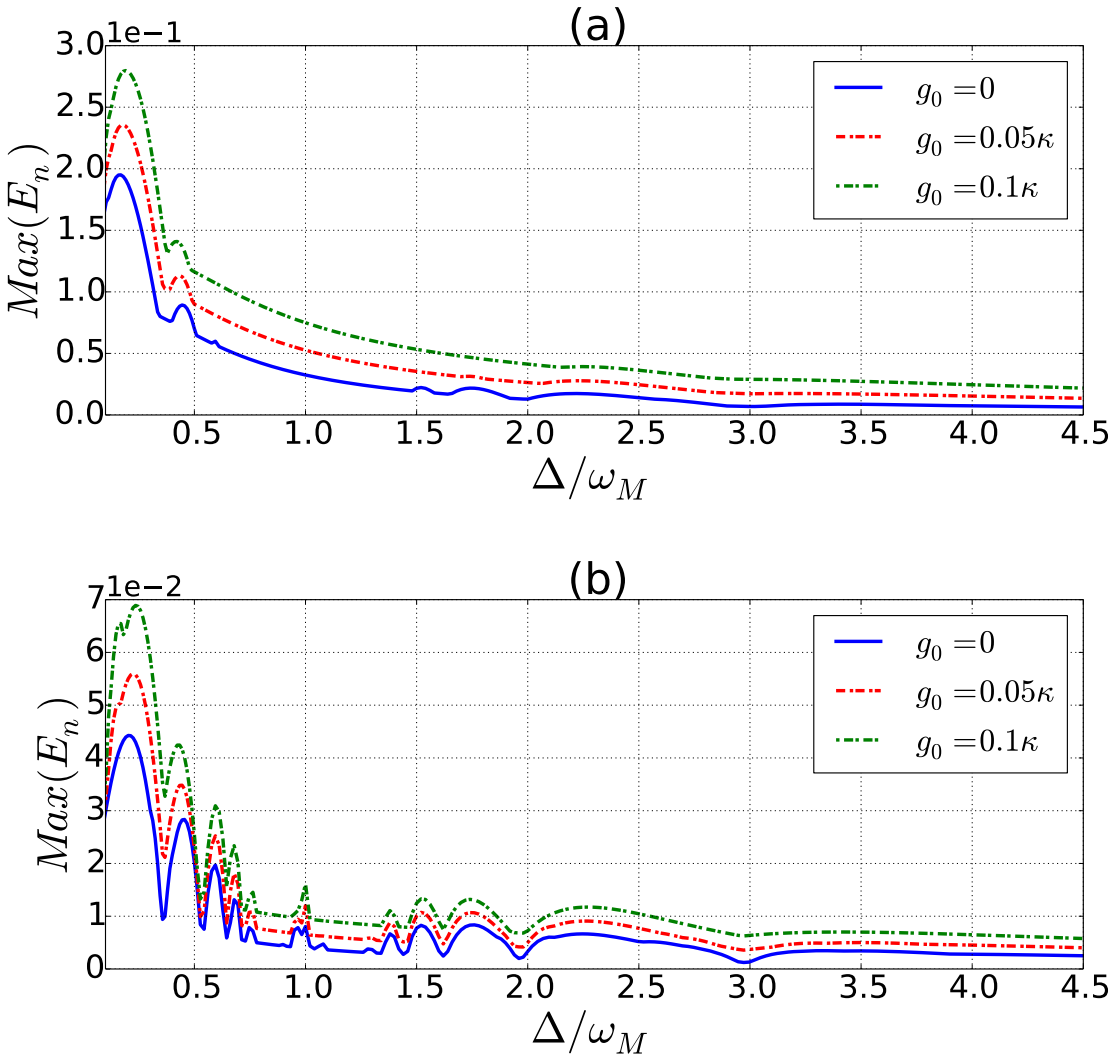

Figure 3.6: (a) The entanglement described by Simon's criteria (b) The entanglement described Duan's criteria. Parameters are: $\omega_M/2\pi = 1$ MHz, $n_{th} = 0$ and $\gamma_M = \omega_M/10^5$, $g = 0.1\omega_M$ and $\kappa = 0.05\omega_M$

and Duan's criteria of [55] with

$$E_n = -det \begin{vmatrix} 1 & \langle \hat{a}_c \rangle & \langle \hat{b}_M^\dagger \rangle \\ \langle \hat{a}_c^\dagger \rangle & \langle \hat{a}_c^\dagger \hat{a}_c \rangle & \langle \hat{a}_c^\dagger \hat{b}_M^\dagger \rangle \\ \langle \hat{b}_M \rangle & \langle \hat{a}_c \hat{b}_M \rangle & \langle \hat{b}_M^\dagger \hat{b}_M^\dagger \rangle \end{vmatrix} \tag{3.30}$$

Our results are reported in Fig. 3.6, where we define the maximum entanglement $Max(E_n)$ as the the maximal E_n achieved during the time evolution of $\tau = 60\pi/\omega_M$. It shows that with an increase of the nonlinear coupling rate g_0, the maximal optomechanical entanglement increases as well, indicating that nonlinear interactions helps the entanglement generation with the parameters used above.

3.5 Conclusions

In this chapter, we developed a new perturbative method to investigate the influence of the nonlinear optomechanical interaction as modifications to the linearized optomechanical model. Our results show that with an intermediate optomechanical coupling, the influence of the nonlinear interaction is not negligible and it affects both the amplitude of the cavity field and the mechanical oscillator, which is consistent with the standard master equation approach with nonlinear interactions. Our results also show that the nonlinear interactions could be used to assist the entanglement generation. However, the perturbative solutions usually have involved form and in this chapter, we only considered the effects from the first order perturbation while the influence of the higher orders on system dynamics are still unclear.

Recently, similar methods were used to investigate the contribution of the nonlinear interaction in the optomechanical dynamics involving two driving fields, and they found that nonlinear optomechanical interaction could lead to the optomechanical induced transparency [38, 39, 40]. In their formalism, the Hamiltonian is diagonalized while assumptions are made about their interactions with environment. But in our method, by employing the analytical solutions for the linear optomechanical model, additional assumptions about the system-bath interaction are unnecessary, leading to slightly different dynamics for the system. Moreover, the theoretical formalism developed here is easy to incorporate with numerical analytics due to its simple matrix form.

Chapter 4

Strongly Coupled Optomechanical System

With a strong optomechanical coupling strength, the influence of the nonlinear optomechanical interaction becomes even more significant than it is in case of weak coupling regime. In the strong coupling regime, both the linear approach (Chapter 2) and perturbative method (Chapter 3) fail to provide correct insight for the system dynamics. To investigate the optomechanical behavior in this regime, new theoretical tools are necessary to deal with the effects of the strong nonlinear optomechanical interaction in the open system dynamics, which are the main topics in this chapter.

In this chapter, we consider an optomechanical system with its bare optomechanical coupling constant g_0 comparable with the mechanical frequency ω_M, which we call the single photon ultra-strong coupling regime. In this regime, the steady-state mechanical displacement produced by a single photon is more than its zero-point fluctuation. The mechanical oscillator is, therefore, strongly coupled to the cavity field, and any fluctuation with the mechanical oscillator immediately shifts the state of the cavity field. To obtain the truly single photon nonlinearity, we also require the cavity decay κ to be small compared to the mechanical frequency ω_M, so that any single photon could live long enough to influence the mechanical dynamics which causes the nontrivial optomechanical effects. Due to such a strong cavity-mechanical coupling, the optomechanical decoherence behaviors change significantly, and the traditional treatment of the standard master equations with an independent decoherence model would not provide a correct insight for the optomechanical dynamics in this regime.

Based on the optomechanical dressed-state basis, a new master equation with a coupled decoherence model is developed in this chapter for the standard optomechanical system in the ultra-strong coupling regime, where we treat the cavity field and mechanical oscillator as a single quantum system and consider the influence of the outside environment via the Born-Markovian master equation approach. The results show that the cavity decoherence is strongly coupled with the mechanical bath due

to the large optomechanical coupling. As a result, both the transient dynamics and the steady-state properties are significantly modified. Beyond the standard optomechanical model, we also studied the optomechanical system with two cavity modes interacting with a single mechanical mode. Our results show that the cavity-cavity entanglement is strongly influenced by the strong optomechanical coupling.

4.1 Introduction

Cavity optomechanics studies the radiation pressure interaction between a cavity field and the motion of a mechanical oscillator. Such a system has been realized in a variety of systems, including a Fabry-Perot cavity with moving mirror(s) [4, 5], cold atoms in a cavity [6, 7], a nanomechanical resonator coupling with superconducting circuits [69] and photonic crystal structures [9, 10, 11]. The study of such systems can lead to advances in precision measurements [12, 13], implementations of quantum information protocols and the testing of macroscopic quantum effects [14]. In recent experiments, many quantum behaviors of the mechanical modes have been demonstrated , which include the cooling to the quantum ground state[69, 70], the demonstration of strong optomechanical coupling[19, 71, 22], and conversion of cavity state to the mechanical mode [72, 73].

In recent theoretical works, the ultra-strong coupling regime — where the strength of bare optomechanical coupling is comparable to the mechanical frequency — was studied [43, 44, 39], where the mechanical displacement, induced by the radiation pressure of a single photon, is comparable to its zero-point uncertainty [41, 44]. Due to the strong nonlinearity in this system, many novel quantum effects can be observed in this regime, such as optomechanical instability [41, 45], photon blockade [43, 44], normal mode splitting of a mechanical mode[74], and nonlinear optomechanical EIT [40, 38, 39].

Most of the previous studies have been focused on the steady-state behavior under the *standard* master equation (SME) [44, 39]. In addition to the usual Born-Markovian approximation for the weak system-bath interaction, the SME was derived under the assumption of weak optomechanical coupling in the non-interacting photon (phonon) basis by integrating out the bath degrees of freedom of the cavity and mechanical modes separately. However, under the strong optomechanical coupling between the cavity and the mechanical modes, this approach needs to be revisited in order to correctly describe the dissipative dynamics of this system.

In this work, we derive the master equation in a more appropriate basis, the eigenbasis of the optomechanical system (OMS), in the ultra-strong coupling regime and obtain a new Lindblad master equation which we call the dressed-state master equation (DSME). We find that the weak coupling assumptions in the SME approach could result in unrealistic cavity dephasing effects for the strongly coupled OMS, which are

absent in our dressed-state approach via considering a more realistic contribution of the strong optomechanical coupling in the system-bath interaction. By comparing the dynamics of these two different approaches, we show that the unrealistic cavity dephasing terms can lead to significantly different behaviors for the transient dynamics of the cavity field as well as the steady-state properties of systems, such as predicting the cavity decoherence time as half of its real value and showing $g^{(2)}(0) > 1$ while the OMS actually undergoes the photon antibunching. Finally, we extend the DSME to the case of two cavity modes interacting with a signal mechanical mode and show that the unrealistic cavity dephasing terms in the SME reduce the coherence time of the cavity-cavity entanglement by half. In all these cases, the dressed-state approach is necessary to reveal the correct dissipative dynamics for OMS in the ultra-strong coupling regime.

The chapter is organized as follows. In Sec.4.2, we present the derivation of the master equation in the dressed-state basis. In Sec.4.3, analytical result of the time-dependence of the system operators is derived. We then apply the dressed-state master equation to study the short-time dynamics of the optomechanical system in Sec.4.4.The correlation functions of the cavity mode, the optomechanical entanglement, and mechanical modes are calculated using the numerical results. Conclusions are given in Sec.4.5. We include technical derivations in Appendix C.

4.2 Dressed-state Master Equation

Consider an optomechanical system with one cavity mode and one mechanical mode interacting via radiation pressure force. The Hamiltonian of this system has the form

$$\hat{H}_s = \hbar\omega_c \hat{a}_c^\dagger \hat{a}_c + \hbar\omega_M \hat{b}_M^\dagger \hat{b}_M - \hbar g_0 \hat{a}_c^\dagger \hat{a}_c \left(\hat{b}_M^\dagger + \hat{b}_M\right), \tag{4.1}$$

where ω_c is the cavity frequency, ω_M is the mechanical frequency, and g_0 is the optomechanical coupling strength. The operator $\hat{a}_c$ ($\hat{b}_M$) is the annihilation operator of the cavity (mechanical) mode. We are interested in the ultra-strong coupling regime where g_0 is comparable to ω_M and one example of such a setup is shown in Fig. 4.1(a). For this coupled system, the eigenbasis can be written as

$$|n, m_{(n)}\rangle = |n\rangle \otimes e^{n\beta_0(\hat{b}_M^\dagger - \hat{b}_M)}|m\rangle, \tag{4.2}$$

where $|n\rangle$ is the cavity photon Fock state and $|m_{(n)}\rangle \equiv e^{n\beta_0(\hat{b}_M^\dagger - \hat{b}_M)}|m\rangle$ denotes the photon displaced mechanical Fock state with displacement $n\beta_0$ and $\beta_0 = g_0/\omega_M$. We call these eigenstates the dressed-state basis. The corresponding eigenenergies are $E_{n,m} = n\hbar\omega_c + m\hbar\omega_M - n^2\hbar g_0^2/\omega_M$ and this is illustrated in more detail in Fig. 4.1(b) where the effects from the external thermal baths have been explained.

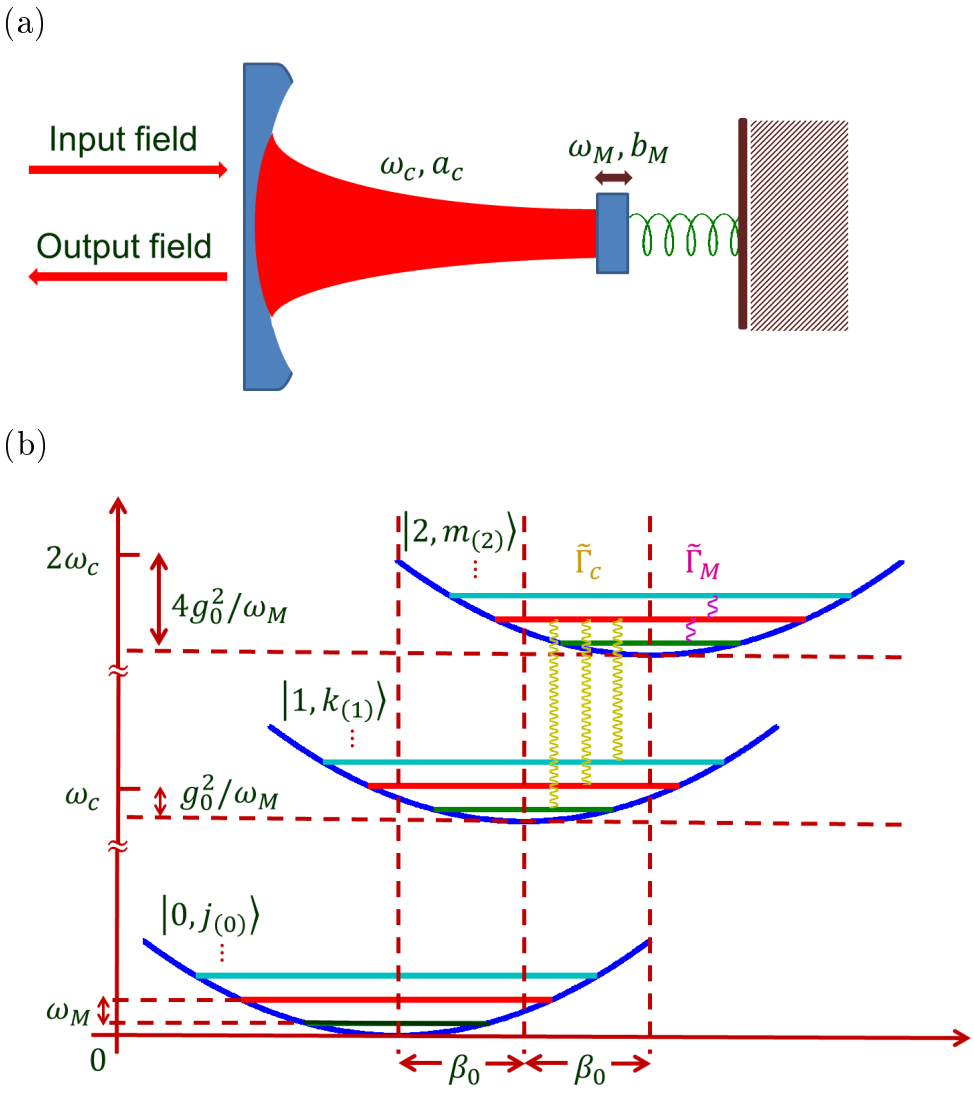

Figure 4.1: (a) Standard cavity optomechanical system. (b) Energy level scheme of the strong coupled optomechanical system. Several possible transitions examples due to couplings of the external thermal bath are indicated. Here $\beta_0 = g_0/\omega_M$, $\tilde{\Gamma}_c$ and $\tilde{\Gamma}_M$ are the operator of the cavity thermal bath and mechanical thermal bath, respectively.

The bath coupled to the cavity mode and to the mechanical mode are both assumed to be an independent bosonic thermal bath, which are charaterized by $H_C^B = \sum_j \hbar\omega_j \hat{a}_j^\dagger \hat{a}_j$ and $H_M^B = \sum_k \hbar\omega_k \hat{b}_k^\dagger \hat{b}_k$ respectively. In the interaction picture of $\hat{H}_s + \hat{H}_C^B + \hat{H}_M^B$, the interaction between the optomechanical system and its environments is described by the Hamiltonian $\tilde{H}_I^B = \tilde{H}_{CB} + \tilde{H}_{MB}$, where the system-bath couplings have the form

$$\tilde{H}_{CB} = \tilde{a}_c(t)^\dagger \tilde{\Gamma}_c(t) + \tilde{a}_c(t)\tilde{\Gamma}_c^\dagger(t), \tag{4.3}$$

$$\tilde{H}_{MB} = \left(\tilde{b}_M(t)^\dagger + \tilde{b}_M(t)\right)\left(\tilde{\Gamma}_M^\dagger(t) + \tilde{\Gamma}_M(t)\right) \tag{4.4}$$

with $\tilde{\Gamma}_c(t) = \sum_{j=0}^{\infty} \lambda_j^c e^{-i\omega_j t}\hat{a}_j$ ($\hat{\Gamma}_M(t) = \sum_{k=0}^{\infty} \lambda_k^M e^{-i\omega_k t}\hat{b}_k$) as coupling operator of the cavity bosonic bath (mechanical bosonic thermal bath) and $\tilde{a}_c(t)$ is defined as $\tilde{a}_c(t) = e^{i\hat{H}_s t}\hat{a}_c e^{-i\hat{H}_s t}$ (similarly for $\tilde{b}_M(t)$). By expanding the operators in the eigenbasis, the cavity operator $\tilde{a}_c(t)$ could be expressed as,

$$\tilde{a}_c(t) = \sum_{n,k,j} e^{-i\Delta_{k,j}^n t} A_{j,k,n} |n-1, j_{(n-1)}\rangle\langle n, k_{(n)}| \tag{4.5}$$

with the transition amplitude $A_{j,k,n} = \sqrt{n}\langle j_{(n-1)}|k_{(n)}\rangle$ and energy difference $\Delta_{k,j}^n = (E_{n,k} - E_{n-1,j})/\hbar = \omega_c + (k-j)\omega_M + (1-2n)g_0^2/\omega_M$. Here, we consider that the cavity field has the optical frequency, i.e. $\omega_c \sim GHz \gg \omega_M$, thus the energy difference can be approximated as $\Delta_{k,j}^n \approx \omega_c$, showing that the optical cavity transition is not influenced by the optomechanical interaction. As a result, Eq.(4.5) could be simplified as $\tilde{a}_c(t) \approx e^{-i\omega_c}\hat{a}_c$, which is the same form as it is in the weak coupling regime, indicating that the dissipative cavity response to the cavity thermal bath is not affected by the strong optomechanical interaction when the cavity mode frequency is in the optical frequency range. Because in this regime, the modification from the strong coupling (in the order of $g_0^2/\omega_M \sim \omega_M \sim MHz$) is small compared with the optical transition energy (in the order of $\omega_c \sim GHz$).

In the interaction picture, the mechanical operator could be expressed as (Appendix C.1)

$$\begin{aligned}\tilde{b}_M(t) &= e^{-i\omega_M t}\sum_{n,\ell}\sqrt{\ell}|n, (\ell-1)_{(n)}\rangle\langle n, \ell_{(n)}| \\ &+ \beta_0 \sum_{n,\ell} n|n, \ell_{(n)}\rangle\langle n, \ell_{(n)}|\end{aligned} \tag{4.6}$$

It shows that the mechanical-mode-bath interaction [see Eq.(4.4)] involves two physical processes: (1) the interaction excites the eigenmode by exchanging one phonon

with the mechanical thermal bath, shown as the first term of Eq.(4.17), causing the OMS has the mechanical transitions with the energy difference of ω_M; (2) the interaction displaces the mechanical oscillator without shifting the system's energy, shown as the second term of Eq.(4.17). In general, the contributions of these two processes are different due to their distinct transition energies and dependent with the spectral density of the mechanical bath.

However, in the SME approach, because of the weak coupling approximation, the energy difference of these two type of transitions are not resolved and the two physical processes are thus treated with equal amplitude, i.e.

$$\begin{aligned}\hat{b}_M(t) \approx e^{-i\omega_M t}\hat{b}_M &\equiv e^{-i\omega_M t}\sum_{n,\ell}\sqrt{\ell}|n,(\ell-1)_{(n)}\rangle\langle n,\ell_{(n)}| \\ &+ e^{-i\omega_M t}\beta_0\sum_{n,\ell} n|n,\ell_{(n)}\rangle\langle n,\ell_{(n)}| \end{aligned} \tag{4.7}$$

The Bohr frequencies of the second physical process are mistakenly treated as ω_M. This assumption is not true for the strongly coupled OMS as it is shown by Eq.(4.17) where the existence of the cavity photon shift the mechanical oscillator with Bohr frequencies as zero. In this study, we are going to investigate the influence of this second physical process with a more realistic contribution.

By using the Born-Markov and the rotating-wave approximation (RWA), the master equation in the Schrödinger picture with the absence of external driving, which we call dressed-state master equation (DSME), takes the following form (Appendix C.2)

$$\begin{aligned}\frac{d\rho(t)}{dt} &= -i[\hat{H}_s,\rho(t)] + \kappa\mathcal{D}[\hat{a}_c]\rho(t) + n_{th}\gamma_M\mathcal{D}[\hat{b}_M^\dagger - \beta_0\hat{N}_c]\rho(t) \\ &+ (n_{th}+1)\gamma_M\mathcal{D}[\hat{b}_M - \beta_0\hat{N}_c]\rho(t) \end{aligned} \tag{4.8}$$

with the Lindblad superoperator defined by $\mathcal{D}[\hat{\Omega}]\rho(t) = \hat{\Omega}\rho(t)\hat{\Omega}^\dagger - \Big(\hat{\Omega}^\dagger\hat{\Omega}\rho(t) + \rho(t)\hat{\Omega}^\dagger\hat{\Omega}\Big)$, the cavity and mechanical decay rates being, respectively, κ and γ_M, and the phonon occupation number $n_{th} = 1/\left(e^{\hbar\omega_M/k_BT} - 1\right)$. Here $\hat{N}_c = \hat{a}_c^\dagger\hat{a}_c$ is the photon number operator. In the limit of weak optomechanical coupling, i.e., $g_0 \ll \omega_M$, the above master equation can be simplified to recover the form of the standard master equation (SME) of

$$\begin{aligned}\frac{d\rho(t)}{dt} &= -i[\hat{H}_s,\rho(t)] + \kappa\mathcal{D}[\hat{a}_c]\rho(t) + n_{th}\gamma_M\mathcal{D}[\hat{b}_M^\dagger]\rho(t) \\ &+ (n_{th}+1)\,\gamma_M\mathcal{D}[\hat{b}_M]\rho(t). \end{aligned} \tag{4.9}$$

To understand the difference of the mechanical dissipative terms between $\mathcal{D}[\hat{b}_M]\rho(t)$ ($\mathcal{D}[\hat{b}_M^\dagger]\rho(t)$) and $\mathcal{D}[\hat{b}_M - \beta_0\hat{N}_c]\rho(t)$ ($\mathcal{D}[\hat{b}_M^\dagger - \beta_0\hat{N}_c]\rho(t)$) in Eq. (4.9) and Eq. (4.8),

respectively, one could work back into the interaction picture with respect to the cavity-mechanical system Hamiltonian $\hat{H}_s$, Eq. (4.1). For example, one obtains, by dropping the fast-oscillating terms using RWA (valid when $\gamma_M \ll \omega_M$, the regime we consider) of Eqs. (4.9) and (4.8),

$$U(t)^\dagger \mathcal{D}[\hat{b}_M]\rho(t)U(t) \approx \mathcal{D}[\hat{b}_M - \beta_0\hat{N}_c]\tilde{\rho}(t) + \mathcal{D}[\beta_0\hat{N}_c]\tilde{\rho}(t), \tag{4.10}$$

$$U(t)^\dagger \mathcal{D}[\hat{b}_M - \beta_0\hat{N}_c]\rho(t)U(t) \approx \mathcal{D}[\hat{b}_M - \beta_0\hat{N}_c]\tilde{\rho}(t), \tag{4.11}$$

where $U(t) = e^{-i\hat{H}_s t}$ and $\tilde{\rho}(t)$ is the reduced density matrix of the cavity-mechanical system in the interaction picture. One can then clearly see that the extra terms in the mechanical damping of the resultant equation from the SME (4.9) is $(2n_{th}+1)\beta_0^2\gamma_M\mathcal{D}[\hat{N}_c]\tilde{\rho}(t)$ and it will affect the non-diagonal components but not the diagonal components (i.e., causing dephasing but not relaxation) of the cavity part of the density matrix $\tilde{\rho}(t)$ (thus also $\rho(t)$ in the photon number basis). As a result, the standard master equation will cause more dephasing of the photon state. In other words, more coherent behavior for the cavity mode due to the missing of these extra dephasing terms in the DSME, Eq. (4.8), is expected.

4.3 Analytical Solutions

In this section, we present analytical solutions for the dynamics of the expectation values of several quantum operators governed by the dressed-state master equation in the undriven case. It can be shown that with Eq.(4.8) the equations of motion for the expectation values of an arbitrary operator Ω are,

$$\begin{aligned}\frac{d\langle\Omega\rangle}{dt} &= -i\langle[\Omega,H]\rangle - \frac{\kappa}{2}\left(\langle[\Omega,\hat{a}_c^\dagger]\hat{a}_c\rangle - \langle\hat{a}_c^\dagger[\Omega,\hat{a}_c]\rangle\right) \\ &- \frac{\gamma_M}{2}\left(\langle[\Omega,\hat{B}_i^\dagger]\hat{B}_i\rangle - \langle\hat{B}_i^\dagger[\Omega,\hat{B}_i]\rangle\right) - n_{th}\frac{\gamma_M}{2}\left(\langle[[\Omega,\hat{B}_i^\dagger],\hat{B}_i]\rangle + \langle[[\Omega,\hat{B}_i],\hat{B}_i^\dagger]\rangle\right),\end{aligned} \tag{4.12}$$

where $\hat{B}_i = \hat{b}_M - \beta_0\hat{a}_c^\dagger\hat{a}_c$. For example, the dynamics of the mean value of the cavity operator $\hat{a}_c$ are given by

$$\begin{aligned}\frac{d\langle\hat{a}_c\rangle}{dt} = &- i\omega_c\langle\hat{a}_c\rangle + ig_0\langle\hat{a}_c\left(\hat{b}_M + \hat{b}_M^\dagger\right)\rangle - \left(\frac{\kappa}{2} + (2n_{th}+1)\beta_0^2\frac{\gamma_M}{2}\right)\langle\hat{a}_c\rangle \\ &+ \beta_0\frac{\gamma_M}{2}\langle\hat{a}_c\left(\hat{b}_M - \hat{b}_M^\dagger\right)\rangle.\end{aligned} \tag{4.13}$$

The cavity mode is now subject to an effective damping rate of $\kappa_{eff} = \kappa + \Delta\kappa$ with $\Delta\kappa = (2n_{th}+1)\beta_0^2\gamma_M$, which strongly depends on the optomechanical coupling and the properties of the mechanical thermal bath. The above equation also shows that the

dynamics of the cavity mode $\langle \hat{a}_c \rangle$ is related to the higher order term $\langle \hat{a}_c \left(\hat{b}_M + \hat{b}_M^\dagger \right) \rangle$. In general, a closed set of operator equations are not available in the single-photon strong coupling regime, and the dynamics could be non-Gaussian.

For several operators, however, the above equation provides analytical solutions. For the cavity photon number operator $\hat{N}_c$, we find that

$$\frac{d\langle \hat{N}_c \rangle}{dt} = -\kappa \langle \hat{N}_c \rangle \tag{4.14}$$

and its solution is

$$\langle \hat{N}_c(t) \rangle = e^{-\kappa t} \langle \hat{N}_c(0) \rangle. \tag{4.15}$$

The dynamics of the cavity photon number $\langle \hat{N}_c \rangle$ is independent of the mechanical damping terms in both the dressed-state-basis master equation and the standard master equation and thus takes the same form for both the master equations. This is because $\hat{N}_c$ commutes with both $\hat{H}_s$ and the operators in the additioanl terms of the mechanical damping terms. For the mechanical mode operator $\hat{b}_M$, we find that

$$\frac{d\langle \hat{b}_M \rangle}{dt} = -i\omega_M \langle \hat{b}_M \rangle + ig_0 \langle \hat{N}_c \rangle - \frac{\gamma_M}{2} \langle \hat{b}_M \rangle + \beta_0 \frac{\gamma_M}{2} \langle \hat{N}_c \rangle. \tag{4.16}$$

Combined with the solution of cavity photon number Eq. (4.15), Eq. (4.16) leads to the solution

$$\langle \hat{b}_M(t) \rangle = e^{-i\omega_M t - \frac{\gamma_M}{2} t} \langle \hat{b}_M(0) \rangle + \frac{ig_0 + \beta_0 \gamma_M/2}{i\omega_M + \frac{\gamma_M}{2} - \kappa} \left(e^{-\kappa t} - e^{-i\omega_M t - \frac{\gamma_M}{2} t} \right) \langle \hat{N}_c(0) \rangle. \tag{4.17}$$

The dynamics of $\langle \hat{b}_M(t) \rangle$ includes an extra term that depends on initial cavity photon numbers, but independent of the mechanical thermal bath temperature.

4.4 Numerical Results

In this section, we use numerical solutions of the dressed-state master equation to illustrate the effect of strong coupling on the system dynamics, and compare these results with that of the standard master equation.

Dynamics of undriven system

We first apply the DSME to study the evolution of photon coherence and focus on the case of the ultra-strong coupling regime, i.e. $g_0/\omega_M = 0.8$. The OMS is initially prepared in the state $|\psi(0)\rangle = (|0\rangle + |3\rangle)_c \otimes |0\rangle_M/\sqrt{2}$. The coherence of the cavity field is well described by $P_{03}(t) := |\langle 0|\tilde{\rho}_c(t)|3\rangle|$ which is the off-diagonal matrix element

of the reduced cavity density matrix in the interaction picture. Fig. 4.2 shows the dynamics of $P_{03}(t)$ for both DSME of Eq.(4.8) (solid curves) and SME of Eq.(4.9) (dashed curves) at two mechanical bath temperatures $n_{th} = 0$ (red color) and $n_{th} = 20$ (blue color).

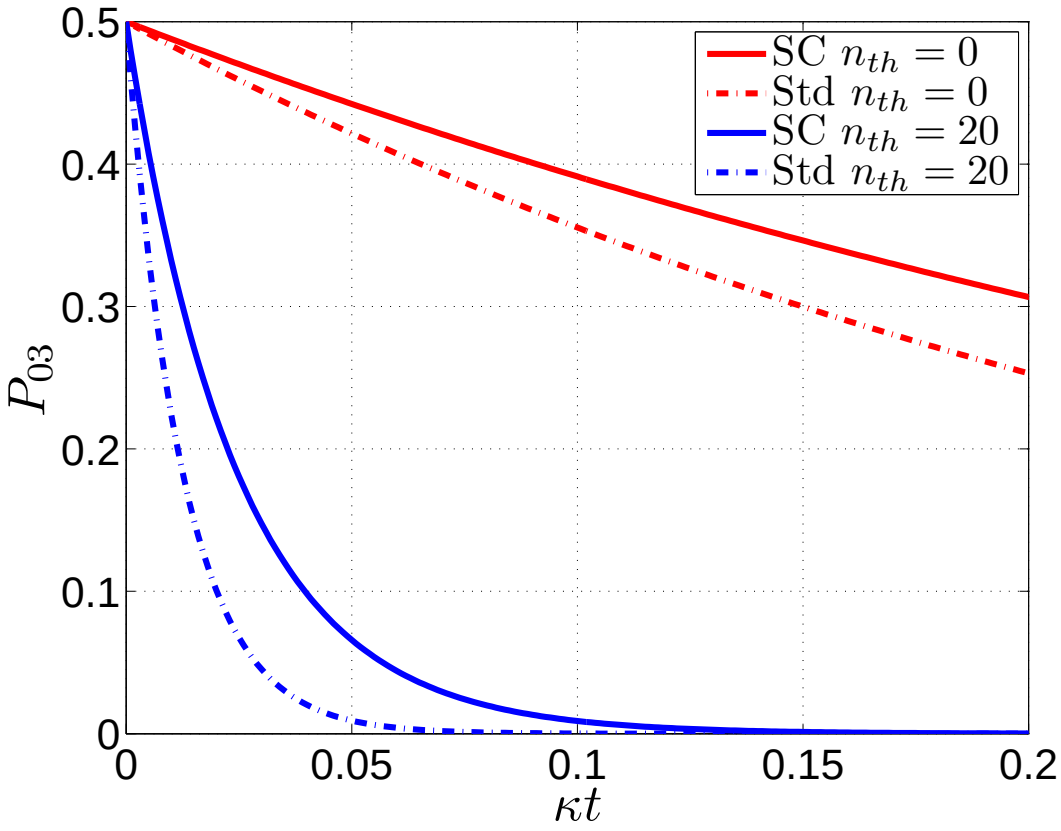

Figure 4.2: Off-diagonal matrix element $P_{03}(t)$. Solid curves are from the dressed-state master equation (DSME) and dashed curves belongs to the standard master equation(SME). Parameters are chosen as: $\omega_M/2\pi = 1$ MHz, $g_0 = 0.8\omega_M$, $\kappa = 0.005\omega_M$, $\gamma_M = \kappa/3$, $n_{th} = 0$ (red) and 20 (blue).

In the ultra-strong coupling regime, the cavity coherence is strongly correlated with the properties of the mechanical bath which are captured by both master equation approaches. It is shown in Fig.4.2 that the cavity coherence $P_{03}(t)$ at higher mechanical bath temperature $n_{th} = 20$ (blue color curves) decays by a factor of twenty faster than the case of $n_{th} = 0$ (red color curves, the full curves are shown in Fig.C.1 of Appendix C.3) whose decay rates are similar with the intrinsic cavity damping rate, i.e. 2κ (with $g_0 = 0$). The SME is based on the assumption that the optomechanical coupling does not have any effect on the interaction between the mechanical mode

and its bath. Then that all the mechanical bath excitations have the same influence on the cavity field causes, through the optomechanical coupling in the Hamiltonian, the cavity field coherence amplitude $P_{03}(t)$ to decay much faster than the intrinsic cavity damping and dependent with mechanical bath temperature. However, the above assumption is actually not true for the strongly coupled optomechanical system, where the optomechanical coupling makes the influence of the mechanical noise dependent on the type of system transitions (see Eq.(4.17)). After including these effects and the property of the spectral density of the mechanical bath, the unrealistic cavity dephasing terms disappear within DSME so that the corresponding decay of $P_{03}(t)$ (solid curves) is obviously weaker than what is expected by the SME (dashed curves). At $n_{th} = 20$, the decay time of $P_{03}(t)$ obtained by DSME (blue solid curve) is over twice longer than it is in SME approach (blue dashed curve). At $n_{th} = 0$ where the mechanical noises are at minimal, both methods provide a similar decay time while DSME always possess a slightly larger amplitude, indicating that more coherent dynamics are revealed by the DSME due to the absence of the unrealistic cavity dephasing, which is consistent with our previous predictions.

Dynamics of driven system

When the cavity is driven with a pump field, we study the properties of the normalized equal time correlation function at steady state, $g^{(2)}(0) := \langle \hat{a}_c^\dagger \hat{a}_c^\dagger \hat{a}_c \hat{a}_c \rangle_{ss} / \langle \hat{a}_c^\dagger \hat{a}_c \rangle_{ss}^2$. It is known that $g^{(2)}(0) < 1$ provides a direct experimental measure for nonclassical antibunching effects of the cavity field, while $g^{(2)}(0) > 1$ indicates the photon bunching effects. By assuming that the pump field is weak, the master equation under driving could be obtained by replacing $\hat{H}_s$ in both Eq.(4.8) and Eq.(4.9) with $\hat{H} = \hat{H}_s + \varepsilon \left(\hat{a}_c e^{i\omega_d t} + \hat{a}_c^\dagger e^{-i\omega_d t} \right)$, where ε is the strength of the pump field and ω_d is the driving frequency. The total master equation takes the following form,

$$\begin{aligned} \frac{d\rho(t)}{dt} &= -i[\hat{H}_s + \varepsilon \left(\hat{a}_c e^{i\omega_d t} + \hat{a}_c^\dagger e^{-i\omega_d t} \right), \rho(t)] + \kappa \mathcal{D}[\hat{a}_c]\rho(t) \\ &+ n_{th}\gamma_M \mathcal{D}[\hat{b}_M^\dagger - \beta_0 \hat{N}_c]\rho(t) + (n_{th}+1)\gamma_M \mathcal{D}[\hat{b}_M - \beta_0 \hat{N}_c]\rho(t) \end{aligned} \tag{4.18}$$

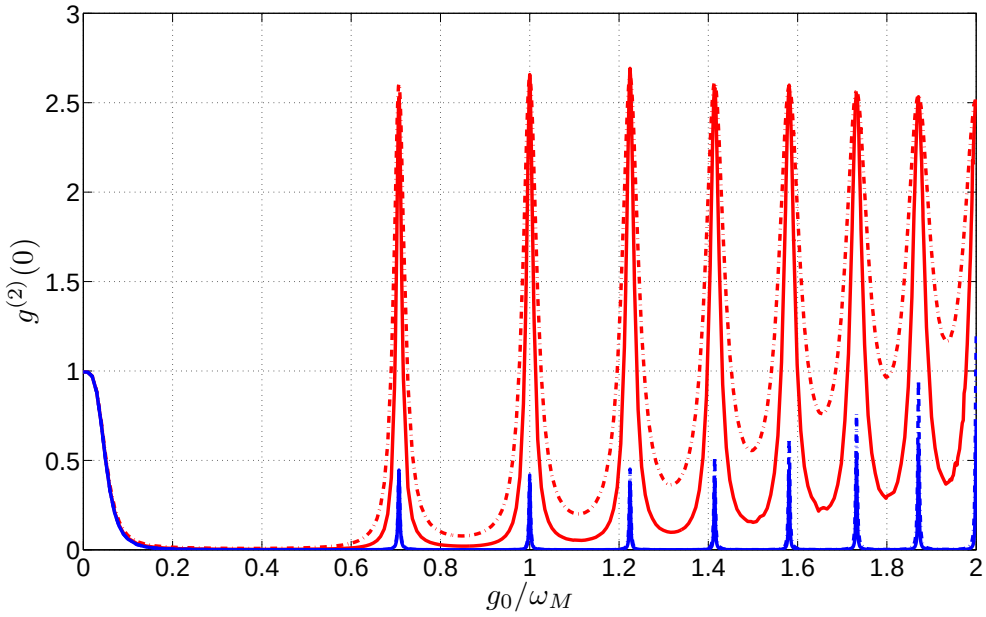

Figure 4.3: $g^{(2)}(0)$ versus g_0/ω_M at cavity detune $\Delta_0 = \omega_c - \omega_d = g_0^2/\omega_M$. Solid curves are from DSME and dashed curves belongs to SME. Parameters are chosen as: $\omega_M/2\pi = 1$, $\kappa = 0.005\omega_M$, $\gamma_M = \kappa/3$, $\varepsilon = \kappa$, $n_{th} = 0$ (lower curves) and 20 (upper curves).

To investigate the influence of the radiation-pressure coupling g_0 and the mechanical bath temperature n_{th} on $g^{(2)}(0)$, we present the dependence of $g^{(2)}(0)$ on g_0 in Fig.4.2 for two different mechanical bath temperatures at cavity detune of $\Delta_0 = \omega_c - \omega_d \equiv g_0^2/\omega_M$, which corresponds to a single photon resonance [75, 76]. The oscillating feature of $g^{(2)}(0)$ as a function of g_0 with the peak positions determined by the two-photon resonance condition $g_0/\omega_M = \sqrt{m/2},\ m = 0, 1, 2, \cdots$ was found in Refs.[75, 76]. Compared with the results of $g^{(2)}(0)$ obtained by SME (dashed curves), the results by DSME (solid curves) show obviously different behavior at large values of g_0 or with high mechanical bath temperature n_{th}. At low mechanical bath temperature, i.e. $n_{th} = 0$, both methods correctly predict the antibunching effect for the OMS. However, at larger g_0, larger resonance peaks were resolved only by DSME approach. With higher mechanical bath temperature, i.e. $n_{th} = 20$, one can see from Fig. 4.2, the DSME predicts stronger photon blockade effect between resonance peaks for the cavity field. More importantly, when $g_0/\omega_M > 1.7$, at many values of g_0, *the DSME predicts antibunching behavior* ($g^{(2)}(0) < 0.5$), *while the SME predicts otherwise* ($g^{(2)}(0) > 1$), showing that at high mechanical thermal bath temperatures with large optomechanical couplings, the unrealistic cavity dephasing terms could cause the SME fails to correctly predict the quantum correlations for the cavity field and it

is necessary to adopt the dressed-state master equation approach for these cases.

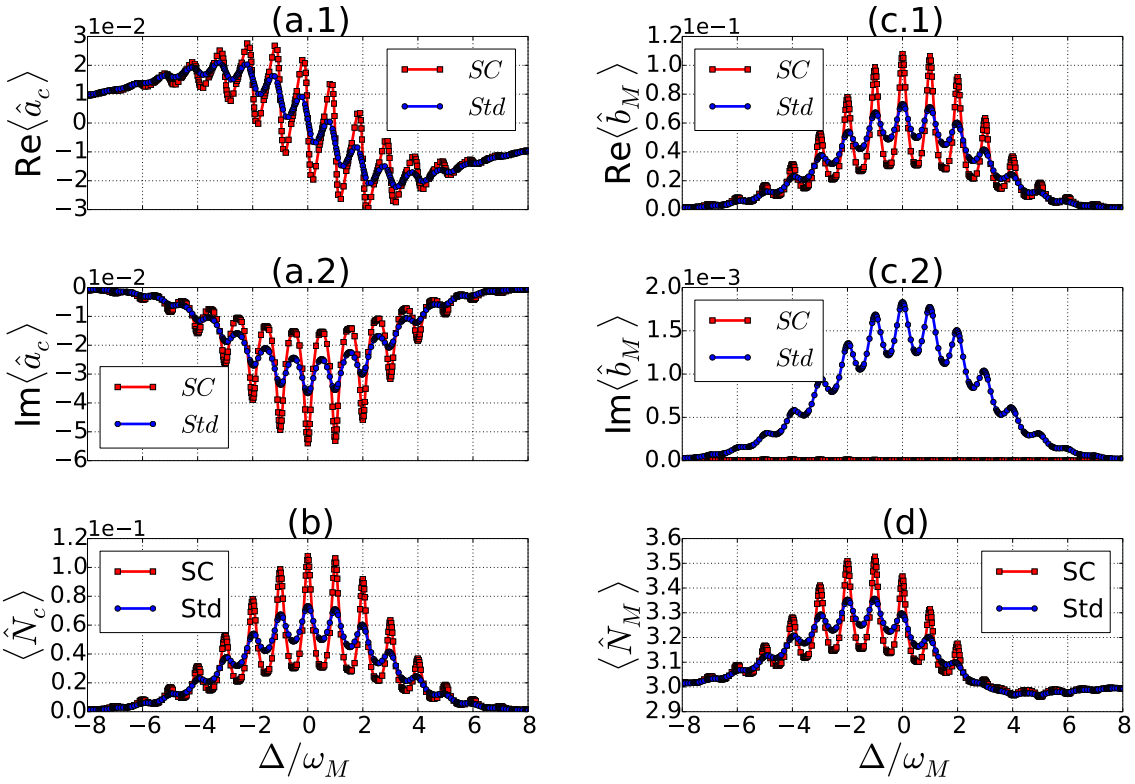

Figure 4.4: Steady-state mean values of $\langle \hat{a}_c \rangle$, $\langle \hat{N}_c \rangle$, $\langle \hat{b}_M \rangle$ and $\langle \hat{N}_M \rangle$ as a function of cavity detuning Δ_0. Red curves show the results of the dressed-state master equation and blue curves are the results of the standard master equation. Parameters used are $\omega_M = 2\pi$ MHz, $\kappa = \omega_M/15$, $\gamma_M = \omega_M/20$, $n_{th} = 3$, $g_0 = \omega_M$ and driving strength $\epsilon = \kappa$.

In contrast to the undriven case where no significant differences in the steady-state properties are observed, the steady-state quantities in the driven case obtained by the two different master equations could display substantial difference. Figure 4.4 shows the steady-state mean values of $\langle \hat{a}_c \rangle$, $\langle \hat{N}_c \rangle$, $\langle \hat{b}_M \rangle$ and $\langle \hat{N}_M \rangle$ as a function of detuning $\Delta_0 = \omega_c - \omega_d$ for the system in the single-photon strong-coupling regime with a low bath temperature of $n_{th} = 3$. The response of the optomechanical system exhibits several resolved resonances in Fig 4.4. Most of the previous studies [44, 39] used the *standard* master equation to study the steady-state behavior. Here, we demonstrate in Fig 4.4 that significant differences in the steady-state quantities obtained between the dressed-state master equation and the standard master equation can be observed, i.e., sharper resonance features for the quantities obtained by the dressed state master equation.

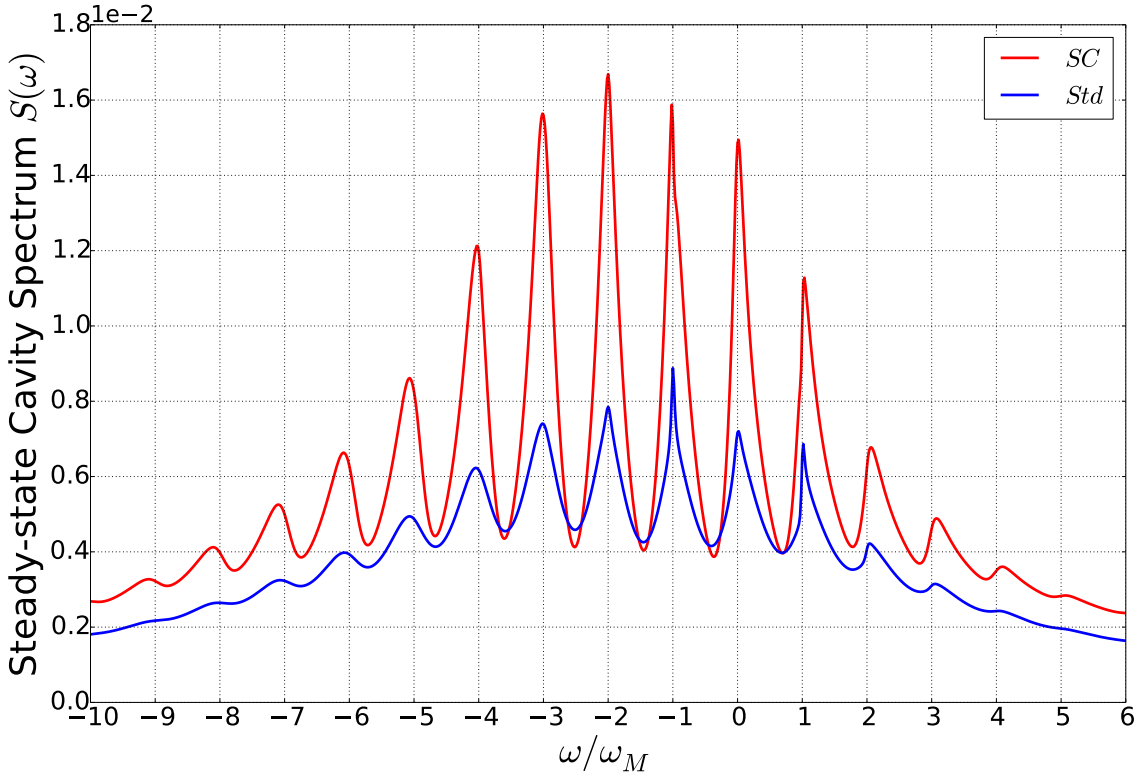

Figure 4.5: Steady-state cavity respond with resonant driving at $\Delta = 0$. Red line shows the result of the dressed-state master equation and blue line is the result of the standard master equation. Parameters are chosen as: $\omega_M = 2\pi$ MHz, $\kappa = \omega_M/15$, $\gamma_M = \omega_M/20$, $n_{th} = 3$, $g_0 = \omega_M$ and driving strength $\epsilon = \kappa$.

Next, we investigate the steady-state cavity output spectrum defined as

$$S(\omega) = \int_{-\infty}^{\infty} \left[\langle \hat{a}_c^\dagger(\tau)\hat{a}_c(0)\rangle - |\langle \hat{a}_c(\tau)\rangle|^2\right], \tag{4.19}$$

where the initial time $t = 0$ should be regarded as a time where the system is in the steady state. The cavity spectrum is related to the Fourier transform of the first-order coherence function

$$g_1(\tau) = \frac{\langle \hat{a}_c^\dagger(\tau)\hat{a}_c(0)\rangle}{\sqrt{\langle \hat{a}_c^\dagger(\tau)\hat{a}_c(\tau)\rangle\langle \hat{a}_c^\dagger(0)\hat{a}_c(0)\rangle}} \tag{4.20}$$

that can be regarded as a measure of the temporal coherence of the cavity field, i.e., how long the cavity field is coherent with the field at an earlier time τ. Figure 4.5 shows the steady-state cavity output spectra $S(\omega)$ at zero detuning, $\Delta_0 = \omega_c - \omega_d = 0$. Both the cavity output spectra obtained by the standard master equation and the

dressed-state master equation have sideband peaks at integer multiples of the mechanical frequency ω_M, which is due to the fact that with $g_0 = \omega_M$ all the mechanical sideband transitions shift the system energy by integers of ω_M. Furthermore, the peaks with widths about the multiple of the mechanical linewidth γ_M are distinguishable, indicating that the system is in the strong-coupling resolved-sideband regime [44]. The fact that more peaks in the spectra appear at negative frequencies exhibits that at a low temperature of $n_{th} = 3$, the cavity photons in the steady state have a larger probability to create one or more phonons and leave the cavity with frequencies smaller than the driving frequency ω_d than to absorb the energy of one or more phonons and leave the cavity with frequencies larger than ω_d. As expected, one can clearly see from Fig. 4.5 that the peaks are more pronounced and resolved in the spectrum obtained by the dressed-state master equation.

Multi-cavity system

In the final part of this chapter, we extend the DSME approach to the case of two cavities coupling with a single mechanical mode and study the entanglement dynamics among the two cavity modes. With the same argument, in the interaction picture of system Hamiltonian, one could obtain the DSME as (see Appendix C.4),

$$\begin{aligned} \frac{d\tilde{\rho}(t)}{dt} &= \sum_i \kappa_i \mathcal{D}[\hat{a}_{ci}]\tilde{\rho}(t) + n_{th}\gamma_M \mathcal{D}[\hat{b}_M^\dagger - \hat{\mathcal{N}}_c]\tilde{\rho}(t) \\ &+ (n_{th}+1)\gamma_M \mathcal{D}[\hat{b}_M - \hat{\mathcal{N}}_c]\tilde{\rho}(t) \end{aligned} \tag{4.21}$$

where $\hat{\mathcal{N}}_c = \beta_1 \hat{N}_{c1} + \beta_2 \hat{N}_{c2}$ and $\beta_i = g_i/\omega_M$ with g_i as the optomechanical coupling of i-th cavity mode to the mechanical mode. Here $\hat{\Omega}_{ci}$ with subscript ci denotes the operator of i-th cavity mode. The OMS is initially prepared in the entangled cavity state $|\psi(0)\rangle = (|0_{c1}\rangle|1_{c2}\rangle + |1_{c1}\rangle|0_{c2}\rangle)\,|0_M\rangle/\sqrt{2}$ and the cavity-cavity entanglement is characterized by the Werner negativity [30]

$$\mathcal{N}(\rho) \equiv log_2\left(||\rho^{T_A}||_1\right) \tag{4.22}$$

with $||A||_1 = tr\sqrt{A^\dagger A}$ being the trace norm of Hermitian operator A, and ρ here being the bipartite density matrix $\rho_C(t) = tr_M(\tilde{\rho}(t))$ for the joint system of the two cavity modes at time t reduced from the solution of the master equation Eq.(4.21). Fig. 4.6 shows the entanglement dynamics for two different set of optomechanical coupling. When $\beta_1 = \beta_2 = 1.5$, due to the fact that photons in the state of $|0_{c1}\rangle|1_{c2}\rangle$ and photons in the state of $|1_{c1}\rangle|0_{c2}\rangle$ shift the mechanical mode equally, the coherence between these two cavity modes as well as entanglement is not affected much by the mechanical mode and its thermal noise. As a result, the two master equations give the exact same dynamics for the cavity-cavity entanglement and their decay

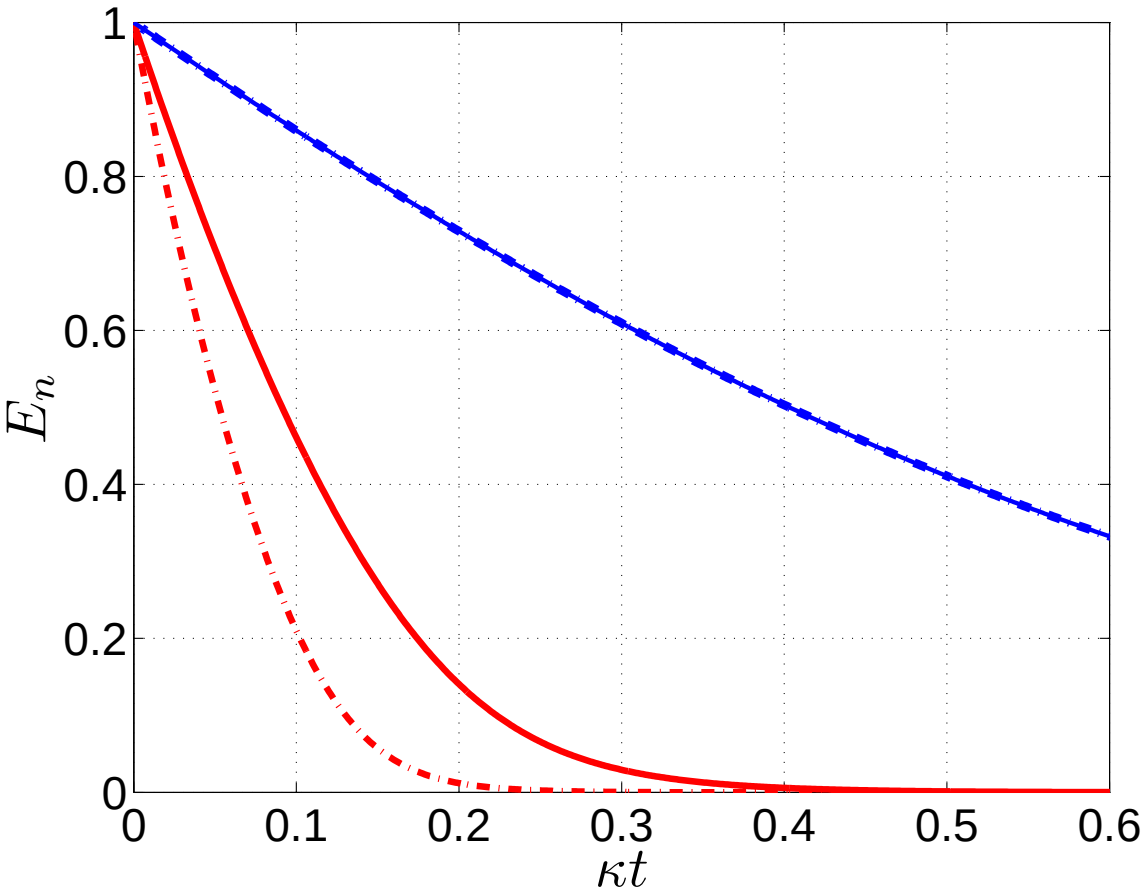

Figure 4.6: Entanglement of two cavity modes measured by Werner negativity of Eq.(4.22). Solid curves are from DSME and dashed curves belongs to the SME. For asymmetric couplings $\beta_1 = 1.5$ and $\beta_2 = 0.5$ (lower curves). For symmetric couplings $\beta_1 = \beta_2 = 1.5$ (upper curves). Parameters are chosen as: $\omega_M/2\pi = 1$, $\kappa_1 = \kappa_2 = 0.005\omega_M$, $\gamma_M = \kappa/3$ and $n_{th} = 20$.

rate is dominated by the cavity decay rate ($\kappa_1 = \kappa_2$). However, once there is a asymmetry in the optomechanical coupling, i.e. $\beta_1 \neq \beta_2$ (blue color curves), the mechanical noises will dominate the dynamics for the cavity-cavity entanglement, where the entanglement under the DSME exists twice as long as it is predicted by the SME approach. This suggests that the SME is insufficient to reveal the entanglement dynamics for the OMS in the strong coupling regime.

4.5 Conclusions

Our results suggest that the influence of the optomechanical coupling should be considered for the dissipative dynamics in the strong coupled optomechanical system, where the dressed-state master equation approach is necessary to reveal the transient dynamics in the time scale of the cavity damping. We showed that in the parameter regimes with high bath temperature or where the mechanical damping is dominant, the transient dynamics of the cavity coherent amplitude and the mechanical quadratures, the decay of the optical coherence function $g^{(2)}(0)$, and the optomechanical entanglement are all influenced by the strong optomechanical interaction and in such situations only the dressed-state master equation Eq.(4.8) is able to reveal the correct dynamics. Using the standard master equation approach Eq.(4.9) in this case will introduce additional unrealistic thermal noises to the cavity field. With no external driving, the dressed-state master equation in the steady state gives the similar results as the standard master equation approach. Therefore if one is only interested in the steady-state behavior of the optomechanical system with zero driving, the standard master equation with the independent bath model is adequate. However, even with a weak external driving field, many steady-state properties of the strong coupled optomechanical system are observed only via the dressed-state master equation approach, indicating that the standard master equation approach is actually inadequate for charactering the steady-state dynamics for optomechanical system in the strong coupling regime. Our result indicates that the form of the dissipative cavity response to the cavity thermal bath in the DSME, Eq. (4.8), is not affected by the strong optomechanical interaction when the cavity mode frequency is in the optical frequency. It is important to note, however, for the general case, the system response to the cavity thermal bath may be strongly influenced by the optomechanical coupling when the cavity field frequency is in the microwave region where the cavity responses are much more complex. However, it is still solvable by our theoretical frame developed here and needs further investigation.

In summary, we have derived a Lindblad master equation for the optomechanical system with dependent decoherence model in the single-photon strong coupling regime based on the optomechanical dressed basis. We applied this master equation to investigate the transient dynamics of optomechanical system in several different parameter regimes and compared the results to the standard master equation method with the independent decoherence model. We found that the dressed-state master equation is capable of revealing more coherent dynamics for the optomechanical system under the strong radiation pressure interaction.

Chapter 5

Conclusions and Future Work

We have theoretically investigated the roles of the nonlinear optomechanical interactions for three different parameter regimes, such as weak coupling, medium coupling and strong coupling regimes. For the weak optomechanical coupling regime, the linearization condition was revisited with focus on the validity of the pulsed scheme for the linearized optomechanical model; subsequently, a linearization time window was proposed to guarantee the linearization approximation and was applied to find new limits on the entanglement generation in pulsed scheme for the blue-detuned unstable optomechanical system. Moreover, a time dependent driving scheme for the three-mode optomechanical system has also been proposed here. It provides additional controls for the entanglement generations of the optomechanical system, which potentially could be applied for a future optomechanical-based quantum communication.

For the nonlinear parameter regime, two theoretical methods have been developed in this dissertation to deal with nonlinear dynamics, i.e. perturbation in the Heisenberg picture and the dressed-state master equation. With its explicit form, the perturbation method could be easily applied for various parameter regimes. The first order perturbation has been implemented to investigate the influence of nonlinear interaction on the modification of the linearized optomechanical model; it shows the amplitude of the field operators, as well as the entanglement dynamics, which are affected by the nonlinear part of the optomechanical interaction. However, the complexity of the perturbation method strongly limited its application. Only some nonlinear properties of the optomechanical system have been revealed by such a method, but most of the interesting optomechanical phenomena are outside the range of the perturbation method. Nevertheless, similar methods have been recently implemented to discover the nonlinear optomechanical induced transparency (OMIT). Due to its different approaches in handling the environmental noises, we expect that the perturbation method developed in this dissertation could yield slightly different pictures for the nonlinear OMIT.

In order to overcome these weaknesses of the operator perturbation method, we constructed a new dressed-state master equation to investigate the influence of nonlinear optomechanical interaction for the open dynamics of the standard optomechanical system. In contrast to the traditional master equation approach, this new master equation treats the mechanical mode and the cavity mode as an integrity, which leads to dependent decoherence dynamics for these two modes. As a result, new transient dynamics, as well as steady state behaviors, have been discovered by this new approach. It is possible that this dressed-state master equation has broad applications for the atomic gas system, in which the parameter regime tends to reveal the difference between our new master equation and the traditional one.

Appendix A

Blue-detuned optomechanical system

A.1 Covariance Matrix under RWA

we only present the analytical results for the blue-detuned cavity driving and assumes the rotating wave approximation (RWA), for which one can show that the covariance matrix V of the system takes the form of,

$$V(t) = \begin{bmatrix} V_{11} & 0 & 0 & V_{14} \\ 0 & V_{11} & V_{14} & 0 \\ 0 & V_{14} & V_{33} & 0 \\ V_{14} & 0 & 0 & V_{33} \end{bmatrix} \tag{A.1}$$

where

$$\begin{aligned} V_{11} &= \frac{1}{2}g^2(\lambda_1,\lambda_3,t) + \left(n_0+\frac{1}{2}\right) f^2(t) + \gamma_M \left(n_{th}+\frac{1}{2}\right)\left(\frac{2g}{\Omega}\right)^2 F(t) \\ &\quad +\kappa G(\lambda_1,\lambda_3,t), \end{aligned} \tag{A.2}$$

$$\begin{aligned} V_{33} &= \frac{1}{2}f^2(t) + \left(n_0+\frac{1}{2}\right) g^2(\lambda_3,\lambda_1,t) + \gamma_M \left(n_{th}+\frac{1}{2}\right)\left(\frac{2g}{\Omega}\right)^2 G(\lambda_3,\lambda_1,t) \\ &\quad +\kappa F(t), \end{aligned} \tag{A.3}$$

$$\begin{aligned} V_{14} &= -f(t)g(\lambda_1,\lambda_3,t) - \left(n_0+\frac{1}{2}\right) f(t) g(\lambda_3,\lambda_1,t) - \gamma_M \left(n_{th}+\frac{1}{2}\right)\xi(A,B) \\ &\quad -\kappa\xi(B,A), \end{aligned} \tag{A.4}$$

with $g(x,y,t) = A \cdot e^{xt} + B \cdot e^{yt}$ and $f(t) = \left(\frac{2g}{\Omega}\right)\left(e^{\lambda_3 t} - e^{\lambda_1 t}\right)$

$$F(t) = \frac{e^{2\lambda_1 t}-1}{2\lambda_1} - 2\frac{e^{(\lambda_1+\lambda_3)t}-1}{(\lambda_1+\lambda_3)} + \frac{e^{2\lambda_3 t}-1}{2\lambda_3}, \tag{A.5}$$

$$G(x,y,t) = A^2 \cdot \frac{e^{2xt}-1}{2x} + 2AB \cdot \frac{e^{(x+y)t}-1}{x+y} + B^2 \cdot \frac{e^{2yt}-1}{2y}, \tag{A.6}$$

$$\xi(x,y,t) = \left(\frac{2g}{\Omega}\right)\left((x-y)\frac{e^{(\lambda_1+\lambda_3)t}-1}{(\lambda_1+\lambda_3)} - x\frac{e^{2\lambda_1 t}-1}{2\lambda_1} + y\frac{e^{2\lambda_3 t}-1}{2\lambda_3}\right), \tag{A.7}$$

Here V_{11} is associated with the cavity mode, V_{33} to the mechanical mode, and V_{14} describing the correlations between these two. The entanglement of the system can be well described by the logarithmic negativity E_N,

$$E_N = \max\left(0, -\ln 2\eta^-\right)$$

where $\eta^- = \frac{1}{\sqrt{2}}\left(\Sigma(V) - \sqrt{\Sigma(V) - 4\det V}\right)^{1/2}$ with $\Sigma(V) = V_{11}^2 + V_{33}^2 + 2V_{14}^2$.

Steady-State Entanglement

When both $\lambda_1 < 0$ and $\lambda_3 < 0$, the system is in the stable and the steady-state covariance matrix V can be obtained by setting $t \to +\infty$,

$$\begin{aligned}(V_{11})_{ss} &= -\gamma_M\left(n_{th}+\frac{1}{2}\right)\left(\frac{2g}{\Omega}\right)^2\left(\frac{1}{2\lambda_1}+\frac{1}{2\lambda_3}-\frac{2}{\lambda_1+\lambda_3}\right)\\ &\quad -\kappa\left(\frac{A^2}{2\lambda_1}+\frac{B^2}{2\lambda_3}+\frac{2AB}{\lambda_1+\lambda_3}\right),\end{aligned} \tag{A.8}$$

$$\begin{aligned}(V_{33})_{ss} &= -\gamma_M\left(n_{th}+\frac{1}{2}\right)\left(\frac{A^2}{2\lambda_1}+\frac{B^2}{2\lambda_3}+\frac{2AB}{\lambda_1+\lambda_3}\right)\\ &\quad -\kappa\left(\frac{2g}{\Omega}\right)^2\left(\frac{1}{2\lambda_1}+\frac{1}{2\lambda_3}-\frac{2}{\lambda_1+\lambda_3}\right),\end{aligned} \tag{A.9}$$

$$\begin{aligned}(V_{14})_{ss} &= \gamma_M\left(n_{th}+\frac{1}{2}\right)\left(\frac{2g}{\Omega}\right)\left(\frac{B-A}{\lambda_1+\lambda_3}-\frac{B}{2\lambda_1}+\frac{A}{2\lambda_3}\right)\\ &\quad +\kappa\left(\frac{2g}{\Omega}\right)\left(\frac{A-B}{\lambda_1+\lambda_3}-\frac{A}{2\lambda_1}+\frac{B}{2\lambda_3}\right),\end{aligned} \tag{A.10}$$

One can show that the above results are equivalent to the steady-state entanglement obtained in [31], which makes our results of the steady-state entanglement generation with the same property of [31], i.e. it is limited by $E_n < \ln 2$ and very sensitive to thermal noise.

A.2 Optomechanical Entanglement between Cavity Output Mode and Mechanical Mode

In practice, people are more interested on the output optical field which could be measured by experiments. In this section, we provide an input-output formalism to describe the entanglement between the output field and the mechanical oscillator.

In order to quantify the entanglement between mechanical mode and the cavity output mode we need to introduce the following integrated output field over a measurement time T_m [77],

$$\hat{a}_{out}(t,Tm) = \frac{1}{\sqrt{T_m}} \int_t^{t+T_m} dt' \hat{a}_{out}(t') \tag{A.11}$$

where $\hat{a}_{out}(t,Tm)$ form a set of dimensionless bosonic operators, with commutators as $[\hat{a}_{out}(t,Tm), \hat{a}^{\dagger}_{out}(t,Tm)] = 1$ and $\hat{a}_{out}(t)$ is the cavity output field operator which is related to the intracavity field $\hat{a}_c(t)$ by the input-output relation,i.e.

$$\hat{a}_{out}(t) = \hat{a}_{in}(t) + \sqrt{2\kappa}\hat{a}_c(t) \tag{A.12}$$

If we choose to measure the output field at the end of the blue-detuned laser pulse with duration of τ, the evolution of $\hat{a}_c(t)$ is actually determined by the following non-linear langevin equations

$$\frac{d}{dt}\hat{b}_M(t) = -i\omega_M \hat{b}_M(t) - \frac{\gamma_M}{2}\left(\hat{b}_M(t) - \hat{b}^{\dagger}_M(t)\right) - ig_0\hat{a}^{\dagger}_c(t)\hat{a}_c(t) - \sqrt{\gamma_M}\hat{b}_{in}(t), \tag{A.13}$$

$$\frac{d}{dt}\hat{a}_c(t) = i\omega_M \hat{a}_c(t) - \kappa\hat{a}_c(t) - ig_0\hat{a}_c(t)\left(\hat{b}_M(t) + \hat{b}^{\dagger}_M(t)\right) - \sqrt{2\kappa}\hat{a}_{in}(t), \tag{A.14}$$

However, g_0 is always much smaller than κ due to zero driving field and therefore we can surely neglect the optomechanical interaction during the measurement time T_m if T_m is in the order of cavity decay time κ^{-1}. As a result after turn off the driving laser we can assume there is only cavity field leaking out and the mechanical mode is only in the free evolution during the measurement time T_m, which leads to the following solutions, i.e. when $t > \tau$

$$\hat{a}_c(t) = e^{-\kappa(t-\tau)}\hat{a}_c(\tau) - \sqrt{2\kappa}\int_\tau^t ds \cdot e^{-\kappa(t-s)}\hat{a}_{in}(s), \tag{A.15}$$

$$\hat{b}_M(t) = \hat{b}_M(\tau), \tag{A.16}$$

where $\hat{a}_c(\tau)$ and $\hat{b}_M(\tau)$ are the solutions of the intracavity optomechanical system at the end of the blue-detuned laser pulse. By definition, the integrated output field operator is

$$\hat{a}_{out}(\tau, T_m) = \alpha(T_m)\,\hat{a}_c(\tau) + \hat{n}^{in}(\tau, T_m)$$

with

$$\alpha\left(T_m\right)=\sqrt{\frac{2\kappa}{T_m}}\left(\frac{1-e^{-\kappa T_m}}{\kappa}\right)$$

and

$$\hat{n}^{in}\left(\tau,T_m\right)=\frac{2}{\sqrt{T_m}}\int_{\tau}^{\tau+T_m}ds\cdot\left(e^{-\kappa(\tau+T_m-s)}-\frac{1}{2}\right)\hat{a}_{in}(s)$$

and the corresponding amplitude and phase quadratures of the cavity output field are

$$\begin{aligned}\hat{X}_c^{out}\left(\tau,T_m\right) &= \alpha\left(T_m\right)\hat{X}_c\left(\tau\right)+\hat{X}_n^{in}\left(\tau,T_m\right),\\ \hat{P}_c^{out}\left(\tau,T_m\right) &= \alpha\left(T_m\right)\hat{P}_c\left(\tau\right)+\hat{P}_n^{in}\left(\tau,T_m\right).\end{aligned}$$

Covariance Matrix for the system of output field mode and mechanical mode

The state of the output field and mechanical oscillator can be completely described by the Covariance Matrix, which in our case are

$$V^{out}=\begin{pmatrix} A & \alpha\left(T_m\right)\cdot C \\ \alpha\left(T_m\right)\cdot C^T & \alpha\left(T_m\right)^2\cdot B+\frac{1-\alpha(T_m)^2}{2}\cdot I_{2\times 2}\end{pmatrix}$$

where $I_{2\times2}$ is the two dimensional identity matrix and the element A, B and C comes from the intracavity Covariance Matrix at the end of the blue-detuned pulse, which is

$$V=\begin{pmatrix} A & C \\ C^T & B\end{pmatrix}$$

and in the blue-detuned laser case

$$A=\begin{pmatrix} V_{11}\left(\tau\right) & 0 \\ 0 & V_{11}\left(\tau\right)\end{pmatrix},B=\begin{pmatrix} V_{33}\left(\tau\right) & 0 \\ 0 & V_{33}\left(\tau\right)\end{pmatrix},C=\begin{pmatrix} 0 & V_{14}\left(\tau\right) \\ V_{14}\left(\tau\right) & 0\end{pmatrix}$$

where $V_{ij}\left(\tau\right)$ is the solution of CM for the intracavity system and the exact expression for $V_{ij}\left(\tau\right)$ is given in Eq.A.4.

With the help of Covariance Matrix V^{out} we can use the lorgrithmic negativity E_N as a quantity to describe the entanglement between the output field mode and mechanical mode. In the continuous variable case E_N can be defined as

$$E_N=\max\left(0,-\ln 2\eta^-\right)$$

where

$$\eta^-=\frac{1}{\sqrt{2}}\left(\Sigma\left(V\right)-\sqrt{\Sigma\left(V\right)-4\det V^{out}}\right)^{1/2}$$

with $\Sigma\left(V\right)=\det\left(A\right)^2+\det\left(\alpha\left(T_m\right)^2\cdot B+\frac{1-\alpha(T_m)^2}{2}\cdot I_{2\times2}\right)^2-2\det\left(\alpha\left(T_m\right)\cdot C\right)^2$.

Appendix B

Perturbation Methods

B.1 Calculation of the Second Moment

To apply the perturbation method, one important step is to have the mathematical expressions for the inhomogeneous term $\langle \mathrm{g}(\hat{u}^{(0)}(t'))\rangle$, which depends on the second moment of $\hat{u}^{(0)}(t)$ of the optomechanical system. In this section we show the details of how to calculate the optomechanical system's second order moment.

From Eq.(3.15) the i-th element of $\hat{u}^{(0)}(t)$ reads,

$$\begin{aligned}\hat{u}_i^{(0)}(t) &= \sum_{k,l,n} U_{ik}^{-1}\delta_{kl}e^{\lambda_k t}U_{ln}\hat{u}_n^{(0)}(0) + \sum_{k,l,n,m} U_{ik}^{-1}\delta_{kl}e^{\lambda_l t}\int_0^t dt'\delta_{ln}e^{-\lambda_n t'}U_{nm}\hat{n}_m(t') \\ &= \sum_{k,n} U_{ik}^{-1}e^{\lambda_k t}U_{kn}\hat{u}_n^{(0)}(0) + \sum_{l,m} U_{il}^{-1}e^{\lambda_l t}\int_0^t dt' e^{-\lambda_l t'}U_{lm}\hat{n}_m(t') \qquad \text{(B.1)}\end{aligned}$$

which leads to the second moment of $\hat{u}^{(0)}(t)$ as,

$$\begin{aligned}\langle \hat{u}_i^{(0)}(t)\hat{u}_j^{(0)}(t)\rangle &= \sum_{k,n} U_{ik}^{-1}e^{\lambda_k t}U_{kn}\sum_{k',n'} U_{jk'}^{-1}e^{\lambda_{k'} t}U_{k'n'}\langle \hat{u}_n^{(0)}(0)\hat{u}_{n'}^{(0)}(0)\rangle \qquad \text{(B.2)} \\ &+ \sum_{l} U_{il}^{-1}e^{\lambda_l t}\sum_{l'} U_{jl'}^{-1}e^{\lambda_{l'} t}\Sigma_{l,l'}(t) \qquad \text{(B.3)}\end{aligned}$$

with the integral as

$$\Sigma_{l,l'}(t) = \int_0^t dt_1 \int_0^t dt_2 e^{-\lambda_l t_1}e^{-\lambda_{l'} t_2}\sum_{m,m'} U_{lm}U_{l'm'}\langle \hat{n}_m(t_1)\hat{n}_{m'}(t_2)\rangle \qquad \text{(B.4)}$$

We choose our initial state so that its second moments are characterized by the matrix

$$V = \langle \hat{u}(\tau = 0)\hat{u}^T(\tau = 0)\rangle \qquad \text{(B.5)}$$

leading to

$$\langle \hat{u}_n^{(0)}(0)\hat{u}_{n'}^{(0)}(0)\rangle = \sum_{i,j} \delta_{n=i,n'=j} V_{ij} \tag{B.6}$$

the nonzero noise correlation function for the standard optomechanical system reads

$$\begin{aligned}
\langle \hat{b}^{in,\dagger}(t)\hat{b}^{in}(t')\rangle &= \bar{n}\delta(t-t'), && \text{(B.7)}\\
\langle \hat{b}^{in}(t)\hat{b}^{in,\dagger}(t')\rangle &= (\bar{n}+1)\delta(t-t'), && \text{(B.8)}\\
\langle \hat{a}^{in}(t)\,\hat{a}^{in,\dagger}(t')\rangle &= \delta(t-t'), && \text{(B.9)}
\end{aligned}$$

which yields the following relations,

$$\langle \hat{n}_m(t_1)\hat{n}_{m'}(t_2)\rangle = \left(\frac{(\bar{n}+1)\tilde{\gamma}_M}{g}\delta_{m=1,m'=2} + \frac{\bar{n}\tilde{\gamma}_M}{g}\delta_{m=2,m'=1} + \frac{2\tilde{\kappa}}{g}\delta_{m=3,m'=4}\right)\delta(t_1-t_2) \tag{B.10}$$

As a result, the integral shows

$$\Sigma_{l,l'}(t) = \frac{1-e^{-(\lambda_l+\lambda_{l'})t}}{(\lambda_l+\lambda_{l'})\,g}\Big(\bar{n}\tilde{\gamma}_M U_{l2}U_{l'1} + (\bar{n}+1)\tilde{\gamma}_M U_{l1}U_{l'2} + 2\tilde{\kappa}U_{l3}U_{l'4}\Big) \tag{B.11}$$

With these relations, one could simplify the second moment as

$$\begin{aligned}
\langle \hat{u}_i^{(0)}(t)\hat{u}_j^{(0)}(t)\rangle &= \sum_{l,l',n,n'} e^{(\lambda_l+\lambda_{l'})t}U_{il}^{-1}U_{jl'}^{-1}U_{ln}U_{l'n'}V_{nn'}\\
&+ \sum_{l,l'}\frac{e^{(\lambda_l+\lambda_{l'})t}-1}{(\lambda_l+\lambda_{l'})\,g}U_{il}^{-1}U_{jl'}^{-1}\Big(\bar{n}\tilde{\gamma}_M U_{l2}U_{l'1} + (\bar{n}+1)\tilde{\gamma}_M U_{l1}U_{l'2} + 2\tilde{\kappa}U_{l3}U_{l'4}\Big)
\end{aligned} \tag{B.12}$$

Next, let us apply the above results to calculate $\langle \hat{u}^{(1)}(\tau)\rangle$, which reads

$$\langle \hat{u}^{(1)}(\tau)\rangle = U^{-1}e^{D\tau}\int_0^\tau dt' e^{-Dt'}U\cdot\langle \mathrm{g}(\hat{u}^{(0)}(t'))\rangle \tag{B.13}$$

with

$$\langle \mathrm{g}\left(\hat{u}^{(0)}(t)\right)\rangle = \begin{pmatrix} -i\langle \hat{u}_4^{(0)}(t)\hat{u}_3^{(0)}(t)\rangle \\ i\langle \hat{u}_4^{(0)}(t)\hat{u}_3^{(0)}(t)\rangle \\ -i\langle \hat{u}_3^{(0)}(t)\left(\hat{u}_1^{(0)}(t)+\hat{u}_2^{(0)}(t)\right)\rangle \\ i\langle \hat{u}_4^{(0)}(t)\left(\hat{u}_1^{(0)}(t)+\hat{u}_2^{(0)}(t)\right)\rangle \end{pmatrix} \tag{B.14}$$

and the i-th element of $\langle \hat{u}^{(1)}(\tau)\rangle$ could be expressed as,

$$\langle \hat{u}^{(1)}(\tau)\rangle_i = i\sum_k U_{ik}^{-1}\Big((U_{k2}-U_{k1})\cdot G_1(k,\tau) - U_{k3}F_1(k,\tau) + U_{k4}F_2(k,\tau)\Big) \tag{B.15}$$

where

$$G_1(k,\tau) = e^{\lambda_k \tau} \int_0^\tau dt' e^{-\lambda_k t'} \langle \hat{u}_4^{(0)}(t') \hat{u}_3^{(0)}(t') \rangle, \tag{B.16a}$$

$$F_1(k,\tau) = e^{\lambda_k \tau} \int_0^\tau dt' e^{-\lambda_k t'} \left(\langle \hat{u}_3^{(0)}(t') \hat{u}_1^{(0)}(t') \rangle + \langle \hat{u}_3^{(0)}(t') \hat{u}_2^{(0)}(t') \rangle \right), \tag{B.16b}$$

$$F_2(k,\tau) = e^{\lambda_k \tau} \int_0^\tau dt' e^{-\lambda_k t'} \left(\langle \hat{u}_4^{(0)}(t') \hat{u}_1^{(0)}(t') \rangle + \langle \hat{u}_4^{(0)}(t') \hat{u}_2^{(0)}(t') \rangle \right), \tag{B.16c}$$

By substituting the exact form of $\langle \hat{u}_i^{(0)}(t) \hat{u}_j^{(0)}(t) \rangle$ in Eq.(B.19), these integral gives,

$$\begin{aligned} G_1(k,\tau) &= \sum_{l,l',n,n'} \frac{e^{(\lambda_l+\lambda_{l'})\tau} - e^{\lambda_k \tau}}{\lambda_l + \lambda_{l'} - \lambda_k} U_{4l}^{-1} U_{3l'}^{-1} U_{ln} U_{l'n'} V_{nn'} \\ &+ \sum_{l,l'} U_{4l}^{-1} U_{3l'}^{-1} \Big(\bar{n}\tilde{\gamma}_M U_{l2} U_{l'1} + (\bar{n}+1)\tilde{\gamma}_M U_{l1} U_{l'2} + 2\tilde{\kappa} U_{l3} U_{l'4} \Big) \\ &\times \frac{1}{(\lambda_l + \lambda_{l'})\, g} \left(\frac{e^{(\lambda_l+\lambda_{l'})\tau} - e^{\lambda_k \tau}}{\lambda_l + \lambda_{l'} - \lambda_k} - \frac{e^{\lambda_k \tau} - 1}{\lambda_k} \right), \end{aligned} \tag{B.17a}$$

$$\begin{aligned} F_1(k,\tau) &= \sum_{l,l',n,n'} \frac{e^{(\lambda_l+\lambda_{l'})\tau} - e^{\lambda_k \tau}}{\lambda_l + \lambda_{l'} - \lambda_k} U_{3l}^{-1} \left(U_{1l'}^{-1} + U_{2l'}^{-1} \right) U_{ln} U_{l'n'} V_{nn'} \\ &+ \sum_{l,l'} \Big(\bar{n}\tilde{\gamma}_M U_{l2} U_{l'1} + (\bar{n}+1)\tilde{\gamma}_M U_{l1} U_{l'2} + 2\tilde{\kappa} U_{l3} U_{l'4} \Big) U_{3l}^{-1} \left(U_{1l'}^{-1} + U_{2l'}^{-1} \right) \\ &\times \frac{1}{(\lambda_l + \lambda_{l'})\, g} \left(\frac{e^{(\lambda_l+\lambda_{l'})\tau} - e^{\lambda_k \tau}}{\lambda_l + \lambda_{l'} - \lambda_k} - \frac{e^{\lambda_k \tau} - 1}{\lambda_k} \right), \end{aligned} \tag{B.17b}$$

$$\begin{aligned} F_2(k,\tau) &= \sum_{l,l',n,n'} \frac{e^{(\lambda_l+\lambda_{l'})\tau} - e^{\lambda_k \tau}}{\lambda_l + \lambda_{l'} - \lambda_k} U_{4l}^{-1} \left(U_{1l'}^{-1} + U_{2l'}^{-1} \right) U_{ln} U_{l'n'} V_{nn'} \\ &+ \sum_{l,l'} \Big(\bar{n}\tilde{\gamma}_M U_{l2} U_{l'1} + (\bar{n}+1)\tilde{\gamma}_M U_{l1} U_{l'2} + 2\tilde{\kappa} U_{l3} U_{l'4} \Big) U_{4l}^{-1} \left(U_{1l'}^{-1} + U_{2l'}^{-1} \right) \\ &\times \frac{1}{(\lambda_l + \lambda_{l'})\, g} \left(\frac{e^{(\lambda_l+\lambda_{l'})\tau} - e^{\lambda_k \tau}}{\lambda_l + \lambda_{l'} - \lambda_k} - \frac{e^{\lambda_k \tau} - 1}{\lambda_k} \right). \end{aligned} \tag{B.17c}$$

B.2 Calculation of the Third Moment

From Eq.(3.15) the i-th element of $\hat{u}^{(0)}(t)$ reads,

$$\hat{u}_i^{(0)}(t) = \sum_{k,n} U_{ik}^{-1} e^{\lambda_k t} U_{kn} \hat{u}_n^{(0)}(0) + \sum_{l,m} U_{il}^{-1} e^{\lambda_l t} \int_0^t dt' e^{-\lambda_l t'} U_{lm} \hat{n}_m(t') \tag{B.18}$$

which leads the third moment of $\hat{u}^{(0)}(t)$ as,

$$\begin{aligned}\langle \hat{u}_i^{(0)}(t)\hat{u}_j^{(0)}(t)\hat{u}_k^{(0)}(\tau)\rangle &= \sum_{\substack{l_1,\ l_2\\ n_1,n_2}} U^{-1}_{il_1}U^{-1}_{jl_2}e^{\left(\lambda_{l_1}+\lambda_{l_2}\right)t}U_{l_1n_1}U_{l_2n_2}\sum_{l_3,n_3}U^{-1}_{kl_3}e^{\lambda_{l_3}\tau}U_{l_3n_3}V_{n_1,n_2,n_3}\\ &+ \sum_{l}U^{-1}_{il}e^{\lambda_l t}\sum_{l'}U^{-1}_{jl'}e^{\lambda_{l'}t}\Sigma_{l,l'}(t,t)\sum_{l_3,n_3}U^{-1}_{kl_3}e^{\lambda_{l_3}\tau}U_{l_3n_3}\langle\hat{u}^{(0)}_{n_3}(0)\rangle\\ &+ \sum_{l}U^{-1}_{il}e^{\lambda_l t}\sum_{l'}U^{-1}_{kl'}e^{\lambda_{l'}\tau}\Sigma_{l,l'}(t,\tau)\sum_{l_2,n_2}U^{-1}_{jl_2}e^{\lambda_{l_2}t}U_{l_2n_2}\langle\hat{u}^{(0)}_{n_2}(0)\rangle\\ &+ \sum_{l}U^{-1}_{jl}e^{\lambda_l t}\sum_{l'}U^{-1}_{kl'}e^{\lambda_{l'}\tau}\Sigma_{l,l'}(t,\tau)\sum_{l_1,n_1}U^{-1}_{il_1}e^{\lambda_{l_1}t}U_{l_1n_1}\langle\hat{u}^{(0)}_{n_1}(0)\rangle\end{aligned} \tag{B.19}$$

with $V_{n_1,n_2,n_3} = \langle \hat{u}^{(0)}_{n_1}(0)\hat{u}^{(0)}_{n_2}(0)\hat{u}^{(0)}_{n_3}(0)\rangle$ and

$$\Sigma_{l,l'}(t,t_2) = \int_0^t ds_1\int_0^{t_2} ds_2 e^{-\lambda_l s_1}e^{-\lambda_{l'}s_2}\sum_{m,m'}U_{lm}U_{l'm'}\langle\hat{n}_m(s_1)\hat{n}_{m'}(s_2)\rangle \tag{B.20}$$

When $t \le t_2$

$$\Sigma_{l,l'}(t,t_2) = \frac{1-e^{-(\lambda_l+\lambda_{l'})t}}{g\cdot(\lambda_l+\lambda_{l'})}\left((\bar{n}+1)\tilde{\gamma}U_{l1}U_{l'2} + \bar{n}\tilde{\gamma}U_{l2}U_{l'1} + 2\tilde{\kappa}U_{l3}U_{l'4}\right) \tag{B.21}$$

Because

$$\langle \hat{u}_i^{(1)}(\tau)\hat{u}_j^{(0)}(\tau)\rangle = \sum_{k,l}U^{-1}_{ik}e^{\lambda_k\tau}U_{kl}\int_0^\tau dt' e^{-\lambda_k t'}\cdot\langle \mathcal{G}_l(\hat{u}^{(0)}(t'))\hat{u}^{(0)}_j(\tau)\rangle \tag{B.22}$$

with the integral given by

$$\langle \hat{u}_i^{(1)}(\tau)\hat{u}_j^{(0)}(\tau)\rangle = \sum_k U^{-1}_{ik}\Big(i\left(U_{k2}-U_{k1}\right)\Lambda_1(k,\tau) - iU_{k3}\Lambda_2(k,\tau) + iU_{k4}\Lambda_3(k,\tau)\Big) \tag{B.23}$$

where

$$\Lambda_1(k,\tau) = e^{\lambda_k\tau}\int_0^\tau dt e^{-\lambda_k t}\langle\hat{u}^{(0)}_4(t)\hat{u}^{(0)}_3(t)\hat{u}^{(0)}_j(\tau)\rangle, \tag{B.24a}$$

$$\Lambda_2(k,\tau) = e^{\lambda_k\tau}\int_0^\tau dt e^{-\lambda_k t}\langle\hat{u}^{(0)}_3(t)\left(\hat{u}^{(0)}_1(t)+\hat{u}^{(0)}_2(t)\right)\hat{u}^{(0)}_j(\tau)\rangle, \tag{B.24b}$$

$$\Lambda_3(k,\tau) = e^{\lambda_k\tau}\int_0^\tau dt e^{-\lambda_k t}\langle\hat{u}^{(0)}_4(t)\left(\hat{u}^{(0)}_1(t)+\hat{u}^{(0)}_2(t)\right)\hat{u}^{(0)}_j(\tau)\rangle, \tag{B.24c}$$

Substituting Eq.(B.19) back into the above equations, one arrives at

$$\begin{aligned}
\Lambda_1(k,\tau) &= \sum_{\substack{l_1,\ l_2,\ l_3\\ n_1,n_2,n_3}} \frac{e^{\left(\lambda_{l_1}+\lambda_{l_2}+\lambda_{l_3}\right)\tau}-e^{\left(\lambda_k+\lambda_{l_3}\right)\tau}}{\lambda_{l_1}+\lambda_{l_2}-\lambda_k} U^{-1}_{4l_1}U^{-1}_{3l_2}U^{-1}_{jl_3}U_{l_1n_1}U_{l_2n_2}U_{l_3n_3}V_{n_1n_2n_3} \\
&- \sum_{l_1,l_2,l_3}\Bigg\{\frac{\sum_{n_3}U_{l_3n_3}\langle\hat{u}(\tau)\rangle_{n_3}}{g\cdot(\lambda_{l_1}+\lambda_{l_2})}\left(\frac{e^{\left(\lambda_k+\lambda_{l_3}\right)\tau}-e^{\lambda_{l_3}\tau}}{\lambda_k}-\frac{e^{\left(\lambda_{l_1}+\lambda_{l_2}+\lambda_{l_3}\right)\tau}-e^{\left(\lambda_k+\lambda_{l_3}\right)\tau}}{\lambda_{l_1}+\lambda_{l_2}-\lambda_k}\right) \\
&\times U^{-1}_{4l_1}U^{-1}_{3l_2}U^{-1}_{jl_3}W_{l_1,l_2}\Bigg\} \\
&- \sum_{l_1,l_2,l_3}\Bigg\{\frac{\sum_{n_2}U_{l_2n_2}\langle\hat{u}(\tau)\rangle_{n_2}}{g\cdot(\lambda_{l_1}+\lambda_{l_3})}\left(\frac{e^{\lambda_{l_2}\tau}-e^{\left(\lambda_{l_3}+\lambda_k\right)\tau}}{\lambda_{l_2}-\lambda_{l_3}-\lambda_k}-\frac{e^{\left(\lambda_{l_1}+\lambda_{l_2}+\lambda_{l_3}\right)\tau}-e^{\left(\lambda_k+\lambda_{l_3}\right)\tau}}{\lambda_{l_1}+\lambda_{l_2}-\lambda_k}\right) \\
&\times U^{-1}_{4l_1}U^{-1}_{jl_3}U^{-1}_{3l_2}W_{l_1l_3}\Bigg\} \\
&- \sum_{l_1,l_2,l_3}\Bigg\{\frac{\sum_{n_1}U_{l_1n_1}\langle\hat{u}(\tau)\rangle_{n_1}}{g\cdot(\lambda_{l_2}+\lambda_{l_3})}\left(\frac{e^{\lambda_{l_1}\tau}-e^{\left(\lambda_{l_3}+\lambda_k\right)\tau}}{\lambda_{l_1}-\lambda_{l_3}-\lambda_k}-\frac{e^{\left(\lambda_{l_2}+\lambda_{l_1}+\lambda_{l_3}\right)\tau}-e^{\left(\lambda_k+\lambda_{l_3}\right)\tau}}{\lambda_{l_1}+\lambda_{l_2}-\lambda_k}\right) \\
&\times U^{-1}_{4l_1}U^{-1}_{jl_3}U^{-1}_{3l_2}W_{l_2l_3}\Bigg\} \qquad \text{(B.25)}
\end{aligned}$$

where $W_{ll'}=(\bar{n}+1)\tilde{\gamma}U_{l1}U_{l'2}+\bar{n}\tilde{\gamma}U_{l2}U_{l'1}+2\tilde{\kappa}U_{l3}U_{l'4}$ and the third order moment for the initial state reads

$$V_{n_1n_2n_3}=\langle\hat{u}^{(0)}_{n_1}(0)\hat{u}^{(0)}_{n_2}(0)\hat{u}^{(0)}_{n_3}(0)\rangle \qquad \text{(B.26)}$$

$$\begin{aligned}
\Lambda_2(k,\tau) &= \sum_{\substack{l_1,\ l_2,\ l_3\\ n_1,n_2,n_3}} \frac{e^{\left(\lambda_{l_1}+\lambda_{l_2}+\lambda_{l_3}\right)\tau}-e^{\left(\lambda_k+\lambda_{l_3}\right)\tau}}{\lambda_{l_1}+\lambda_{l_2}-\lambda_k} U^{-1}_{3l_1}\left(U^{-1}_{1l_2}+U^{-1}_{2l_2}\right)U^{-1}_{jl_3}U_{l_1n_1}U_{l_2n_2}U_{l_3n_3}V_{n_1n_2n_3} \\
&- \sum_{l_1,l_2,l_3}\Bigg\{\frac{\sum_{n_3}U_{l_3n_3}\langle\hat{u}(\tau)\rangle_{n_3}}{g\cdot(\lambda_{l_1}+\lambda_{l_2})}\left(\frac{e^{\left(\lambda_k+\lambda_{l_3}\right)\tau}-e^{\lambda_{l_3}\tau}}{\lambda_k}-\frac{e^{\left(\lambda_{l_1}+\lambda_{l_2}+\lambda_{l_3}\right)\tau}-e^{\left(\lambda_k+\lambda_{l_3}\right)\tau}}{\lambda_{l_1}+\lambda_{l_2}-\lambda_k}\right) \\
&\times U^{-1}_{3l_1}\left(U^{-1}_{1l_2}+U^{-1}_{2l_2}\right)U^{-1}_{jl_3}W_{l_1,l_2}\Bigg\} \\
&- \sum_{l_1,l_2,l_3}\Bigg\{\frac{\sum_{n_2}U_{l_2n_2}\langle\hat{u}(\tau)\rangle_{n_2}}{g\cdot(\lambda_{l_1}+\lambda_{l_3})}\left(\frac{e^{\lambda_{l_2}\tau}-e^{\left(\lambda_{l_3}+\lambda_k\right)\tau}}{\lambda_{l_2}-\lambda_{l_3}-\lambda_k}-\frac{e^{\left(\lambda_{l_1}+\lambda_{l_2}+\lambda_{l_3}\right)\tau}-e^{\left(\lambda_k+\lambda_{l_3}\right)\tau}}{\lambda_{l_1}+\lambda_{l_2}-\lambda_k}\right) \\
&\times U^{-1}_{3l_1}U^{-1}_{jl_3}\left(U^{-1}_{1l_2}+U^{-1}_{2l_2}\right)W_{l_1l_3}\Bigg\} \\
&- \sum_{l_1,l_2,l_3}\Bigg\{\frac{\sum_{n_1}U_{l_1n_1}\langle\hat{u}(\tau)\rangle_{n_1}}{g\cdot(\lambda_{l_2}+\lambda_{l_3})}\left(\frac{e^{\lambda_{l_1}\tau}-e^{\left(\lambda_{l_3}+\lambda_k\right)\tau}}{\lambda_{l_1}-\lambda_{l_3}-\lambda_k}-\frac{e^{\left(\lambda_{l_2}+\lambda_{l_1}+\lambda_{l_3}\right)\tau}-e^{\left(\lambda_k+\lambda_{l_3}\right)\tau}}{\lambda_{l_1}+\lambda_{l_2}-\lambda_k}\right) \\
&\times U^{-1}_{3l_1}U^{-1}_{jl_3}\left(U^{-1}_{1l_2}+U^{-1}_{2l_2}\right)W_{l_2l_3}\Bigg\} \qquad \text{(B.27)}
\end{aligned}$$

$$
\begin{aligned}
\Lambda_3(k,\tau) &= \sum_{\substack{l_1,\ l_2,\ l_3\\ n_1,n_2,n_3}} \frac{e^{\left(\lambda_{l_1}+\lambda_{l_2}+\lambda_{l_3}\right)\tau}-e^{\left(\lambda_k+\lambda_{l_3}\right)\tau}}{\lambda_{l_1}+\lambda_{l_2}-\lambda_k} U_{4l_1}^{-1}\left(U_{1l_2}^{-1}+U_{2l_2}^{-1}\right)U_{jl_3}^{-1}U_{l_1n_1}U_{l_2n_2}U_{l_3n_3}V_{n_1n_2n_3} \\
&- \sum_{l_1,l_2,l_3}\Bigg\{\frac{\sum_{n_3}U_{l_3n_3}\langle\hat{u}(\tau)\rangle_{n_3}}{g\cdot\left(\lambda_{l_1}+\lambda_{l_2}\right)}\left(\frac{e^{\left(\lambda_k+\lambda_{l_3}\right)\tau}-e^{\lambda_{l_3}\tau}}{\lambda_k}-\frac{e^{\left(\lambda_{l_1}+\lambda_{l_2}+\lambda_{l_3}\right)\tau}-e^{\left(\lambda_k+\lambda_{l_3}\right)\tau}}{\lambda_{l_1}+\lambda_{l_2}-\lambda_k}\right) \\
&\quad\times U_{4l_1}^{-1}\left(U_{1l_2}^{-1}+U_{2l_2}^{-1}\right)U_{jl_3}^{-1}W_{l_1,l_2}\Bigg\} \\
&- \sum_{l_1,l_2,l_3}\Bigg\{\frac{\sum_{n_2}U_{l_2n_2}\langle\hat{u}(\tau)\rangle_{n_2}}{g\cdot\left(\lambda_{l_1}+\lambda_{l_3}\right)}\left(\frac{e^{\lambda_{l_2}\tau}-e^{\left(\lambda_{l_3}+\lambda_k\right)\tau}}{\lambda_{l_2}-\lambda_{l_3}-\lambda_k}-\frac{e^{\left(\lambda_{l_1}+\lambda_{l_2}+\lambda_{l_3}\right)\tau}-e^{\left(\lambda_k+\lambda_{l_3}\right)\tau}}{\lambda_{l_1}+\lambda_{l_2}-\lambda_k}\right) \\
&\quad\times U_{4l_1}^{-1}U_{jl_3}^{-1}\left(U_{1l_2}^{-1}+U_{2l_2}^{-1}\right)W_{l_1l_3}\Bigg\} \\
&- \sum_{l_1,l_2,l_3}\Bigg\{\frac{\sum_{n_1}U_{l_1n_1}\langle\hat{u}(\tau)\rangle_{n_1}}{g\cdot\left(\lambda_{l_2}+\lambda_{l_3}\right)}\left(\frac{e^{\lambda_{l_1}\tau}-e^{\left(\lambda_{l_3}+\lambda_k\right)\tau}}{\lambda_{l_1}-\lambda_{l_3}-\lambda_k}-\frac{e^{\left(\lambda_{l_2}+\lambda_{l_1}+\lambda_{l_3}\right)\tau}-e^{\left(\lambda_k+\lambda_{l_3}\right)\tau}}{\lambda_{l_1}+\lambda_{l_2}-\lambda_k}\right) \\
&\quad\times U_{4l_1}^{-1}U_{jl_3}^{-1}\left(U_{1l_2}^{-1}+U_{2l_2}^{-1}\right)W_{l_2l_3}\Bigg\}
\end{aligned}
\tag{B.28}
$$

For $\langle\hat{u}_i^{(0)}(\tau)\hat{u}_j^{(1)}(\tau)\rangle$, one have

$$
\langle\hat{u}_i^{(0)}(\tau)\hat{u}_j^{(1)}(\tau)\rangle = \sum_{k,l}U_{jk}^{-1}e^{\lambda_k\tau}U_{kl}\int_0^\tau dt' e^{-\lambda_k t'}\cdot\langle\hat{u}_i^{(0)}(\tau)\mathrm{g}_l(\hat{u}^{(0)}(t'))\rangle \tag{B.29}
$$

with the integral given by

$$
\langle\hat{u}_i^{(0)}(\tau)\hat{u}_j^{(1)}(\tau)\rangle = \sum_k U_{jk}^{-1}\Big(i\left(U_{k2}-U_{k1}\right)\Lambda_1'(k,\tau)-iU_{k3}\Lambda_2'(k,\tau)+iU_{k4}\Lambda_3'(k,\tau)\Big) \tag{B.30}
$$

where

$$
\Lambda_1'(k,\tau) = e^{\lambda_k\tau}\int_0^\tau dt e^{-\lambda_k t}\langle\hat{u}_i^{(0)}(\tau)\hat{u}_4^{(0)}(t)\hat{u}_3^{(0)}(t)\rangle \tag{B.31a}
$$

$$
\Lambda_2'(k,\tau) = e^{\lambda_k\tau}\int_0^\tau dt e^{-\lambda_k t}\langle\hat{u}_i^{(0)}(\tau)\hat{u}_3^{(0)}(t)\left(\hat{u}_1^{(0)}(t)+\hat{u}_2^{(0)}(t)\right)\rangle \tag{B.31b}
$$

$$
\Lambda_3'(k,\tau) = e^{\lambda_k\tau}\int_0^\tau dt e^{-\lambda_k t}\langle\hat{u}_i^{(0)}(\tau)\hat{u}_4^{(0)}(t)\left(\hat{u}_1^{(0)}(t)+\hat{u}_2^{(0)}(t)\right)\rangle \tag{B.31c}
$$

$\Lambda_i'(k,\tau)$ different from $\Lambda_i(k,\tau)$ by replacing the term of $V_{n_1n_2n_3}$ in the first lines of $\Lambda_i(k,\tau)$ into $V_{n_3n_1n_2}$ and switch $W_{l_il_3}$ into $W_{l_3l_i}$ for all the last two lines.

B.3 Coefficient Matrix Under RWA

In this section, we consider two special situations for which the analytical form of U as well as λ_i could be analytically obtained where the mechanical damping γ_M is small so that M could be simplified as

$$M' = \begin{pmatrix} -i\tilde{\omega}_M - \frac{\tilde{\gamma}_M}{2} & 0 & -i & -i \\ 0 & i\tilde{\omega}_M - \frac{\tilde{\gamma}_M}{2} & i & i \\ -i & -i & -i\tilde{\Delta} - \tilde{\kappa} & 0 \\ i & i & 0 & i\tilde{\Delta} - \tilde{\kappa} \end{pmatrix} \tag{B.32}$$

By putting M into the above form, we have neglected a fast oscillating term for the mechanical damping, one could prove that this term is oscillating with frequency $2\omega_M$ and proportional to $\gamma_M/2$. With this approximation, the eigenvalues of the coefficient matrix λ_i and U are greatly simplified, especially at $\Delta = \omega_M$ it yields,

$$\lambda_{1,2} = -\frac{\tilde{\kappa} + \tilde{\gamma}_M/2}{2} \pm \sqrt{(\Gamma + i\tilde{\omega}_M)^2 - 1} \tag{B.33}$$

$$\lambda_{3,4} = -\frac{\tilde{\kappa} + \tilde{\gamma}_M/2}{2} \pm \sqrt{(\Gamma - i\tilde{\omega}_M)^2 - 1} \tag{B.34}$$

with $\Gamma = \sqrt{(\frac{\tilde{\kappa} - \tilde{\gamma}_M/2}{2})^2 + 1}$. However, the analytical form of matrix U is too complex to show here.

Appendix C

Dressed-state Master Equation

C.1 Operators in the Dressed-state Basis

This appendix is devoted to the derivation of the mechanical system annihilation operator $\tilde{b}_M(t)$ in the dressed-state basis in the interaction picture. The mechanical oscillator is coupled to its thermal bath via the system operator $\hat{b}_M$ [see Eq.(4.4)] and its contribution to the system dynamics could be understood by its form in the interaction picture, i.e. $\tilde{b}_M(t)$. By using the completeness of dressed-state basis, it can be shown that

$$\begin{aligned}
\tilde{b}_M(t) &\equiv e^{i\hat{H}_s t}\hat{b}_M e^{-i\hat{H}_s t} && \text{(C.1)}\\
&= e^{i\hat{H}_s t}\left(\sum_{n,\ell}|n,\ell_{(n)}\rangle\langle n,\ell_{(n)}|\right) I\otimes\hat{b}_M \\
&\times \left(\sum_{n',\eta}|n',\eta_{(n')}\rangle\langle n',\eta_{(n')}|\right) e^{-i\hat{H}_s t} && \text{(C.2)}\\
&= \sum_{n,\ell,\eta} e^{i(\ell-\eta)\omega_M t} B_{n,\ell,\eta}|n,\ell_{(n)}\rangle\langle n,\eta_{(n)}| && \text{(C.3)}
\end{aligned}$$

where $B_{n,\ell,\eta} = \langle n,\ell_{(n)}|\hat{b}_M|n,\eta_{(n)}\rangle$ that is transition element of $\hat{b}_M$ in the dressed-state basis has two contributions, i.e.,

$$\begin{aligned}
B_{n,\ell,\eta} &= \langle\ell|e^{-n\beta_0(\hat{b}_M^\dagger-\hat{b}_M)}\hat{b}_M^\dagger e^{n\beta_0(\hat{b}_M^\dagger-\hat{b}_M)}|\eta\rangle \\
&= \sqrt{\ell}\ \delta_{\ell,\eta+1} + n\beta_0\ \delta_{\ell,\eta} && \text{(C.4)}
\end{aligned}$$

In arriving at Eq. (C.4), the definition of displaced Fock state Eq. (C.50) has been used. As a result,

$$\tilde{b}_M(t) = e^{-i\omega_M t}\sum_{n,\ell}\sqrt{\ell}|n,(\ell-1)_{(n)}\rangle\langle n,\ell_{(n)}| + \beta_0\sum_{n,\ell} n|n,\ell_{(n)}\rangle\langle n,\ell_{(n)}| \quad \text{(C.5)}$$

$$= e^{-i\omega_M t}\left(\hat{b}_M - \beta_0\hat{N}_c\right) + \beta_0\hat{N}_c. \quad \text{(C.6)}$$

Equation (C.5) indicates that the coupling between the mechanical mode and its thermal bath would perturb the optomechanical system energy levels by two different physical process: (1) exciting the eigenmode by exchanging one phonon with mechanical thermal bath; (2) displacing the optomechanical system without altering the system energy. These two process actually have different effects to the system dynamics depending on the mechanical bath properties, which will be discussed in details in the next section.

C.2 Dressed-state Master Equation

In this Appendix, we present the derivation of the master equation (4.8) starting from the Born-Markov master equation,

$$\frac{d\tilde{\rho}(t)}{dt} = -\int_0^t ds Tr_R[\tilde{H}_I(t),[\tilde{H}_I(t-s),\tilde{\rho}(t)\otimes\tilde{R}_c\otimes\tilde{R}_M]] \quad \text{(C.7)}$$

with operators in the interaction picture denoted as a tilde on top,

$$\tilde{\Omega}(t) = U^\dagger(t)\hat{\Omega}U(t), \quad U(t) = e^{-i(\hat{H}_s+\hat{H}_C^B+\hat{H}_M^B)t}. \quad \text{(C.8)}$$

Here $\tilde{\rho}(t)$ is the reduced density matrix of the cavity-mechanical system in the interaction picture after tracing out the environment (bath) degrees of freedom. While $\tilde{R}_c$ denotes the density matrix of cavity thermal bath (an effectively zero-temperature bath due to the high cavity frequency) and $\tilde{R}_M$ is the density matrix for mechanical thermal bath in a thermal state at temperature T. In order to simplify our notations, let us define a superoperator $\mathcal{L}$ on density matrix as following,

$$\frac{d\tilde{\rho}(t)}{dt} = -\mathcal{L}\tilde{\rho}(t). \quad \text{(C.9)}$$

Due to the fact that the bath coupled to the cavity mode and the bath coupled to the mechanical mode are assumed to be independent and the fact that $\tilde{a}_c(t)$ and $\tilde{b}_M(t)$ commute, the superoperator could be expressed as two parts: one due to the cavity bath and the other due to the mechanical bath, i.e.,

$$\mathcal{L}\tilde{\rho}(t) = \mathcal{L}_c\tilde{\rho}(t) + \mathcal{L}_M\tilde{\rho}(t). \quad \text{(C.10)}$$

with

$$\begin{aligned}\mathcal{L}_c\tilde{\rho}(t) &= \int_0^t ds\mathcal{R}_1(s)\left(\tilde{a}_c(t)\tilde{a}_c^\dagger(t-s)\tilde{\rho}(t)-\tilde{a}_c^\dagger(t-s)\tilde{\rho}(t)\tilde{a}_c(t)\right)\\ &\quad +h.c.\\ &+ \int_0^t ds\mathcal{R}_2(s)\left(\tilde{a}_c^\dagger(t)\tilde{a}_c(t-s)\tilde{\rho}(t)-\tilde{a}_c(t-s)\tilde{\rho}(t)\tilde{a}_c^\dagger(t)\right)\\ &\quad +h.c. \end{aligned} \tag{C.11}$$

where $\mathcal{R}_1(s) = Tr_R\left(\tilde{\Gamma}_c^\dagger(t)\tilde{\Gamma}_c(t-s)R_c\right)$, $\mathcal{R}_2(s) = Tr_R\left(\tilde{\Gamma}_c(t)\tilde{\Gamma}_c^\dagger(t-s)R_c\right)$ and $h.c.$ denotes the Hermitian conjugate of the previous term, and

$$\begin{aligned}\mathcal{L}_M\tilde{\rho}(t) &= \int_0^t ds\mathcal{R}_M(s)\left(\tilde{X}_M(t)\tilde{X}_M(t-s)\tilde{\rho}(t)-\tilde{X}_M(t-s)\tilde{\rho}(t)\tilde{X}_M(t)\right)\\ &+ \quad h.c., \end{aligned} \tag{C.12}$$

where $\tilde{X}_M(t) = \tilde{b}_M(t)+\tilde{b}_M^\dagger(t)$, $\mathcal{R}_M(s) = Tr_R\{\tilde{X}_\Gamma(t)\tilde{X}_\Gamma(t-s)\tilde{R}_M\}$ and $\tilde{X}_\Gamma(t) = \tilde{\Gamma}_M(t)+\tilde{\Gamma}_M^\dagger(t)$.

I. Cavity bath contribution $\mathcal{L}_c$

By expanding $\tilde{a}_c(t)$ in the eigen-basis $|n, m_{(n)}\rangle$ of H_s, one can simplify $\mathcal{L}_c\tilde{\rho}(t)$ into following form;

$$\begin{aligned}\mathcal{L}_c\tilde{\rho}(t) &= \sum_{\substack{n,j,k\\ m,\ell,\eta}} \mathcal{C}_1\left(\hat{A}_{j,k}^n(t)\hat{A}_{\ell,\eta}^{m,\dagger}(t)\tilde{\rho}(t)-\hat{A}_{\ell,\eta}^{m,\dagger}(t)\tilde{\rho}(t)\hat{A}_{j,k}^n(t)\right)+h.c.\\ &+ \sum_{\substack{n,j,k\\ m,\ell,\eta}} \mathcal{C}_2\left(\hat{A}_{\ell,\eta}^{m,\dagger}(t)\hat{A}_{j,k}^n(t)\tilde{\rho}(t)-\hat{A}_{j,k}^n(t)\tilde{\rho}(t)\hat{A}_{\ell,\eta}^{m,\dagger}(t)\right)+h.c., \end{aligned} \tag{C.13}$$

where $\hat{A}_{j,k}^n(t) = e^{-i\Delta_{k,j}^n t}A_{j,k,n}|n-1, j_{(n-1)}\rangle\langle n, k_{(n)}|$, with the transition amplitude $A_{j,k,n} = \sqrt{n}\langle j_{(n-1)}|k_{(n)}\rangle$ and $\Delta_{k,j}^n = (E_{n,k}-E_{n-1,j})/\hbar = \omega_c+(k-j)\omega_M+(1-2n)g_0^2/\omega_M$. Here the correlation of the optical thermal bath gives

$$\mathcal{C}_1 = \int_0^t ds e^{-i\Delta_{\ell,\eta}^m s}\mathcal{R}_1(s) = \int_0^\infty d\omega\int_0^t ds\, e^{i(\omega-\Delta_{\ell,\eta}^m)s}g_c(\omega)|\lambda_c(\omega)|^2\bar{n}(\omega,T), \tag{C.14}$$

where $g_c(\omega)$ and $\lambda_c(\omega)$ are the density of state of and coupling strength to the optical thermal bath, respectively. Making the Markovian approximation by extending the

upper limit of the integration with respect to the variable s to $t \to \infty$ and using the relation

$$\int_0^\infty ds e^{i(\omega-\omega')s} = \pi\delta(\omega-\omega') + i\ P.V.\frac{1}{\omega-\omega'} \tag{C.15}$$

with P.V. denoting the Cauchy principal value, one obtains

$$\mathcal{C}_1 \approx \pi g_c(\Delta^m_{\ell,\eta})|\lambda_c(\Delta^m_{\ell,\eta})|^2\bar{n}(\Delta^m_{\ell,\eta},T), \tag{C.16}$$

where the imaginary part with the P.V. contribution which can be in principle put into the renormalized frequency of the cavity mode has been neglected. We consider that ω_c is in the optical frequency range in the order of 10^{15}Hz, much larger than ω_M and g_0. Thus it dominates the energy difference due to the photon number change, i.e., $\Delta^m_{\ell,\eta} \sim \omega_c$. As a result, a constant cavity decay rate can be defined as $\kappa = 2\pi g_c(\omega_c)|\lambda_c(\omega_c)|^2$, independent of the quantum number changes (transitions) of the mechanical mode and $\mathcal{C}_1$ is simplified as,

$$\mathcal{C}_1 \approx \bar{n}(\omega_c,T)\kappa \tag{C.17}$$

Similarly, one obtains

$$\mathcal{C}_2 = \int_0^t ds e^{i\Delta^n_{j,k}s}\mathcal{R}_2(s) \approx \frac{\kappa}{2}\left[\bar{n}(\omega_c,T)+1\right]. \tag{C.18}$$

Furthermore, the large value of $\omega_c \gg k_BT/\hbar$ effectively makes $\bar{n}(\omega_c,T) \sim 0$ (an effective zero temperature bath). As a result, $\mathcal{C}_1 \approx 0$ and $\mathcal{C}_2 \approx \kappa/2$. From Eq. (C.13), one then has

$$\begin{aligned}\mathcal{L}_c\tilde{\rho}(t) &= \frac{\kappa}{2}\sum_{\substack{n,j,k\\m,\ell,\eta}}\left(\hat{A}^{m,\dagger}_{\ell,\eta}(t)\hat{A}^n_{j,k}(t)\tilde{\rho}(t) - \hat{A}^n_{j,k}(t)\tilde{\rho}(t)\hat{A}^{m,\dagger}_{\ell,\eta}(t)\right)\\ &+ h.c.\end{aligned} \tag{C.19}$$

which is actually the term of $\kappa\mathcal{D}[\hat{a}_c]\rho(t)$ in the interaction picture of $\hat{H}_s$. Here the superoperator $\mathcal{D}[\hat{\Omega}]\rho(t) = \hat{\Omega}\rho(t)\hat{\Omega}^\dagger - \left(\hat{\Omega}^\dagger\hat{\Omega}\rho(t) + \rho(t)\hat{\Omega}^\dagger\hat{\Omega}\right)$.

Therefore, in the strong coupling regime the dissipative terms of the cavity decay is still in the form of

$$\mathcal{L}_c\rho(t) = \kappa\mathcal{D}[\hat{a}_c]\rho(t), \tag{C.20}$$

the same as that in the standard master equation. We will see in the next section that it is , however, not the case for the dissipative terms of the decay of the mechanical mode. The essential difference between the cavity decay and mechanical decay is that the optical cavity mode has a very high energy change when it is excited by its thermal bath, and this makes the energy modifications from the optomechanical interaction insignificant. Therefore all the transitions have the same contribution (or the same decay rate κ), leading to the same decoherence terms as the standard cavity decay.

II. Mechanical bath contribution $\mathcal{L}_M$

In this section we present the derivation for the dissipative terms in the dressed-state master equation for the mechanical mode. The first term in $\mathcal{L}_M\tilde{\rho}(t)$ of Eq. (C.12) has the following terms, i.e.,

$$\mathcal{L}_M^{(1)}\tilde{\rho}(t) = \int_0^t ds\ \mathcal{R}_M(s)\tilde{X}_M(t)\tilde{X}_M(t-s)\tilde{\rho}(t) \tag{C.21}$$

with $\tilde{X}_M(t) = \tilde{b}_M(t) + \tilde{b}_M^\dagger(t)$. It immediately follows that

$$\mathcal{L}_M^{(1)}\tilde{\rho}(t) = \sum_{i,j=\pm} \mathcal{L}_M^{(i,j)}\tilde{\rho}(t) \tag{C.22}$$

with

$$\begin{aligned}
\mathcal{L}_M^{(+,+)}\tilde{\rho}(t) &= \int_0^t ds\ \mathcal{R}_M(s)\tilde{b}_M^\dagger(t)\tilde{b}_M^\dagger(t-s)\tilde{\rho}(t),\\
\mathcal{L}_M^{(-,-)}\tilde{\rho}(t) &= \int_0^t ds\ \mathcal{R}_M(s)\tilde{b}_M(t)\tilde{b}_M(t-s)\tilde{\rho}(t),\\
\mathcal{L}_M^{(+,-)}\tilde{\rho}(t) &= \int_0^t ds\ \mathcal{R}_M(s)\tilde{b}_M^\dagger(t)\tilde{b}_M(t-s)\tilde{\rho}(t),\\
\mathcal{L}_M^{(-,+)}\tilde{\rho}(t) &= \int_0^t ds\ \mathcal{R}_M(s)\tilde{b}_M(t)\tilde{b}_M^\dagger(t-s)\tilde{\rho}(t).
\end{aligned}$$

Substituting Eq. (C.6) for $\tilde{b}_M(t)$ and $\tilde{b}_M^\dagger(t)$, one can obtain

$$\begin{aligned}
\mathcal{L}_M^{(+,+)}\tilde{\rho}(t) &= C_0\beta_0^2\hat{N}_c\hat{N}_c\tilde{\rho}(t) + e^{2i\omega_M t}C_-\hat{B}_M^\dagger\hat{B}_M^\dagger\tilde{\rho}(t)\\
&+ e^{i\omega_M t}\left(C_0 + C_-\right)\beta_0\hat{B}_M^\dagger\hat{N}_c\tilde{\rho}(t),
\end{aligned}$$

$$\begin{aligned}
\mathcal{L}_M^{(-,-)}\tilde{\rho}(t) &= C_0\beta_0^2\hat{N}_c\hat{N}_c\tilde{\rho}(t) + e^{-2i\omega_M t}C_+\hat{B}_M\hat{B}_M\tilde{\rho}(t)\\
&+ e^{i\omega_M t}\left(C_0 + C_+\right)\beta_0\hat{B}_M\hat{N}_c\tilde{\rho}(t),
\end{aligned}$$

$$\begin{aligned}
\mathcal{L}_M^{(+,-)}\tilde{\rho}(t) &= C_0\beta_0^2\hat{N}_c\hat{N}_c\tilde{\rho}(t) + C_+\hat{B}_M^\dagger\hat{B}_M\tilde{\rho}(t)\\
&+ \left(e^{i\omega_M t}C_0\hat{B}_M^\dagger + e^{-i\omega_M t}C_+\hat{B}_M\right)\beta_0\hat{N}_c\tilde{\rho}(t),
\end{aligned}$$

$$\begin{aligned}
\mathcal{L}_M^{(-,+)}\tilde{\rho}(t) &= C_0\beta_0^2\hat{N}_c\hat{N}_c\tilde{\rho}(t) + C_+\hat{B}_M\hat{B}_M^\dagger\tilde{\rho}(t)\\
&+ \left(e^{-i\omega_M t}C_0\hat{B}_M + e^{i\omega_M t}C_-\hat{B}_M^\dagger\right)\beta_0\hat{N}_c\tilde{\rho}(t),
\end{aligned}$$

with $\hat{B}_M = \hat{b}_M - \beta_0 \hat{N}_c$ and the coefficients defined by

$$\begin{aligned} C_0 &= \int_0^t ds \mathcal{R}_M(s), \quad C_- = \int_0^t ds e^{-i\omega_M s}\, \mathcal{R}_M(s), \\ C_+ &= \int_0^t ds e^{i\omega_M s}\, \mathcal{R}_M(s). \end{aligned}$$

Here $\mathcal{R}_M(t)$ is defined under Eq. (C.12). Several fast-oscillating terms , i.e., terms proportional to $e^{\pm ni\omega_M}$, in the above expressions have very small contributions and are neglected due to the fact that the case we consider is in the regime where $\omega_M \gg \gamma_M$, where γ_M is the mechanical decay rate and its definition will be given later . This is called the rotating-wave approximation. The above expressions, after neglecting these fast-oscillating terms, becomes

$$\mathcal{L}_M^{(1)} \tilde{\rho}(t) = \left(4C_0 \beta_0^2 \hat{N}_c \hat{N}_c + C_- \hat{B}_M \hat{B}_M^\dagger + C_+ \hat{B}_M^\dagger \hat{B}_M \right) \tilde{\rho}(t), \tag{C.23}$$

where the coefficients are given

$$C_0 = \int_0^t ds Tr_R \left(\tilde{X}_\Gamma(t) \tilde{X}_\Gamma(t-s) \tilde{R}_M \right), \tag{C.24}$$

$$C_- = \int_0^t ds e^{-i\omega_M s} Tr_R \left(\tilde{\Gamma}_M^\dagger(t) \tilde{\Gamma}_M(t-s) \tilde{R}_M \right), \tag{C.25}$$

$$C_+ = \int_0^t ds e^{i\omega_M s}\, Tr_R \left(\tilde{\Gamma}_M(t) \tilde{\Gamma}_M^\dagger(t-s) \tilde{R}_M \right). \tag{C.26}$$

Let us look at more details of a typical bath contributions from Eq. (C.24)

$$\int_0^t ds Tr_R \left(\tilde{\Gamma}_M^\dagger(t) \tilde{\Gamma}_M(t-s) R_M \right) = \int_0^t ds \int_0^\infty d\omega\, e^{-i\omega s} g_M(\omega) |\lambda_M(\omega)|^2 n(\omega, T) \tag{C.27}$$

and the contribution from (C.25)

$$\begin{aligned} &\int_0^t ds e^{-i\omega_M s} Tr_R \left(\tilde{\Gamma}_M^\dagger(t) \tilde{\Gamma}_M(t-s) R_M \right) \\ &= \int_0^t ds \int_0^\infty d\omega\, e^{-i(\omega-\omega_M)s} g_M(\omega) |\lambda_M(\omega)|^2 n(\omega, T) \end{aligned} \tag{C.28}$$

where the trace of the bath correlation functions have been converted to the bath frequency integration with $g_M(\omega)$ and $\lambda_M(\omega)$ being the density of states of and the coupling strength to the mechanical bath, respectively.

With Markovian approximation, one requires that $Tr_R\left(\tilde{\Gamma}_M^\dagger(t)\tilde{\Gamma}_M(t-s)R_M\right)$ decays in a very short time, i.e., the bath correlation time is very short compared to the typical system response time. In this case, Eq. (C.28) could be calculated by letting upper limit of the integration $t \to \infty$, i.e.,

$$\begin{aligned}
&\int_0^t ds \int_0^\infty d\omega\ e^{-i(\omega-\omega_M)s} g_M(\omega)|\lambda_M(\omega)|^2 n(\omega,T) \\
=\ &\int_0^\infty d\omega \Big(\int_0^\infty ds e^{-i(\omega-\omega_M)s} \Big) g_M(\omega)|\lambda_M(\omega)|^2 n(\omega,T) \\
=\ &\int_0^\infty d\omega \pi\delta(\omega-\omega_M) g_M(\omega)|\lambda_M(\omega)|^2 n(\omega,T) + i\,P.V.\int_0^\infty d\omega \frac{g_M(\omega)|\lambda_M(\omega)|^2 n(\omega,T)}{\omega_M-\omega} \\
=\ &\pi g_M(\omega_M)|\lambda_M(\omega_M)|^2 n(\omega_M,T) + i\ P.V.\int_0^\infty d\omega \frac{g_M(\omega)|\lambda_M(\omega)|^2 n(\omega,T)}{\omega_M-\omega}. \qquad \text{(C.29)}
\end{aligned}$$

In the second step, we have used Eq. (C.15). Therefore Eq. (C.28) can be written as

$$\int_0^t ds e^{-i\omega_M s} Tr_R\left(\tilde{\Gamma}_M^\dagger(t)\tilde{\Gamma}_M(t-s)R_M\right) = \frac{\gamma_M}{2} n_{th}(\omega_M) + i\ ImC_- \quad \text{(C.30)}$$

where $n_{th}(\omega_M) = n(\omega,T)$ is the average occupation number of the thermal mechanical bath modes, $\gamma_M = 2\pi g_M(\omega_M)|\lambda_M(\omega_M)|^2$ is the decay rate of the mechanical mode, and ImC_- is the imaginary part defined through the P.V. term of Eq. (C.29) and will contribute to the effective Hamiltonian. However, the contribution of Eq. (C.27) is quite different and can be neglected as compared to Eq. (C.28). To give a concrete estimate, let us employ the same assumption of short bath correlation time τ_c and assume the bath correlation function, without losing any generality, in a form of exponential decay as

$$Tr_R\left(\tilde{\Gamma}_M^\dagger(t)\tilde{\Gamma}_M(t-s)R_M\right) \sim C_R e^{-s/\tau_c}. \quad \text{(C.31)}$$

We then find for Eq. (C.27)

$$\int_0^t ds Tr_R\left(\tilde{\Gamma}_M^\dagger(t)\tilde{\Gamma}_M(t-s)R_M\right) \sim C_R\int_0^t ds e^{-s/\tau_c} = C_R(1-e^{-t/\tau_c})\tau_c. \quad \text{(C.32)}$$

As a result, the contribution of C_0 proportional to the very short bath correlation time τ_c can be neglected as compared to those of C_- and C_+. We note here that obtaining the vanishing result for Eq. (C.27) is equivalent to assuming no significant low-frequency contribution near $\omega = 0$ from the spectral density $J(\omega) = g_M(\omega)|\lambda_M(\omega)|^2$ of the mechanical bath. This can be understood as follows. If one follows the similar calculation for Eq. (C.28) in Eq. (C.29) by setting $\omega_M = 0$ in Eq. (C.29) for the

evaluation of Eq. (C.27), then the contribution of Eq. (C.27) is tiny if $J(\omega = 0)$ is very small as compared to $J(\omega = \omega_M)$. Thus we have

$$C_0 = \int_0^t ds Tr_R \left(\tilde{X}_\Gamma(t) \tilde{X}_\Gamma(t-s) \tilde{R}_M \right) \approx 0 \tag{C.33}$$

$$\begin{aligned} C_- &= \int_0^t ds e^{-i\omega_M s} Tr_R \left(\tilde{\Gamma}_M^\dagger(t) \tilde{\Gamma}_M(t-s) \tilde{R}_M \right) \\ &= n_{th}\gamma_M + i\ ImC_- \end{aligned} \tag{C.34}$$

$$\begin{aligned} C_+ &= \int_0^t ds e^{i\omega_M s}\ Tr_R \left(\tilde{\Gamma}_M(t) \tilde{\Gamma}_M^\dagger(t-s) \tilde{R}_M \right) \\ &= (n_{th}+1)\gamma_M + i\ ImC_+ \end{aligned} \tag{C.35}$$

Notice in the standard master equation that the C_0 term is kept and is assumed to have the same contributions as C_- and C_+, but this is not true in the strong coupling regime. Actually this C_0 term generates dephasing to the cavity mode and the disappearance of this term in the strong coupling regime indicates that the strong optomechanical interaction could help the cavity mode from dephsing which is confirmed from our simulations. In summary, it is this coefficient C_0 that has negligible contribution in the strongly coupling regime and thus in turn makes the resultant dressed-state master equation deviate from the standard master equation. By Going Backing to the Schrödinger picture, the real part of the coefficients leads to

$$\begin{aligned} U(t) \left(\mathcal{L}_M^{(1)} \tilde{\rho}(t) \right) U^\dagger(t) &= \gamma_M n_{th}(\omega_M) \left(\hat{b}_M - \beta_0 \hat{N}_c \right) \left(\hat{b}_M^\dagger - \beta_0 \hat{N}_c \right) \rho(t) \\ &+ \gamma_M (n_{th}(\omega_M)+1) \left(\hat{b}_M^\dagger - \beta_0 \hat{N}_c \right) \left(\hat{b}_M - \beta_0 \hat{N}_c \right) \rho(t) \end{aligned} \tag{C.36}$$

Using the similar arguments and calculations for each part of $\mathcal{L}_M \rho(t)$ in Eq. (C.12), one can show that

$$\mathcal{L}_M \rho(t) = (n_{th}+1)\gamma_M \mathcal{D}[\hat{b}_M - \beta_0 \hat{N}_c]\rho(t) + \gamma_M \cdot n_{th} \mathcal{D}[\hat{b}_M^\dagger - \beta_0 \hat{N}_c]\rho(t). \tag{C.37}$$

The imaginary parts of the coefficients will contribution to a modification to the system Hamiltonian, i.e.

$$\hat{H}' = \mathcal{C} \left(\hat{b}_M^\dagger \hat{b}_M - \beta_0 \hat{a}_c^\dagger \hat{a}_c (\hat{b}_M^\dagger + \hat{b}_M) + \beta_0^2 \hat{a}_c^\dagger \hat{a}_c \hat{a}_c^\dagger \hat{a}_c \right), \tag{C.38}$$

where the coefficient $\mathcal{C} = ImC_+ + ImC_-$ is in the order of lamb shift and normally could be neglected.

C.3 Master Equations in the Interaction Picture

In this section, we present both the dressed-state master equation and the standard master equation in the interaction picture of $\hat{H}_s$. Due to the fact that in the interaction picture of $\hat{H}_s$, one could have the following form for the Heisenberg operators,

$$\begin{aligned}
\tilde{a}_c(t) &= \sum_{n,k,j} e^{-i\Delta^n_{k,j}t} A_{j,k,n} |n-1, j_{(n-1)}\rangle\langle n, k_{(n)}| \approx e^{-i\omega_c}\hat{a}_c && \text{(C.39)}\\
\tilde{b}_M(t) &= e^{-i\omega_M t}\sum_{n,\ell}\sqrt{\ell}|n,(\ell-1)_{(n)}\rangle\langle n,\ell_{(n)}| \\
&+ \beta_0\sum_{n,\ell} n|n,\ell_{(n)}\rangle\langle n,\ell_{(n)}| \\
&= e^{-i\omega_M t}\left(\hat{b}_M - \beta_0\hat{a}_c^\dagger\hat{a}_c\right) + \beta_0\hat{a}_c^\dagger\hat{a}_c && \text{(C.40)}
\end{aligned}$$

so that we have the following relations,

$$U^\dagger\mathcal{D}[\hat{b}_M]\rho(t)U \approx \mathcal{D}[\hat{b}_M - \beta_0\hat{N}_c]\tilde{\rho}(t) + \mathcal{D}[\beta_0\hat{N}_c]\tilde{\rho}(t) \quad \text{(C.41)}$$

$$U^\dagger\mathcal{D}[\hat{b}_M - \beta_0\hat{N}_c]\rho(t)U \approx \mathcal{D}[\hat{b}_M - \beta_0\hat{N}_c]\tilde{\rho}(t) \quad \text{(C.42)}$$

where we have used the RWA to drop the fast oscillating terms. As a result, the dressed-state master equation could expressed as,

$$\begin{aligned}
\frac{d\tilde{\rho}(t)}{dt} &= \kappa\mathcal{D}[\hat{a}_c]\tilde{\rho}(t) + n_{th}\gamma_M\mathcal{D}[\hat{b}_M^\dagger - \beta_0\hat{N}_c]\tilde{\rho}(t) \\
&+ (n_{th}+1)\gamma_M\mathcal{D}[\hat{b}_M - \beta_0\hat{N}_c]\tilde{\rho}(t) && \text{(C.43)}
\end{aligned}$$

while the standard master equation could be expressed as

$$\begin{aligned}
\frac{d\tilde{\rho}(t)}{dt} &= \kappa\mathcal{D}[\hat{a}_c]\tilde{\rho}(t) + n_{th}\gamma_M\mathcal{D}[\hat{b}_M^\dagger - \beta_0\hat{N}_c]\tilde{\rho}(t) \\
&+ (n_{th}+1)\gamma_M\mathcal{D}[\hat{b}_M - \beta_0\hat{N}_c]\tilde{\rho}(t) \\
&+ (n_{th}+1)\beta_0^2\gamma_M\mathcal{D}[\hat{N}_c]\tilde{\rho}(t) \\
&+ n_{th}\beta_0^2\gamma_M\mathcal{D}[\hat{N}_c]\tilde{\rho}(t) && \text{(C.44)}
\end{aligned}$$

Therefore compared with the dressed-state master equation, the standard master equation clearly show two additional terms related with the cavity dephasing. In our paper, we showed the result of $P_{03}(t) := |\langle 0|\tilde{\rho}_c(t)|3\rangle|$ in the interaction picture, however P_{03} is closely related with the off diagnoal element of $\rho_{03}(t) := |\langle 0|\rho_c(t)|3\rangle|$ which we can show in the following,

$$\begin{aligned}
\rho_{03} = tr_M[\rho_s(t)|0\rangle\langle 3|\otimes I_M] &= tr_M[\tilde{\rho}_s(t)e^{i\hat{H}_s t}|0\rangle\langle 3| \\
&\quad \otimes I_M e^{-i\hat{H}_s t}] && \text{(C.45)}
\end{aligned}$$

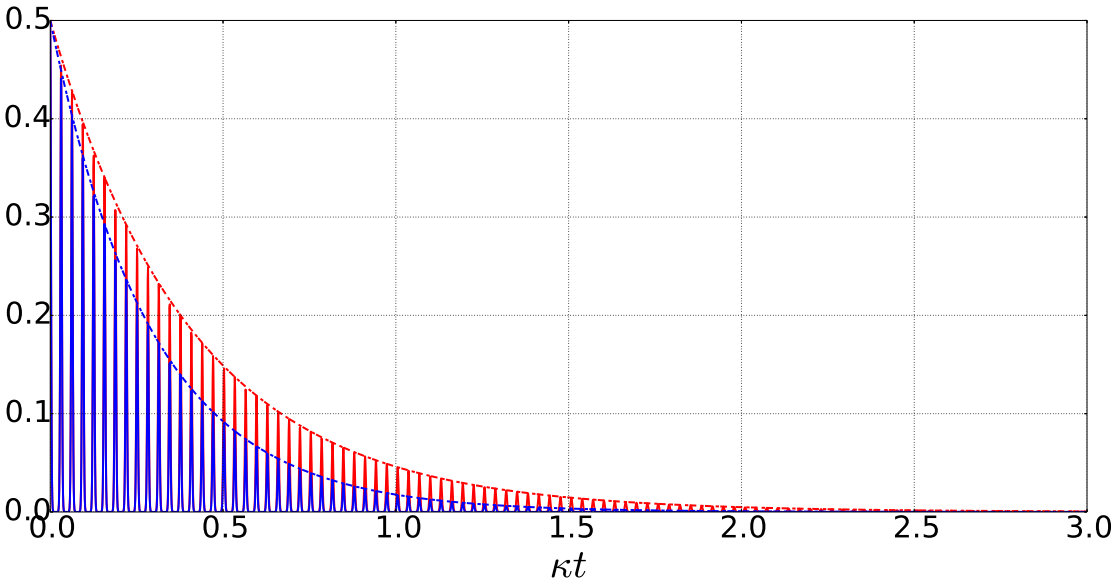

Figure C.1: Off-diagonal matrix element $P_{03}(t)$ (dashed curves) and the Schrödinger picture element $|\rho_{03}|$ (Solid curves). Red curves are from the dressed-state master equation and blue curves belongs to the standard master equation. Parameters are chosen as: $\omega_M/2\pi = 1$, $g_0 = 0.8\omega_M$, $\kappa = 0.005\omega_M$, $\gamma = \kappa/3$, $n_{th} = 0$

It can be shown that

$$\begin{aligned} e^{i\hat{H}_s t}|0\rangle\langle 3| \otimes I_M e^{-i\hat{H}_s t} &= e^{-3i\omega_c t} e^{9i\beta_0^2 \omega_M t}|0\rangle\langle 3| \otimes e^{i\omega_M t \hat{b}_M^\dagger \hat{b}_M} \\ &\times e^{-i\omega_M t\left(\hat{b}_M^\dagger - 3\beta_0\right)\left(\hat{b}_M - 3\beta_0\right)} \end{aligned} \tag{C.46}$$

and Using the fact that

$$e^{i\omega_M t \hat{b}_M^\dagger \hat{b}_M} e^{-i\omega_M t\left(\hat{b}_M^\dagger - 3\beta_0\right)\left(\hat{b}_M - 3\beta_0\right)} = e^{-i9\beta_0^2 sin(\omega_M t)} e^{3\beta_0\left(\left(e^{i\omega_M t}-1\right)\hat{b}_M^\dagger - \left(e^{-i\omega_M t}-1\right)\hat{b}_M\right)} \tag{C.47}$$

one could obtain

$$\rho_{03} = A \cdot tr_M[\tilde{\rho}_s(t)|0\rangle\langle 3| \otimes e^{3\beta_0\left(\left(e^{i\omega_M t}-1\right)\hat{b}_M^\dagger - \left(e^{-i\omega_M t}-1\right)\hat{b}_M\right)}] \tag{C.48}$$

with the constant phase factor as $A = e^{-3i\omega_c t + 9i\beta_0^2(\omega_M t - sin(\omega_M t))}$. Therefore P_{03} is not exactly $|\rho_{03}|$ but the difference is the oscillating shift operator in the above equation. One example of $P_{03}(t)$ for the relationship between the interaction picture and Schrödinger picture is shown in Fig.C.1.

C.4 Two-cavity Dressed-state Master Equation

We consider the following optomechanical system Hamiltonian, i.e. two cavity modes interacting with a single mechanical mode,

$$\hat{H}_s = \sum_i \hbar\omega_{ci}\hat{a}_i^\dagger\hat{a}_i + \hbar\omega_M\hat{b}_M^\dagger\hat{b}_M - \sum_i \hbar g_{0i}\hat{a}_i^\dagger\hat{a}_i\left(\hat{b}_M^\dagger + \hat{b}_M\right) \tag{C.49}$$

where operator of the form Ω_{ci} indicates the operator belongs to the ith cavity mode and $\hat{a}_{ci}$ ($\hat{b}_M$) is the annihilation operator for the ith cavity mode (mechanical mode). The eigen-basis of H_s are known as

$$|n_1, n_2, \tilde{m}(n_1, n_2)\rangle = |n_1\rangle \otimes |n_2\rangle \otimes e^{\left(\sum_i n_i\beta_i\right)\left(\hat{b}_M^\dagger - \hat{b}_M\right)}|m\rangle \tag{C.50}$$

with $\beta_i = g_{0i}/\omega_M$ and the corresponding eigen-energy (dressed-state bais) is given by

$$E_{n_1,n_2,m} = n_1\hbar\omega_{c1} + n_2\hbar\omega_{c2} + m\hbar\omega_M - \left(n_1\beta_1 + n_2\beta_2\right)^2\hbar\omega_M \tag{C.51}$$

For the cavity modes in the optical frequency we still have the following approximation, Applying the same arguement, one could also approximate,

$$\tilde{a}_{ci}(t) \approx e^{-i\omega_{ci}t}\hat{a}_{ci} \tag{C.52}$$

However, for the mechanical mode it becomes

$$\begin{aligned}
\tilde{b}_M(t) &= e^{-i\omega_M t}\sum_{n_1,n_2,\ell}\sqrt{\ell}|n_1, n_2, \tilde{\ell}(n_1, n_2)\rangle\langle n_1, n_2, \tilde{\ell}(n_1, n_2)| \\
&\quad + \sum_{n_1,n_2,\ell}\left(n_1\beta_1 + n_2\beta_2\right)|n_1, n_2, \tilde{\ell}(n_1, n_2)\rangle\langle n_1, n_2, \tilde{\ell}(n_1, n_2)| \\
&= e^{-i\omega_M t}\left(\hat{b}_M - \hat{N}_c\right) + \hat{N}_c.
\end{aligned} \tag{C.53}$$

where $\hat{N}_c = \beta_1\hat{N}_{c1} + \beta_2\hat{N}_{c2}$ and we have used the following relations,

$$\begin{aligned}
& e^{\left(-\sum_i n_i\beta_i\right)\left(\hat{b}_M^\dagger - \hat{b}_M\right)}\hat{b}_M^\dagger\hat{b}_M e^{\left(\sum_i n_i\beta_i\right)\left(\hat{b}_M^\dagger - \hat{b}_M\right)} \\
= \; & \hat{b}_M^\dagger\hat{b}_M + \left(n_1\beta_1 + n_2\beta_2\right)^2 + \left(n_1\beta_1 + n_2\beta_2\right)\left(\hat{b}_M^\dagger + \hat{b}_M\right)
\end{aligned} \tag{C.54}$$

$$\begin{aligned}
& e^{\left(\sum_i n_i\beta_i\right)\left(\hat{b}_M^\dagger - \hat{b}_M\right)}\left(\hat{b}_M^\dagger + \hat{b}_M\right)e^{-\left(\sum_i n_i\beta_i\right)\left(\hat{b}_M^\dagger - \hat{b}_M\right)} \\
= \; & \left(\hat{b}_M^\dagger + \hat{b}_M\right) - 2\left(n_1\beta_1 + n_2\beta_2\right)
\end{aligned} \tag{C.55}$$

which could be easily proved by the Hadamard lemma. Based on these two facts, one could easily arrive at the dressed-state master equation for the two cavity modes case

as (in the interaction picture of $\hat{H}_s$),

$$\begin{aligned}\frac{d\tilde{\rho}(t)}{dt} &= \sum_i \kappa_i \mathcal{D}[\hat{a}_{ci}]\tilde{\rho}(t) + (n_{th}+1)\gamma_M \mathcal{D}[\hat{b}_M - \hat{N}_c]\tilde{\rho}(t) \\ &+ n_{th}\gamma_M \mathcal{D}[\hat{b}_M^\dagger - \hat{N}_c]\tilde{\rho}(t)\end{aligned} \tag{C.56}$$

where $\hat{N}_c = \beta_1 \hat{N}_{c1} + \beta_2 \hat{N}_{c2}$.

Bibliography

[1] J. Kepler. "De Cometis". In: (1619).

[2] V. B. Braginsky and A. B. Manukin. In: *Sov. Phys. JETP* 25 (1967), p. 25.

[3] V. B. Braginsky, A. B. Manukin, and M.Y. Tikhonov. In: *Sov. Phys. JETP* 31 (1970), p. 829.

[4] A. Abramovici et al. In: *Science* 256 (1992), p. 325.

[5] T. Corbitt et al. In: *Phys.Rev. Lett.* 99 (2007), p. 160801.

[6] K. W. Murch et al. In: *Nature Phys.* 4 (2008), p. 561.

[7] Monika H. Schleier-Smith et al. In: *Phys. Rev. Lett.* 107 (2011), p. 143005.

[8] J. D. Teufel et al. In: *Nature (London)* 475 (2011), p. 359.

[9] M. Eichenfield et al. In: *Nature (London)* 459 (2009), p. 550.

[10] M. Eichenfield et al. In: *Nature (London)* 462 (2009), p. 78.

[11] E. Gavartin et al. In: *Phys. Rev. Lett* 106 (2011), p. 203902.

[12] M. D. LaHaye et al. In: *Science* 304 (2004), p. 74.

[13] C. Bradaschia et al. In: *Phys. Res. A* 289 (1990), p. 518.

[14] W. Marshall et al. In: *Phys. Rev. Lett* 91 (2003), p. 130401.

[15] A. D. O'Connell et al. In: *Nature* 464 (2010), p. 697.

[16] C. K. Law. In: *Phys. Rev. A* 51 (1995), p. 2537.

[17] A. Schliesser et al. In: *Phys. Rev. Lett.* 97 (2006), p. 243905.

[18] Dustin Kleckner et al. "Optomechanical trampoline resonators". In: *Opt. Express* 19.20 (2011), p. 19708.

[19] S. Groblacher et al. In: *Nature (London)* 460 (2009), p. 724.

[20] O. Arcizet et al. "Radiation-pressure cooling and optomechanical instability of a micromirror". In: *Nature (London)* 444 (2006), p. 71.

[21] B. D. Cuthbertson et al. In: *Rev. Sci. Inst.* 67 (1996), p. 2435.

[22] E. Verhagen et al. In: *Nature (London)* 482 (2012), p. 63.

[23] J. Chan et al. In: *Nature (London)* 478 (2011), p. 89.

[24] T. J. Kippenberg and K. J. Vahala. In: *Science* 321 (2008), p. 1172.

[25] J. Eisert and M. B. Plenio. In: *Int. J. Quant. Inf.* 1 (2003), p. 479.

[26] Lin Tian and Hailin Wang. In: *Phys. Rev. A* 82 (2010), p. 053806.

[27] V. Fiore et al. In: *Phys. Rev. Lett.* 107 (2011), p. 133601.

[28] A. A. Clerk et al. In: *Rev. Mod. Phys.* 82 (2010), p. 1155.

[29] D. Vitali et al. In: *Phys. Rev. Lett.* 98 (2007), p. 030405.

[30] G. Vidal and R. F. Werner. In: *Phys. Rev. A* 65 (2002), p. 032314.

[31] M. Paternostro et al. In: *Phys. Rev. Lett.* 99 (2007), p. 250401.

[32] A. Mari and J. Eisert. In: *New Journal of Physics* 14 (2012), p. 075014.

[33] A. Mari and J. Eisert. In: *Phys. Rev. Lett.* 103 (2009), p. 213603.

[34] A. Farace and V. Giovannetti. In: *Phys. Rev. A* 86(1) (2012), p. 013820.

[35] G. S. Agarwal and Sumei Huang. In: *Phys. Rev. A* 81 (2010), 041803(R).

[36] S. Weis et al. In: *Science* 330 (2010), p. 1520.

[37] A. H. Safavi-Naeini et al. In: *Nature* 472 (2011), p. 69.

[38] K. Borkje et al. In: *Phys. Rev. Lett.* 111 (2013), p. 053603.

[39] Andreas Kronwald and Florian Marquardt. In: *Phys. Rev. Lett.* 111 (2013), p. 133601.

[40] M.A. Lemonde, N. Didier, and A.A. Clerk. In: *Phys. Rev. Lett.* 111 (2013), p. 053602.

[41] M. Ludwig, B. Kubala, and F. Marquardt. In: *New J. Phys.* 10 (2008), p. 095013.

[42] F. Marquardt, J. G. E. Harris, and S. M. Girvin. In: *Phys. Rev. Lett.* 96 (2006), p. 103901.

[43] P. Rabl. In: *Phys. Rev. Lett.* 107 (2011), p. 063601.

[44] A. Nunnenkamp, K. Borkje, and S.M. Girvin. In: *Phys. Rev. Lett.* 107 (2011), p. 063602.

[45] Jiang Qian et al. In: *Phys. Rev. Lett.* 109 (2012), p. 253601.

[46] C. Genes et al. In: *Phys. Rev. A* 77 (2008), p. 033804.

[47] F. Marquardt et al. In: *Phys. Rev. Lett.* 99 (2007), p. 93902.

[48] I. Wilson-Rae et al. In: *Phys. Rev. Lett.* 99 (2007), p. 093901.

[49] S. Bose, K. Jacobs, and P. L. Knight. In: *Phys. Rev. A* 56 (1997), p. 4175.

[50] S. Mancini, D. Vitali, and P. Tombesi. In: *Phys. Rev. Lett.* 90 (2003), p. 137901.

[51] Jing Zhang, Kunchi Peng, and Samuel L. Braunstein. In: *Phys. Rev. A* 68 (2003), p. 013808.

[52] S. Pirandola et al. In: *Phys. Rev. Lett.* 97 (2006), p. 150403.

[53] S. Pirandola et al. In: *J. Mod. Opt.* 51 (2004), p. 901.

[54] Sebastian G. Hofer et al. In: *Phys. Rev. A* 84 (2011), p. 052327.

[55] L.-M. Duan et al. In: *Phys. Rev. Lett.* 84 (2000), p. 2722.

[56] P. Komar et al. In: *Phys. Rev. A* 87 (2013), p. 013839.

[57] Lin Tian. In: *Phys. Rev. Lett.* 110 (2013), p. 233602.

[58] Ying-Dan Wang and Aashish A. Clerk. In: *Phys. Rev. Lett.* 110 (2013), p. 253601.

[59] P. Van Loock and A. Furusawa. In: *Phys. Rev. A* 67 (2003), p. 052315.

[60] S. Gigan et al. "Self-cooling of a micromirror by radiation pressure". In: *Nature (London)* 444 (2006), p. 67.

[61] C. Hohberger-Metzger and K. Karrai. "Radiation-pressure cooling and optomechanical instability of a micromirror". In: *Nature (London)* 432 (2004), p. 1002.

[62] T. Corbitt et al. "An all-optical trap for a gramscale mirror". In: *Phys.Rev. Lett.* 98 (2007), p. 150802.

[63] M. Vogel et al. In: *Applied Physics Letters* 83 (2003), p. 1337.

[64] K.Jacobs et al. "Quantum noise in the position measurement of a cavity mirror undergoing Brownian motion". In: *Phys. Rev. A* 60 (1999), p. 538.

[65] C. Fabre et al. In: *Phys. Rev. A* 49 (1994), p. 1337.

[66] S. Mancini and P. Tombesi. In: *Phys. Rev. A* 49 (1994), p. 4055.

[67] E. Shchukin and W. Vogel. "Inseparability Criteria for Continuous Bipartite Quantum States". In: *Phys. Rev. Lett.* 95 (2005), p. 230502.

[68] R. Simon. In: *Phys. Rev. Lett.* 84 (2000), p. 2726.

[69] J. D. Teufel et al. "Sideband cooling of micromechanical motion to the quantum ground state". In: *Nature* 475 (2011), p. 359.

[70] A. D. O'Connell et al. "Quantum ground state and single-phonon control of a mechanical resonator". In: *Nature* 464 (2010), p. 697.

[71] J. D. Teufel et al. "Circuit cavity electromechanics in the strong-coupling regime". In: *Nature* 471 (2011), p. 204.

[72] Ying-Dan Wang and Aashish A. Clerk. "Using Interference for High Fidelity Quantum State Transfer in Optomechanics". In: *Phys. Rev. Lett.* 108 (15 Apr. 2012), p. 153603. DOI: 10.1103/PhysRevLett.108.153603. URL: http://link.aps.org/doi/10.1103/PhysRevLett.108.153603.

[73] T. A. Palomaki et al. "Coherent state transfer between itinerant microwave fields and a mechanical oscillator". In: *Nature* 495 (2013), p. 210.

[74] J.M.Dobrindt, I. Wilson-Rae, and T.J.Kippenberg. In: *Phys. Rev. Lett.* 101 (2008), p. 263602.

[75] Jie-Qiao Liao and C. K. Law. In: *Phys. Rev. A* 87 (2013), p. 043809.

[76] Xun-Wei Xu, Yuan-Jie Li, and Yu-xi Liu. In: *Phys. Rev. A* 87 (2013), p. 025803.

[77] D. Vitali et al. In: *New Journal of Physics* 10 (2008), p. 033025.